

CLIMATE VARIABILITY AND VADOSE ZONE CONTROLS ON DAMPING OF
TRANSIENT RECHARGE FLUXES

AS
36
2016
GEOL
-C67

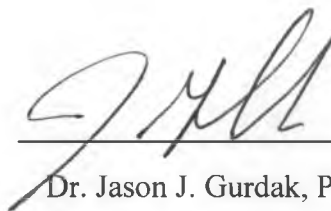
A Thesis submitted to the faculty of
San Francisco State University
In partial fulfillment of
The requirements for
The Degree

Master of Science
In
Geosciences

by
Claudia Rebecca Corona
San Francisco, California
May 2016

CERTIFICATION OF APPROVAL

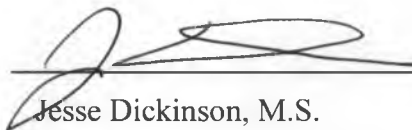
I certify that I have read *Climate Variability and Vadose Zone Controls on Damping of Transient Recharge Fluxes* by Claudia Rebecca Corona, and that in my opinion this work meets the criteria for approving a thesis submitted in partial fulfillment of the requirement for the degree Master of Science in Geosciences at San Francisco State University.



Dr. Jason J. Gurdak, Ph.D.
Associate Professor of Geosciences



Dr. Alexander Stine, Ph.D.
Assistant Professor of Oceanography



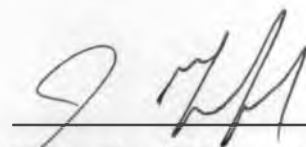
Jesse Dickinson, M.S.
Hydrologist, U. S. Geological Survey

CLIMATE VARIABILITY AND VADOSE ZONE CONTROLS ON DAMPING OF TRANSIENT RECHARGE FLUXES

Claudia Rebecca Corona
San Francisco, California
May 2016

I investigate the effects of interannual to multidecadal climate variability on groundwater resources by exploring the physical processes in the vadose zone that partially control transient infiltration and recharge fluxes. Climate signal flux propagation and variation with depth is influenced by highly nonlinear interactions of vadose zone controls, specifically the local layer texture, period (time interval), and mean amplitude of the flux. The depth at which the flux variation damps to 5% of its initial variation at land surface is defined as the damping depth. When the damping depth is above the water table, recharge may be considered steady; when the damping depth is not reached at the water table, recharge may be considered transient. I examined controls on the damping depth by modeling transient water fluxes through the vadose zone, using the Gardner-Kozeny soil model for diffuse unsaturated flow in the subsurface flow model, HYDRUS 1-D. Homogeneous profiles show that shorter-period oscillations, smaller mean fluxes, and finer-grained soil textures with poor sorting, cause shallower damping depths. Two-layered systems show similar, but more complicated responses. In two-layered systems, coarse-grained soils cause the greatest deviations from homogeneous damping depths, most evidently if they make up the lower layer of the profile. Flow simulations show that coupled finer-grained soil profiles cause damping depths that are more similar to their homogeneous counterparts and are closer to land surface, relative to coupled fine-grained/coarse-grained profiles. Linear superposition is possible in simulations of flux variations with short periods and finer-grained soils. Flux simulations with longer periods and coarser-grained soils fail to provide evidence for linear superposition. Findings from this study will enhance our understanding of how the vadose zones influences the teleconnections between climate variability modes and groundwater levels.

I certify that the Abstract is a correct representation of the content of this thesis.



Chair, Thesis Committee

5-24-2016

Date

ACKNOWLEDGEMENTS

The pursuit of a Master's Degree pushes us to learn and grow in ways that our younger selves never could have imagined, and I have my thesis advisor and science mentor, Dr. Jason Gurdak, to thank for this opportunity. Dr. Gurdak not only supported me during my time at SFSU, but he went above and beyond as an advisor, helping me attain many phenomenal academic and professional opportunities. I would also like to thank my amazing mentor from afar, USGS scientist Jesse Dickinson for his weekly guidance as I learned about the world of computer models and vadose zone hydrology. I would like to thank Dr. Zan Stine, for his wisdom and encouragement in my pursuit of knowledge. A special thanks to the Department of Hydrology and Water Resources at the University of Arizona, namely Jesse Dickinson and Dr. Ty Ferré for their incredible brainpower and cooperation—I aspire to be a hydrologist of their caliber. I am also grateful for the support by the National Science Foundation (NSF) Hydrologic Science program award #EAR-1316553, the ARCS Foundation and the SFSU College of Science and Engineering. I want to thank my fellow grad students in the Department of Earth and Climate Sciences for their boundless creativity, good-natured humor and energy, without which I wouldn't be. All in all, it has been a great pleasure to work with current and future scientists at the forefront of scientific discovery.

TABLE OF CONTENTS

LIST OF FIGURES.....	VIII
LIST OF TABLES	XI
1.0. INTRODUCTION.....	1
1.1. Background and Problem Statement	1
1.2. Climate Variability and Groundwater Levels.....	1
1.3. Infiltration in the Vadose Zone	3
1.4. Previous Studies	5
1.4.1. Climate Variability Signals in Groundwater.....	5
1.4.2. Vadose Zone Controls in Subsurface Flow Models	6
1.5. Superposition Approaches.....	7
1.6. Objectives and Hypothesis	8
2.0 METHODOLOGY	9
2.1 Theory	9
2.2. Numerical Modeling Approach.....	11
2.3 Flux Variations with Depth in Homogeneous Systems.....	13
2.4. Flux Variations with Depth in Two-Layered Systems	14
2.5 Testing for Linearity in Damping.....	15
2.6 Nonparametric Testing	19
3.0. RESULTS OF SINUSOIDAL FLUX VARIATIONS WITH DEPTH.....	20
3.1. How Does Soil Texture Influence Damping in a Homogeneous System?	20
Clay and Loamy Sand Profiles.....	21
3.2. Effects of Varying Layer Thickness on Damping Depth	25
Clay as the upper layer	25
Silt as the upper layer	26

<i>Loam as the upper layer</i>	26
<i>Loamy Sand as the upper layer</i>	26
3.3. Does the interaction of soil layers influence the damping of variable water flux?	27
<i>For a 30-day period with an applied flux variation of 1.0 mm/day</i>	28
<i>For a 90-day period with an applied flux variation of 1.0 mm/day,</i>	28
<i>For a 365-day period with an applied flux variation of 1.0 mm/day,</i>	29
3.4. Is linear superposition accurate in two-layered systems?	29
<i>Clay as the upper layer</i>	29
<i>Silt as the upper layer</i>	30
<i>Loam as the upper layer</i>	30
<i>Loamy Sand as the upper layer</i>	31
3.5. Diffusivity and Damping Depth	31
<i>Clay Overlying Loamy Sand</i>	32
<i>Loamy Sand Overlying Clay</i>	33
3.6. Using Statistical Tools to Understand Parameter Influence	33
4.0 IMPLICATIONS.....	34
5.0 CONCLUSIONS	35
6.0 REFERENCES.....	37
7.0 FIGURES	40
8.0 TABLES.....	59
9.0 APPENDIX	95
Model Input.....	95
Model Output	95

LIST OF FIGURES

- Figure 1. Damping of a sinusoidal vertical flux, q_z , applied at land surface, where $z = 0$. Profiles of the flux with depth. The flux travels vertically downward and has a steady component, q_s , plus a sinusoidal component with amplitude q_p 40
- Figure 2. Soil textural triangle showing percentages of sand, silt and clay for the 12 USDA soil texture classifications. The shaded polygons are the selected reference soil textures used in the two-layered system. 41
- Figure 3. Damping of sinusoidal flux applied at land surface ($z = 0$) to some depth, d_{num} . Layer thickness for model runs are quarter-fractions of the total d_{num} , representing thin, intermediate, and thick upper layers relative to the respective soil. 42
- Figure 4(a, b, c). Damping of sinusoidal flux applied at land surface ($z = 0$) in (a) a silt homogeneous system, a (b) a two-layered system of silt (soil #1) underlain by clay (soil #2) and a discontinuous homogeneous system with a revised amplitude. The sinusoidal envelope represents flux variations with depth at different times, t . The flux has a steady component q_s plus a sinusoidal component with amplitude q_p 43
- Figure 5(a, b). Damping of sinusoidal flux in (a) made of two distinct homogeneous layers, an upper layer (silt) and bottom layer (clay). (b) Plot of q_s , q_s and q_p for the lower layer, where the lower line defines an amplitude of 0.99 and the higher line denotes the revised amplitude. The box indicates the node at which the flux variation is 5% of what it was of the revised, starting at q_a 44
- Figure 6. Damping depths (m) from 588 simulations of homogeneous profiles of 12 soil textures, using a range of mean fluxes (0.01 to 2.0 mm/day) and periods (30 to 3,652 days). The range of mean fluxes represents long-term net infiltration flux of climate and land-cover regions of the U.S., and the range of periods represents variability on monthly, seasonal, annual, and interannual timescales. 45
- Figure 7. Comparison of the damping depths for all twelve soil texture classes. The flux amplitude damps to 5% of the applied flux variation over a period, $P = 90$ days, where the steady flux component $q_s = 1.00 \times 10^3$ m/d, plus a sinusoidal component with amplitude $q_p = 0.99 \times 10^3$ m/d..... 46
- Figure 8. Comparison of (a) flux, q_z , (b) hydraulic conductivity, K , (c) initial pressure head condition, ψ , (d) water content θ , and (e) diffusivity, D , profiles at times $P/4$ and $3P/4$, where P is the sinusoidal wave period, and the envelopes encompass the variations in the profiles of clay and loamy sand layers for a period of 90 days, and a mean flux $q_s = 1.00 \times 10^3$ m/d..... 47

LIST OF FIGURES (CONTINUED)

- Figure 9. Damping of 0.1 mm/day flux over time ranging from a monthly period (30 days) to a possible 10 years (3,652 days). Color differentiates soil tendency for shallow damping (reds) compared to deep damping (blues), with in-between damping depths in yellow. Small symbols represent fine-grained soils, and large circles represent sandy loam, loamy sand and sand—all coarse-grained textures. 48
- Figure 10. Damping depths of 1.0 mm/day flux over time ranging from a monthly period (30 days) to a possible 10 years (3,652 days). Color differentiates soil tendency for shallow damping (reds) compared to deep damping (blues), with in-between damping depths in yellow. Small symbols represent fine-grained soils, and large circles represent sandy loam, loamy sand and sand—all coarse-grained textures. 49
- Figure 11. Damping of 2.0 mm/day flux over time ranging from a monthly period (30 days) to a possible 10 years (3,652 days). Color differentiates soil tendency for shallow damping (reds) compared to deep damping (blues), with in-between damping depths in yellow. Small symbols represent fine-grained soils, and large circles represent sandy loam, loamy sand and sand—all coarse-grained textures. 50
- Figure 12(a, b). Damping in the vadose zone for clay, silt, loam, and loamy sand with four increasing infiltration fluxes: (a) 0.01mm/day, (b) 0.1mm/day, over time that may represent irrigation patterns (30 days), seasonal patterns (90 days), annual cycles (365 days) and the lower end of climate variability modes like El Niño (730.5 days). 51
- Figure 13(a ,b). Damping in the vadose zone for clay, silt, loam, and loamy sand with four increasing infiltration fluxes: (a) 1.0mm/day and (b) 2.0mm/day over time that may represent irrigation patterns (30 days), seasonal patterns (90 days), annual cycles (365 days) and the lower end of climate variability modes like El Niño (730.5 days). 52
- Figure 14. Comparison of damping depths between the homogeneous clay layer and the two-layered cases where clay is the upper layer. Comparisons are made with varying layer thickness that were calculated by dividing the total damping depth of the clay by quarters over 30, 90, and 365 days. 53
- Figure 15. Comparison of damping depths between the homogeneous silt layer and the two-layered cases where silt is the upper layer. Comparisons are made with varying layer thickness that were calculated by dividing the total damping depth of the clay by quarters over 30, 90, and 365 days. 53

LIST OF FIGURES (CONTINUED)

- Figure 16. Comparison of damping depths between the homogeneous loam layer and the two-layered cases where loam is the upper layer. Comparisons are made with varying layer thickness that were calculated by dividing the total damping depth of the clay by quarters over 30, 90, and 365 days. 54
- Figure 17. Comparison of damping depths between the homogeneous loam layer and the two-layered cases where loam is the upper layer. Comparisons are made with varying layer thickness that were calculated by dividing the total damping depth of the clay by quarters over 30, 90, and 365 days. 54
- Figure 18. Comparison of all two-layered damping depths with all homogeneous damping depths. Comparisons are made with varying layer thickness that were calculated by dividing the total damping depth of the clay by quarters over 30, 90, and 365 days. In light blue are two-layered systems where loamy sand is the upper layer, ranging from -5% to -65%. Negative percent differences highlight two-layered systems that had shallower damping depths than that of their homogeneous upper layer. Two-layered systems where loamy sand was the lower layer, show damping depth differences of over 100%, with the percent difference becoming more pronounced as the upper layer thins and the bottom layer of loamy sand thickens..... 55
- Figure 19(a, b, c). Comparison of the damping depth of the two-layered system and the homogeneous system with the revised amplitude for thin, intermediate, and thick upper layers ($\frac{1}{4}d_{num}$, $\frac{1}{2}d_{num}$, $\frac{3}{4}d_{num}$) for a q_z of 1 mm/day and (a) a 30-day period, a (b) 90-day period and a (c) 365-day period. 56
- Figure 20(a-e). Two-layered system of a clay layer (upper layer) overlying a loamy sand layer (lower layer) for a period of 90 days, and a mean flux $q_s = 1.00 \times 10^3$ m/d.. Comparison of (a) flux, q_z , (b) hydraulic conductivity, K , (c) initial pressure head condition, ψ , (d) water content θ , and (e) diffusivity, D , profiles at times $P/4$ and $3P/4$, where P is the sinusoidal wave period. The black envelope represents the water flux response in the two-layered system. 57
- Figure 21(a-e). Two-layered system of a loamy sand (upper layer) overlying a clay layer (lower layer) for a period of 90 days and a mean flux $q_s = 1.00 \times 10^3$ m/d. Comparison of (a) flux, q_z , (b) hydraulic conductivity, K , (c) initial pressure head condition, ψ , (d) water content θ , and (e) diffusivity, D , profiles at times $P/4$ and $3P/4$, where P is the sinusoidal wave period. The black envelope represents the water flux response in the two-layered system. 58

LIST OF TABLES

Table 1. Model conditions and parameters.	73
Table 2. Infiltration rates represented. Regions from Sanford and Selnick, 2013.	73
Table 3. Water flux values used with conversions to potential annual flux in mm. From Sanford and Selnick, 2013.	74
Table 4. USDA soil textural classes and Gardner hydraulic properties employed in flow simulations (modified from Dickinson et al., 2014).	74
Table 5. Numerical solution, d_{num} , of a climate signal in a 30-day period.	75
Table 6. Numerical solution, d_{num} , of a climate signal in a 90-day period.	78
Table 7. Numerical solution, d_{num} , of a climate signal in a 180-day period.	80
Table 8. Numerical solution, d_{num} , of a climate signal in a 365-day period.	83
Table 9. Numerical solution, d_{num} , of a climate signal in a 731-day period.	86
Table 10. Numerical solution, d_{num} , of a climate signal in a 2556-day period.	89
Table 11. Numerical solution, d_{num} , of a climate signal in a 3652-day period.	92
Table 12. Two-layered profile with clay as the upper layer and different bottom layers. Changes from the one-layer d_{num} are based on varying later thickness and varying lower layer for a q_z of 1 mm/day and period of 30 days.	95
Table 13. Two-layered profile with clay as the upper layer and different bottom layers. Changes from the one-layer d_{num} are based on varying later thickness and varying lower layer for a q_z of 1 mm/day and period of 90 days.	95
Table 14. Two-layered profile with clay as the upper layer and different bottom layers. Changes from the one-layer d_{num} are based on varying later thickness and varying lower layer for a q_z of 1 mm/day and period of 365 days.	96
Table 15. Two-layered profile with silt as the upper layer and different bottom layers. Changes from the one-layer d_{num} are based on varying later thickness and varying lower layer for a q_z of 1 mm/day and period of 30 days.	96

LIST OF TABLES (CONTINUED)

Table 16. Two-layered profile with silt as the upper layer and different bottom layers. Changes from the one-layer d_{num} are based on varying later thickness and varying lower layer for a q_z of 1 mm/day and period of 90 days.....	97
Table 17. Two-layered profile with silt as the upper layer and different bottom layers. Changes from the one-layer d_{num} are based on varying later thickness and varying lower layer for a q_z of 1 mm/day and period of 365 days.....	97
Table 18. Two-layered profile with loam as the upper layer and different bottom layers. Changes from the one-layer d_{num} are based on varying later thickness and varying lower layer for a q_z of 1 mm/day and period of 30 days.....	98
Table 19. Two-layered profile with loam as the upper layer and different bottom layers. Changes from the one-layer d_{num} are based on varying later thickness and varying lower layer for a q_z of 1 mm/day and period of 90 days.....	98
Table 20. Two-layered profile with loam as the upper layer and different bottom layers. Changes from the one-layer d_{num} are based on varying later thickness and varying lower layer for a q_z of 1 mm/day and period of 365 days.....	99
Table 21. Two-layered profile with loamy sand as the upper layer and different bottom layers. Changes from the one-layer d_{num} are based on varying later thickness and varying lower layer for a q_z of 1 mm/day and period of 30 days.....	99
Table 22. Two-layered profile with loamy sand as the upper layer and different bottom layers. Changes from the one-layer d_{num} are based on varying later thickness and varying lower layer for a q_z of 1 mm/day and period of 90 days.....	100
Table 23. Two-layered profile with loamy sand as the upper layer and different bottom layers. Changes from the one-layer d_{num} are based on varying later thickness and varying lower layer for a q_z of 1 mm/day and period of 365 days.....	100
Table 24. Percent change in damping depth comparisons for clay for a q_z of 1.0 mm/day and a period of 30 days. A difference of less than 10% between the two-layered and the one-layered systems indicates possible linear superposition.	101
Table 25. Percent change in damping depth comparisons for silt for a q_z of 1.0 mm/day and a period of 30 days. A difference of less than 10% between the two-layered and the one-layered systems indicates possible linear superposition.	101

LIST OF TABLES (CONTINUED)

Table 26. Percent change in damping depth comparisons for loam for a q_z of 1.0 mm/day and a period of 30 days. A difference of less than 10% between the two-layered and the one-layered systems indicates possible linear superposition.	102
Table 27. Percent change in damping depth comparisons for loamy sand for a q_z of 1.0 mm/day and a period of 30 days. A difference of less than 10% between the two-layered and the one-layered systems indicates possible linear superposition.	102
Table 28. Percent change in damping depth comparisons for clay for a q_z of 1.0 mm/day and a period of 90 days. A difference of less than 10% between the two-layered and the one-layered systems indicates possible linear superposition.	103
Table 29. Percent change in damping depth comparisons for silt for a q_z of 1.0 mm/day and a period of 90 days. A difference of less than 10% between the two-layered and the one-layered systems indicates possible linear superposition.	103
Table 30. Percent change in damping depth comparisons for loam for a q_z of 1.0 mm/day and a period of 90 days. A difference of less than 10% between the two-layered and the one-layered systems indicates possible linear superposition.	104
Table 31. Percent change in damping depth comparisons for loamy sand for a q_z of 1.0 mm/day and a period of 90 days. A difference of less than 10% between the two-layered and the one-layered systems indicates possible linear superposition.	104
Table 32. Percent change in damping depth comparisons for clay for a q_z of 1.0 mm/day and a period of 365 days. A difference of less than 10% between the two-layered and the one-layered systems indicates possible linear superposition.	104
Table 33. Percent change in damping depth comparisons for silt for a q_z of 1.0 mm/day and a period of 365 days. A difference of less than 10% between the two-layered and the one-layered systems indicates possible linear superposition.	105
Table 34. Percent change in damping depth comparisons for loam for a q_z of 1.0 mm/day and a period of 365 days. A difference of less than 10% between the two-layered and the one-layered systems indicates possible linear superposition.	105
Table 35. Percent change in damping depth comparisons for loamy sand for a q_z of 1.0 mm/day and a period of 365 days. A difference of less than 10% between the two-layered and one-layered systems indicates possible linear superposition.	106

LIST OF TABLES (CONTINUED)

Table 36. The False Discovery Rate (FDR) p-values of mean flux, period, and K_{sat} , shown alongside a statistically significant level of $\alpha = 0.05$	107
Table 37. The FDR LogWorth values highlight the statistically significant influence that the flux and period have on the damping depth.	107

1.0 INTRODUCTION

1.1. Background and Problem Statement

Understanding the processes that control groundwater response to climate variability has important implications for decisions about sustainable groundwater management and policy. As water resources become more limited in many parts of the world, many regions are increasing their reliance on groundwater to supplement existing surface-water resources (Earman and Dettinger, 2011; Taylor et al., 2012). Hydrologic models are commonly used to evaluate the impact of water use, management strategies, and climate forcings on groundwater sustainability.

1.2. Climate Variability and Groundwater Levels

Climate variability occurs on all temporal scales that extend beyond individual weather events. Climate variability is defined as the difference between current climate conditions and the mean state, where the mean state is representative of “normal” conditions computed over a larger temporal scale (Kuss and Gurdak, 2014). On global scales, the variability is often characterized using climate indices that combine sea surface temperatures, sea level pressures, geo-potential heights, and wind speed, among other atmosphere-ocean variables (Ghil, 2002; Stoner et al., 2009).

The four leading atmospheric-ocean circulation systems that affect North American interannual to multidecadal climate variability are the El Niño-Southern Oscillation (ENSO), the Pacific Decadal Oscillation (PDO), the North Atlantic Oscillation (NAO), and the Atlantic Multidecadal Oscillation (AMO). Currently, the most widely acknowledged quasi-periodic cycles are: 2-7 years (ENSO), 15-30 years (PDO), 3-6 years (NAO), and 50-70 years (AMO) (Ghil, 2002; Mantua and Hare, 2002; Kuss and Gurdak, 2014).

ENSO and NAO are considered high-frequency climate variability modes (interannual, annual), while PDO and AMO are considered low-frequency climate variability modes (multidecadal). Low-frequency climate variability modes partially control precipitation patterns, drought frequency and severity, snowstorms, stream-water

flux and other surface processes that influence infiltration rates in the vadose zone and ultimately affect recharge rates (Hanson et al., 2004; Gurdak et al., 2007; Kuss and Gurdak, 2014). In contrast, high-frequency climate variability modes create short-term hydrologic responses in surface water that are not always preserved in long-term groundwater fluxes (Gurdak et al., 2007; Velasco et al., 2015).

Infiltration events from both high-frequency and low-frequency climate variability modes can be examined by modeling downward flow in the vadose zone (Bakker and Nieber, 2004; Dickinson et al., 2004; and Dickinson et al., 2009). In the modeling environment, the downward flow can be defined as a cyclical sinusoidal flux representative of a climate cycle (Bakker and Nieber, 2004; Dickinson et al., 2009). The use of a cyclical sinusoid in the modeling environment serves as an all-encompassing representation of episodic and periodic variations in fluxes at land surface. These sinusoids result in time-varying water content and transient vertical fluxes within the vadose zone that may ultimately result in time-varying recharge.

Previous studies have found teleconnections between interannual to multidecadal climate variability and fluctuations in groundwater levels (Hanson et al., 2004; Fleming and Quilty, 2006; Gurdak et al., 2007; Holman et al., 2011; Tremblay et al., 2011, and Kuss and Gurdak, 2014). For example, ENSO and PDO were found to have a greater control on variability in groundwater levels across the U.S. than either NAO or AMO, especially in the western and central principal aquifers (PAs) (Kuss and Gurdak, 2014). The associated wet periods of the positive PDO, in particular, were found to result in greater recharge flux in the western and central Principal Aquifers. Kuss and Gurdak, (2014) suggest that the local vadose zone controls of the western and central principal aquifers (PAs) may be influencing infiltrating water to overcome the predominantly upward total potential gradients found in vadose zones of semi-arid and arid regions, resulting in greater recharge fluxes.

1.3. Infiltration in the Vadose Zone

The vadose zone is the variably saturated region of soil and aquifer that vertically extends downward from the ground surface to the water table. Depending on the climate, the thickness of the vadose zone is generally < 1 meter in humid regions to $>10\text{--}100$ meters in semiarid and arid regions (Fan et al., 2007). Therefore, processes in the vadose zone connect the atmosphere, land surface and groundwater systems by influencing infiltration and recharge events.

Water that infiltrates into the vadose zone can do so in the form of precipitation or irrigation water, or sometimes by industrial and municipal spills (Radcliffe and Simunek, 2010). Infiltration events may become a part of evaporation or can be absorbed by plant roots and returned to the atmosphere by transpiration. Water that does not undergo evaporation or transpiration, jointly known as evapotranspiration, may flow downward through the vadose zone until it reaches the water table, where it is considered recharge (Nimmo, 2005; Radcliffe and Simunek, 2010).

In the vadose zone, the hydraulic properties of soil and driving forces, primarily gravity and pressure head gradients, control water flux through the vertical profile (Nimmo, 2005). Darcy's law describes the properties of importance in steady-state water flux through the vadose zone (Richards, 1931).

Water Flux

As applied in the vadose zone, Darcy's law states that the flux q [$L\ T^{-1}$] is proportional to hydraulic conductivity K [$L\ T^{-1}$] multiplied by the driving force, which may equal the recharge rate under certain conditions (Nimmo, 2005). For one-dimensional steady water flux driven by gravity and matric pressure gradients, Darcy's law may be written as:

$$q = -K(\theta) \left[\frac{\partial \psi}{\partial z} + pg \right] \quad \text{eqn. 1}$$

where θ (dimensionless) is the water content, ψ [L] is the pressure head, K [$L\ T^{-1}$] is hydraulic conductivity (a constant of proportionality in Darcy's law), p [$M\ L^{-3}$] is the

density of water, g [$L^3 M^{-1} T^{-2}$] is the acceleration due to gravity, and z [L] is vertical distance. When modeling steady-state water flux in a region of constant downward movement in the vadose zone, gravity is the sole driver of downward flow. Long-term average recharge rates may be quantified if the K (hydraulic conductivity) and uniform pressure head, ψ are known (Nimmo, 2005). In modeling environments, recharge may be considered steady when the flux variation at a depth in the vadose zone is significantly less than that which was applied at land surface (Dickinson et al., 2014). However, if a significant percent of the flux variation is preserved, then recharge may be considered transient.

Transient, vertical flux in the vadose zone can be described by the one-dimensional Richards equation (Richards, 1931a; Bakker and Nieber, 2009; Radcliffe, D.E., 2010; Dickinson et al., 2014a):

$$\frac{\partial \theta}{\partial \psi} \frac{\partial \psi}{\partial t} = \frac{\partial}{\partial z} \left(K \frac{\partial \psi}{\partial z} \right) - \frac{\partial K}{\partial z} \quad \text{eqn. 2}$$

here θ (dimensionless) is the water content, Ψ [L] is the pressure head, t [T] is time, and $K(\Psi)$ [$L T^{-1}$] is the hydraulic conductivity, more of which will be discussed in the methods section (eqn. 8).

For transient water flux, the most important parameters are the water retention relation, $\theta(\psi)$, the hydraulic conductivity $K(\psi)$, and the hydraulic capacity function $C(\psi)$ (Nimmo, 2005; Radcliffe and Simunek, 2010). The parameters that govern transient vadose water flux depend on the pressure head and pore-size distribution of the given vadose zone. The unsaturated hydraulic conductivity may vary by orders of magnitude with pressure head. $K(\psi)$ is sensitive to the same parameters that affect the proportionality constant, K_s : texture, structure, and mineralogy (Radcliffe and Simunek, 2010). If the hydraulic conductivity varies, the flux is transient, implying hard-to-quantify fluctuations in travel times, distance, frequency and amplitude as a result of vadose zone texture, thickness, and layering. Such characteristics influence water flux behavior from infiltration to recharge.

1.4. Previous Studies

1.4.1. Climate Variability Signals in Groundwater

The teleconnections between climate variability modes and time-varying recharge rates can be examined by studying the behavior and damping depth of the flux variation in a vadose zone profile (Dickinson et al., 2014a). The damping depth is defined as the depth z below which $< 5\%$ of the applied variation is preserved (Dickinson et al., 2014a). When the flux variation damps at a depth above the water table, groundwater recharge may be considered steady. If the flux variation remains $> 5\%$ below the water table, recharge may be considered transient. The influence of climate variability modes on groundwater levels may be understood by conducting a sensitivity analysis of damping depths with varying vadose zone materials, periods, and fluxes (Bakker and Nieber, 2009; Dickinson et al., 2014a; Kuss and Gurdak, 2014).

The damping of water flux with depth is influenced by vadose zone controls, specifically the local layer texture, period (time interval), and mean amplitude of the flux (Dickinson et al., 2014a). For example, flux variations in two-layered profiles where finer-textured clay layers overlay coarser layers, damp at shallower depths. With respect to climate variability, high-frequency climate signals in such profiles consistently reach a damping depth closer to land surface (Rimon et al., 2007; Velasco et al., 2015). Dickinson et al. (2014) found that damping of a sinusoidal flux is critically influenced by layer texture. Their study looked at how a flux applied at land surface was influenced in two separate soil textures—clay and sand. They found that given a 30-d period, with a constant infiltration flux, damping occurred at a depth of 1 m in the clay profile and 6.4 m in the sand profile (Dickinson et al., 2014). They discovered that with greater periods, damping occurred shallower depths in clay (finer-grained material) compared to sand (coarser-grained material).

Clay and sand are two of twelve soil classification textures used to describe local soils by the U.S. Department of Agriculture (USDA, 2016). The question of how the remaining ten soil textures and their interactions influence the variability of a water flux is necessary for our overall understanding of when an infiltration event from a climate

signal has reached the water table and recharged an aquifer. Such information has great potential in informing sustainable artificial recharge projects or groundwater pumping schedules, both of which require better understanding of water flux behavior from infiltration to recharge (Kuss and Gurdak, 2014).

1.4.2. Vadose Zone Controls in Subsurface Flow Models

Current research-level approaches use large-scale, detailed models and extensive computing resources to simulate the interactions of atmospheric, land surface, and groundwater flow processes. In regional subsurface flow models, approaches for simulating recharge and infiltration include the kinematic wave approximation and the one-dimensional numerical solution of the Richards equation (Bakker and Nieber, 2009; Dickinson et al, 2014). A calibrated, transient saturated groundwater-flow model with the necessary long-term head and discharge measurements can deliver accurate assessments at the watershed-scale (Dickinson et al., 2014).

However, large-scale models rarely represent fluxes through vadose zone directly, due to the complexity of the rates and timing of vertical fluxes. Instead, recharge rates are derived from regional water budgets, time-averaged across temporal discretization of the model and spatially averaged across subregions of the model, with little to no representation of the influence of the vadose zone (Dickinson et al., 2014). Often, there is sparsely available or plainly absent groundwater time series data, severely limiting the use of the model for understanding the role of the vadose zone in influencing atmospheric forcings as time-varying recharge to the saturated zone. In response, recent research has begun to consider the influence of hydraulic diffusivity on the linearized Richards equations and subsequent steady-state and transient-state solutions that represent flow processes in the vadose zone (Bakker et al., 2004; Dickinson et al., 2004; Dickinson and Pool, 2007; Bakker and Nieber, 2009).

Bakker and Nieber (2009) derived an analytical solution to the linearized, transient Richards equation with a surface boundary condition represented by a sinusoidally varying flux. The sinusoidally varying flux was the product of infiltration into and

evaporation out of the soil profile and dampened with depth in the vadose zone such that beyond a certain depth, the flow could be approximated as steady (Bakker and Nieber, 2009). In watershed models, the vadose zone is assumed to dampen water content variations from sequential events of episodic infiltration at the surface. This damping effect is the reason for assigning slowly varying or constant recharge rates to watershed-scale models. Bakker and Nieber (2009) analytical solution for such damping assumed that a level of accuracy could be maintained even when water content variations were small enough that hydraulic diffusivity may be approximated as constant. Expanding on this idea, Dickinson et al. (2014) derived a numerical solution that solved for the damping depth, d_{num} , with the subsurface flow program, HYDRUS 1-D (Simunek et al., 1995). The damping depth is the depth where the ratio of the flux variation at any depth “z” to the flux variation at “z=0” is reasonably equal to 0.05.

1.5. Superposition Approaches

Characterizing the complete input-output parameters of a complex system, such as the vadose zone, requires exhaustive measurement that is usually impossible to achieve. When a system, be it an atmospheric simulation, water budget, or subsurface model, qualifies as a linear system, it is possible to use the responses to a small set of inputs to predict the response to any possible input (Reilly et al., 1984). This can save scientists large amounts of work and water managers valuable time because linearity makes it possible to characterize the system completely. The implications of linearity are far-reaching, and yet, the mathematical definition is simple. A system is linear if the following relationship holds true:

$$\text{if } y_1 = f(x_1) \text{ and } y_2 = f(x_1) \quad \text{eqn. 3}$$

$$\text{then } f(x_1 + x_2) = y_1 + y_2 \quad \text{eqn. 4}$$

where the system responds to a certain input (x_1) with a certain output (y_1) (Tompkins, 1993). The system then responds to another input (x_2) with some other output (y_2) (eqn. 3). The superposition principle states that a linear system will result in a net response

equal to the summation of the two outputs (eqn. 3). Considering that the inputs and outputs may be affected by time, eqns. 2 and 3 can be stated as:

$$\text{if } y_1(t) = f(x_1(t)) \text{ and } y_2(t) = f(x_2(t)) \quad \text{eqn. 5}$$

$$\text{then } f(x_1(t) + x_2(t)) = y_1(t) + y_2(t) \quad \text{eqn. 6}$$

Superposition allows for prediction of system behavior under circumstances that were not actually measured. While linear systems in the natural world may be a rare occurrence, many systems have a range of inputs to which they react linearly, a range that I look to identify in the numerical modeling of damping depths. One of the main objectives of my research is to investigate if the damping in two separate soil textures can be added linearly to accurately estimate damping depth, or if interactions among soils do not behave linearly and make the assumption of linear superposition inaccurate.

1.6. Objectives and Hypothesis

In Dickinson et al. (2014), we are presented with the idea that soil water pressure heads and water contents have an important influence on water flow from infiltration to recharge. Dickinson et al. (2014) showed that the diffusivity in sand and clay caused significant differences in the damping depth of the two homogeneous soils. Using results from hundreds of numerical simulations to understand and model infiltration and water flux through the vadose zone, this study addresses six main questions: (1.1) How does soil texture influence damping in a homogeneous system?, (1.2) What are the effects of layer thickness on damping depth?, (1.3) How do layer interactions influence the damping depth?, (1.4) Is linear superposition accurate in two-layered systems?, (1.5) How does diffusivity influence the damping depth of two-layered systems? and (1.6) What model parameters—hydraulic conductivity (representative of soil texture), period (time), and flux (infiltration) have a statistically significant influence the damping depth? In sum, this thesis quantifies and creates a basis from observed behaviors that arise from differing vadose zone controls for a wide range of fluxes, periods, and soil textures.

2.0 METHODOLOGY

There are various ways to study flux variability in the vadose zone, one of the most effective being computer modeling. Analytical models may be used as a first-step analysis of transient flux in one-layered soils, but numerical models are deemed the more accurate method because they compute a variable diffusivity (Leconte and Brisette, 2001; Dickinson et al., 2014a). Bakker and Nieber (2009) use analytical models that assume a constant diffusivity, where water content variations are considered small enough that hydraulic diffusivity can be approximated as steady (Bakker and Nieber, 2009; Dickinson et al., 2014). Numerical models compute a variable diffusivity based on a nonlinear relation between diffusivity and water content (Dickinson et al., 2014). Numerical models may be used to estimate deep drainage below the root zone or recharge in response to above-surface forcings, like climate variability, with strong reliability (Scanlon et al., 2002; Dickinson et al., 2014a; Velasco et al., 2015). HYDRUS-1D is a numerical modeling computer program that simulates saturated and unsaturated water flux by solving Richards' Equation (Richards, 1931; Radcliffe and Simunek, 2010, eqn.8). I employ the HYDRUS-1D environment to conduct a sensitivity analysis quantifying the damping of a water flux variability in differing homogeneous soil textures, and the damping of flux variations in two-layered systems with a wide range of fluxes, periods and layer combinations.

2.1 Theory

Bakker and Nieber (2009) presented an analytical solution for damping of water flux in the vadose zone that assumes negligible changes in a profile's water content, such that hydraulic diffusivity may be approximated as constant. The analytical solution is based on a linearization of the Richards' equation that sets the vadose zone diffusivity equal to a constant.

In analytical and numerical solutions for periodic groundwater flow conditions, the vadose zone can be constructed as a one-dimensional profile where periodic flow travels

downward vertically along the z-axis. In such systems, flow is governed by the one-dimensional Richards equation:

$$\frac{\partial \theta}{\partial \psi} \frac{\partial \psi}{\partial t} = \frac{\partial}{\partial z} \left(K \frac{\partial \psi}{\partial z} \right) - \frac{\partial K}{\partial z} \quad \text{eqn. 7}$$

where θ (dimensionless) is the water content, Ψ [L] is the pressure head, t [T] is time, and $K(\Psi)$ [L T⁻¹] is the hydraulic conductivity. At the top of the model boundary ($z=0$), we specify a vertical flux, q_z , [L T⁻¹]:

$$q_z(z = 0, t) = q_s + q_p \sin(\omega t) \quad \text{eqn. 8}$$

where the vertical flux, q_z , consists of a steady component q_s [L T⁻¹] plus a sinusoidal component with amplitude q_p [L T⁻¹] over a period P [T] (Figure 1). The term “ ω ” defines the angular frequency, where $\omega = 2\pi/P$. The components of q can represent varying infiltration in basin floors, stream channels, and areas of continued water use, where the steady component, q_s , could represent a long-term average flux and the periodic component, q_p , may represent variations from the steady component.

The magnitudes of q_s and q_p are independent, with the limitation that the amplitude q_p never exceeds the steady component of the flux, q_s (Bakker and Nieber, 2009; Dickinson et al., 2014a). This results in a flux that is always either zero or positive in the downward direction. The range of flux rates chosen thus represent the range of recharge rates inferred at sites across the United States (Sanford and Selnick, 2013; Dickinson et al., 2014; Velasco et al., 2015). Combined, q_s and q_p components can represent the net infiltration below the root zone that results from the infiltration of precipitation, runoff, and the uptake of water by evapotranspiration.

The relation between pressure head and hydraulic conductivity is determined using the Gardner model (Gardner, 1958):

$$K = K_s \exp[\alpha(\psi - \psi_e)] \quad \psi < \psi_e \quad \text{eqn. 9}$$

where K_s [$L\ T^{-1}$] is the hydraulic conductivity at saturation, ψ_e [L] is the air-entry pressure, and α [L^{-1}] is a fitting parameter based on the pore-size distribution. The water content θ is a function of the pressure-head and is approximated with the Gardner-Kozeny model, where n_0 is the porosity (dimensionless) and μ is a fitting parameter [L^{-1}] (Mathias and Butler, 2006):

$$\theta = n_0 \exp[\mu(\psi - \psi_e)] \quad \psi < \psi_e \quad \text{eqn. 10}$$

In the Bakker and Nieber (2009) analytical solution, the vadose zone diffusivity D [$L^2\ T^{-1}$] is set equal to a constant (see Bakker and Nieber, 2009; Dickinson et al., 2014 for full derivation):

$$D = \frac{K}{C} = \frac{K_s}{n_0 \mu} \left(\frac{\theta_{st}}{n_0} \right)^{\frac{\alpha}{\mu-1}} \quad \text{eqn. 11}$$

where C is the water capacity [L^{-1}] and θ_{st} is the water content corresponding to steady flow, q_s :

$$\theta_{st} = n_0 \left(\frac{q_s}{K_s} \right)^{\frac{\mu}{\alpha}} \quad \text{eqn. 12}$$

Building upon the derivations of Bakker and Nieber (2009), Dickinson et al. (2014) created a numerical solution that simulates a variable diffusivity and is considered the more accurate solution. For both the analytical and numerical solutions, the vertical flux (q_z) is represented by a single sinusoidal component that damps to a degree that is a function of q_s , also described as the mean flux at land surface $z = 0$ m (mm/d), period (days), layer thickness (m), soil type (1-12 U.S. Department of Agriculture soil texture classification) and soil hydraulic parameters (K , θ , Ψ , α , ϕ).

2.2. Numerical Modeling Approach

Numerical simulations were used to evaluate the previously stated research questions, including how hydraulic properties of the vadose zone, such as K_h and D_h and properties of the periodic net infiltration flux (q_z) affect the damping depth (z) in

homogeneous and heterogeneous textural profiles of the vadose zone. I use the same approach as Dickinson et al. (2014) and define damping depth as the depth z below which <5% of the surface applied q_z variation is preserved. The HYDRUS-1D computer code (Šimůnek et al., 2008) was used to simulate a variably saturated, one-dimensional vertical flux in the vadose zone profile above the capillary fringe of the water table.

The modeling approach uses a periodic vertical, net infiltration flux (q_z) (eqn. 2) that is defined by a mean downward flux value and dampens with depth in the vadose zone. The q_z is simulated using a single sinusoidal component that damps to a degree that is a function of the mean flux (mm/d) (Table 1), period (days), layer thickness (m), soil (sediment textural) type, and hydraulic parameters (K , θ , Ψ , α , ϕ) of the vadose zone. A range of simulated mean flux values (0.010 to 2.00 mm/d, Table 2) were used to represent long-term (1971–2000) mean net infiltration flux of climate and land-cover regions of the U.S., and were calculated as the difference between mean annual precipitation and mean annual evapotranspiration for the conterminous U.S. reported by Sanford and Selnick (2013).

The mean flux values range from 0.01 mm/d (3.65 mm/year) representative of arid, desert regions to 2.0 mm/d (730 mm/year) representative of humid, marsh regions (Table 3). While mean flux values >2.0 mm/d are possibly in some humid regions, include the Northeast and Pacific Northwest regions of the U.S., mean flux values > 2.0 mm/d resulted in unrealistically deep damping depths and thus are not presented here. The period (days) represent q_z variability on monthly (30-day Period), seasonal (90-day Period), and annual (365-day Period) timescales. In addition, longer periods of 731, 2,556, and 3,652 days (2, 7, and 10 years) simulate q_z variability that is consistent with natural climate variability cycles, including the El Niño/Southern Oscillation (ENSO) that has a 2–7 year quasi-periodic cycle and has been demonstrated to affect recharge rates of the conterminous U.S. (Gurdak et al., 2007; Kuss and Gurdak, 2014a; Velasco et al., 2015).

The vadose zone soil texture and hydraulic properties in HYDRUS-1D were parameterized using the 12 U.S. Department of Agriculture (USDA) soil textural classes

and the Gardner (1958) and Gardner-Kozeny (Mathias and Butler, 2006) soil hydraulic models, except for the saturated hydraulic conductivity (K_s) values that were obtained from the Rosetta soil catalog (Schaap et al., 2001) (Table 4). The Gardner α and Gardner-Kozeny n_0 and μ parameter values were estimated by linear regression as detailed in Dickinson et al. (2014) and Bakker and Nieber (2009).

The numerical simulations were used to evaluate the controls on damping depth in both homogeneous and heterogeneous textural profiles of the vadose zone. Although the vadose zone of most aquifers has heterogeneous, layered soil textures, the simulations of homogeneous profiles allowed for a simplified evaluation of the controls on damping depth and builds on the findings from the simulations of homogeneous sand and clay profiles reported by Dickinson et al. (2014). In this study, the simulations of heterogeneous profiles allow for evaluation of the controls on damping depth in a layered profile as compared to a homogeneous profile, particularly how the transition between the soil layers and superposition processes control the damping depth. The following sections describe this specific model conditions and parameters for simulations of homogeneous and heterogeneous profiles of the vadose zone.

2.3 Flux Variations with Depth in Homogeneous Systems

Flux variation with depth in the soil was examined by simulating one-dimensional downward flow through a homogenous, one-layer soil and using the assumption that flux varies sinusoidally at land surface. In the numerical models, I examined how the flux varied by generating plots of the flux with depth at different times. The profiles were created for all twelve soils (Figure 2) to examine how different characteristics of the flux at the land surface could affect the variability in the profiles. I made profiles for systems where the mean flux, q_s , varied from 0.01 mm/day to 2.0 mm/day and the amplitude of the flux varied from 0.0099 mm/day to 1.98 mm/day and the period of the flux variability ranged from 30 days to 3,652 days (Tables 5-11).

The numerical solution employed HYDRUS-1D to compute the damping depth. A specified flux was defined at the top boundary, considered land surface and free drainage

was defined as the bottom boundary, to simulate deep percolation in a thick vadose zone. The profile is composed of 1,001 nodes whose vertical node spacing is equal and sums up to the specified bottom boundary of the model. To observe the damping depth in homogeneous system, the bottom boundary of the model was extended downward as the infiltration rate increased, as the period increased or as coarser soils were used, to ensure that the damping depth was within the model domain.

The homogeneous simulations used the 12 USDA soil textural classes as defined by the Gardner (1958) and Gardner-Kozeny (Mathias and Butler, 2006) soil models (Table 4). K_s values were obtained from the Rosetta soil catalog (Schaap et al., 2001). The Gardner α and Gardner-Kozeny η_0 and μ parameter values were estimated by linear regression as detailed in Dickinson et al. (2014) and Bakker and Nieber (2009). For site-specific applications, the desired Gardner and Gardner-Kozeny soil properties could be estimated using ROSETTA or the fitting procedure of Wraith and Or (1998), though that is out of the scope of this research. The set of homogeneous simulations with varying periods, fluxes, and soil textural classes resulted in a catalog of damping depths that would be used to predict the ideal bottom boundaries in the two-layered system.

2.4. Flux Variations with Depth in Two-Layered Systems

The general modeling approach for the two-layered system used a 90-day period with a 1 mm/day infiltration rate for any two soil combinations of four selected reference soils (clay, silt, loam and loamy sand) that represent the edges and center of the USDA soil texture triangle (Figure 2). Similar to the homogeneous simulations, the profile was composed of 1,001 nodes whose vertical node spacing is equal and sums up to the specified bottom boundary of the model. To investigate the damping depth in two-layer systems, the total vertical length of the model was set to a depth of 10 m for any two-soil combination of clay, silt or loam. Simulations with loamy sand had a bottom boundary of 50 m due a deeper homogeneous damping depth of ~ 30 m.

In addition to the depth of damping in two-layered systems, I examined how the water flux was influenced by varying the layer soil thickness. Recall that the hydraulic

diffusivity describes the nonlinear relationships between water capacity (C), and hydraulic diffusivity (D). By observing the mean change in diffusivity between the upper and lower soil layer, I observed the effects of layering on flux variability and damping depths.

First, I created ten two-layer profiles composed of either clay, silt, loam or loamy sand. Six of the two-layered systems had a bottom boundary of $z = 10$ m, and four profiles had a bottom boundary of $z = 50$ m. In the two-layered profile, the thickness of the upper layer is set to be a quarter fraction ($\frac{1}{4}$, $\frac{1}{2}$, or $\frac{3}{4}$) of the damping depth (d_{num}) of the upper layer's homogeneous damping depth. This results in a set of three possible upper layer thicknesses per two-layered profile (Figure 3). Once the upper layer thickness is set, the lower layer makes up the rest model domain. Using the same input parameters as the homogeneous simulations, the two-layered model simulates a vertical water flux (q_z) traveling from the upper layer to the lower layer, resulting in a unique damping depth. I later explore whether such two-layered systems could be represented by one-layer linearity.

Example System of Layer Thickness

Suppose that for a homogenous system of silt with a $q_z = 1.0 \times 10^{-3}$ m/d and $P = 90$ d, the resulting damping depth (d_{num}) is $z = 6.4$ m (Figure 4a). Therefore, any of the 10 two-layered systems with silt as the upper layer will have an intermediate thickness of 3.2 m, which is defined as $\frac{1}{2} d_{num}$ ($z = 6.4$ m) (Figure 4b). The corresponding thin ($\frac{1}{4}d_{num}$) and thick ($\frac{3}{4}d_{num}$) upper layer thickness for silt in the two-layered systems are 1.6 and 4.8 m, respectively. In this example of $\frac{1}{2}d_{num}$ for an upper layer composed of silt, the lower layer is clay and has a thickness of 6.8 m ($10 \text{ m} - 3.2 \text{ m}$).

2.5 Testing for Linearity in Damping

The objective of the linear superposition tests is twofold. First, I evaluate whether the damping depths are influenced by varying the upper layer thickness (i.e., thin ($\frac{1}{4}d_{num}$), intermediate ($\frac{1}{2}d_{num}$), and thick ($\frac{3}{4}d_{num}$) upper layers). Second, I compared and quantify the differences in damping depths between two-layered systems and homogeneous systems with revised amplitudes. A homogeneous system with a revised amplitude is a

discontinuous system of two homogeneous simulations added together, with the q_a at the end of the upper layer thickness should equal the q_a at the bottom of the upper layer.

Knowing the parameters and thickness, I ran a separate bottom layer simulation with the same input parameters. At the bottom of the upper layer, a separate soil, is added (Figure 4c, 5a). The emplaced soil can be substituted into the system because it shares the same q_s component as the upper layer as well as the flux amplitude at the bottom of the upper layer (Figure 5a). This layer substitution method aims to answer the question of how layer thickness influences the propagation of the mean infiltration flux and ultimately, the damping depth.

The amplitude component (q_a) of the homogeneous and two-layered systems is set at a value this is 99% of the steady component of the flux, q_s . However, the depth at which a soil has been emplaced has a q_s value that is smaller, from that which began at land surface, where the flux variation (q_s) was 100%. From the emplaced soil then, we take the damping depth as being the value where the flux variability relative to the inherently smaller q_s of the emplaced soil, is 5% of the land variation (Figure 5b). This q_s is considered the vertical extension in meters, that the flux variability was preserved to before damping. This q_s is summed to the fraction mark of the upper layer, to find the revised system damping depth.

$$\begin{aligned}
 &= \text{upper layer } (\frac{1}{4}, \frac{1}{2}, \frac{3}{4} * d_{num}) + \text{bottom layer with, revised amplitude } (d_{num}) \\
 &= \text{revised system damping depth}
 \end{aligned}
 \tag{eqn. 13}$$

If the net sum of the separate responses of the upper layer and the lower layer is equal or within 10% of the two-layered system, then this may be considered a possible case of linear superposition. Systems may indicate linear superposition if the sum damping depth from the additive responses varies from the two-layered system by no more than a 10% difference.

Example System for Testing of Linearity of Damping

Suppose the model setup for testing of linearity is initially similar to the previous example system of layer thickness, where an upper silt layer and lower clay layer were simulated as a two-layered system with an initial infiltration mean flux of 1.0×10^{-3} m/d and $P = 90$ days. To test for the possibility of linear superposition, I revise the initial amplitude for a separate homogeneous model run of the bottom layer. First, I use the upper layer's q_a (i.e., thin ($\frac{1}{4}d_{num}$), intermediate ($\frac{1}{2}d_{num}$), and thick ($\frac{3}{4}d_{num}$) upper layers), to define the q_a of the lower layer, in this case, a q_a at a depth of 3.2 m ($\frac{1}{2}d_{num}$). I characterize this as a homogeneous clay model run with a revised amplitude. This revision represents the flux amplitude at the bottom of the upper silt layer in a two-layered profile. The total d_{num} of the homogeneous system with the revised amplitude is the sum of the resulting damping depth from the bottom layer clay system with the revised amplitude and the thickness ($\frac{1}{2}d_{num}$) of the upper silt layer. I use the same procedure for the thin layer ($\frac{1}{4}d_{num}$) and the thick layer ($\frac{3}{4}d_{num}$) variations of the upper layer of silt and lower layer of clay.

The resulting d_{num} from the amplitude-driven system are compared to the d_{num} from the continuous two-layered systems. The purpose of this comparison is to identify systems where linear superposition (linear sums of the amplitude-driven system) is a reasonable assumption. To quantify the comparison, I solve for the percent difference between the d_{num} from the amplitude-driven system and the d_{num} from the continuous two-layered systems:

$$\frac{\text{Homogeneous with revised amplitude } d_{num} - \text{Two layered } d_{num}}{\text{Two layered } D_{num}} * 100\% = \text{Percent difference} \quad \text{eqn. 14}$$

where percent difference of less than $\pm 10\%$ indicates the possibility of linear superposition. If the percent difference between damping depths is 10% or less, then there is indication that the damping of the water flux in a layered system is largely driven by the upper layer, with little to no effect on damping by the bottom layer. Cases of linear

superposition provide evidence that a simple, homogeneous model can be used to reasonably simulate damping depths in a more complex, two-layered system. Comparisons with percent differences $> 10\%$ indicate inaccurate linear superposition where:

$$\begin{aligned} & (+) \text{ Difference: } (> 10\%) \text{ indicates deeper damping;} \\ & \text{Homogeneous with revised amplitude } d_{num} > \text{Two-layered } d_{num} \quad \text{eqn. 15} \end{aligned}$$

$$\begin{aligned} & (-) \text{ Difference: } (< 10\%) \text{ indicates shallower damping;} \\ & \text{Homogeneous with revised amplitude } d_{num} < \text{Two-layered } d_{num} \quad \text{eqn. 16} \end{aligned}$$

For example, in a test for possible linear superposition, the homogeneous system with the revised amplitude results in a linearly summed damping depth of 5.8 m:

$$\begin{aligned} & \text{top soil (Fraction of } d_{num}) + \text{bottom soil (} d_{num}, \text{ revised amplitude)} \quad \text{eqn. 17} \\ & = \text{revised damping depth} \end{aligned}$$

It follows that the damping depth in a silt layer for this scenario occurs at $d_{num} = 6.4$ m. I am interested in understanding how the flux variability dampens with a silt layer thickness of half that depth. I calculate $\frac{1}{2} d_{num}$, or $z = 3.2$ m ($\frac{1}{2} * d_{num}$ of silt layer), then find the amplitude at that depth and obtain a new d_{num} , of 2.6 m (d_{num} of silt with revised amplitude). I plug these values into equation 17:

$$\begin{aligned} & = 3.2 \text{ m } (\frac{1}{2} * d_{num} \text{ of silt layer}) + \quad \text{eqn. 18} \\ & 2.6 \text{ m } (d_{num} \text{ of silt with revised amplitude)} \\ & = 5.1 \text{ m } (\text{depth of new system}) \end{aligned}$$

Plugging these values in eqn. 13 results in:

$$\frac{5.8 \text{ m} - 5.1 \text{ m}}{5.1 \text{ m}} * 100\% = (+) 13\% \text{ Difference} \quad \text{eqn. 19}$$

where a 13% difference indicates a system of over-prediction (>10%) and the assumption of linear superposition is inaccurate.

2.6 Nonparametric Testing

The goal of nonparametric testing was to identify the sensitivity of the damping depth to three factors: hydraulic conductivity (representative of the soil properties of vadose zone sediments), mean infiltration flux, and period (time).

I used the False Discovery Rate (FDR) technique as described in Benjamini and Hochberg (1995) to conduct the nonparametric factor test. The FDR p-value adjustment is an efficient technique to control for the rate of false positives among a large number test. The FDR p-values ($p_{(i), FDR}$) are computed as:

$$p_{(i), FDR} = \text{Minimum} [p(i + 1, FDR), (m/i)p(i)] \quad \text{eqn. 20}$$

Such that the independently calculated p-values have an FDR adjusted p-value that falls below α , then the parameter shows that the data is statistically significant at the 0.05 level (Benjamini and Hochberg, 1995). To provide an appropriate scale for visualization, I used the FDR LogWorth transformation, where:

$$\begin{aligned} -\log_{10}(FDR P - Value) &= 1.3 \\ \log_{10}(0.05) &= 1.3 \end{aligned} \quad \text{eqn. 21}$$

If the FDR LogWorth values exceed 1.3, it is an indication that the effects are significant at the 0.05 level. With this transformation, we can attempt to reject the null hypothesis that the flux, period and parameters do not influence the damping depth. In addition to the FDR LogWorth values, I present their respective R^2 value, the coefficient of determination that measures the proportion of variation accounted for by the model simulation and describes how well the regression line approximates the real data points. The sensitivity of each factor was quantified using nonparametric testing because the data was not normally distributed and did not have equal variances (Helsel and Hirsch, 1992).

3.0. RESULTS OF SINUSOIDAL FLUX VARIATIONS WITH DEPTH

The results are organized in two parts. First, I present the model results of climate variability signal damping in the subsurface. Second, I discuss the influence of soil texture, time period, and flux variation on infiltration events in the vadose zone with the use of statistical tools.

I ran 588 simulations in homogeneous systems with seven periods and seven mean flux values to observe how the damping depth varied with varying soil textures and parameters. Figure 6 and 7 illustrate the importance of soil texture and associated hydraulic properties in controlling the characteristics of the flux amplitude profiles and damping depths. The simulated damping depth (d_{num}) was unique for each homogeneous system and behaved differently for each of the 12 soil textures. For all simulations, the variability of the flux reached deeper damping depths with greater periods and larger fluxes (Figure 6).

Simulations are the result of unique combinations of q_z and P inputs, with damping depths ranging from $z = 0.1$ m to $z = 100,000$ m. Overall, flux variations were preserved at greater depths with increasing q_z and P , as shown in Dickinson et al. (2014). Also shown is a trend of shallower damping depths with a decrease in either or both, q_z and P . Though some damping depths are $> 1,000$ m, the discussions will focus on damping depths $< 1,000$ m because the main interest lies in understanding how the behavior of flux variations arise from vadose zone controls and how the behavior varies with differing vadose zone controls at real-world depths.

3.1. How Does Soil Texture Influence Damping in a Homogeneous System?

To illustrate how soil texture influence damping depth, consider the results for a 1.0 mm/day water flux and 90-day period for each of the 12 soils textures (Figure 7). For this scenario, damping depths ranged from 4 m in silty clay loam to 76 m in sand. In addition to sand, the damping depths in the other coarser-grained textures (sandy loam and loamy sand) were greater than then damping depths of the finer-grained soil textures. The

damping depth was 14 m in sandy loam and 30 m in loamy sand, while the damping depths ranged from 4 to 9 m for other relatively finer-grained soil textures (Figure 7). Overall, the damping depths are relatively greater in coarser-grained soils, like sandy loam, loamy sand and sand, than finer-grained soils (Figures 6, 7). To illustrate the differences, I describe an example differentiating a finer-grained soil, clay, and a coarser-grained soil, loamy sand.

Clay and Loamy Sand Profiles

The flux (q_z), hydraulic conductivity (K), initial pressure head condition (ψ), water content (θ) and diffusivity (D) profiles from water flux simulations in soil profiles composed of clay and loamy sand were compared at times P (Figure 8). While the pattern and damping of the q_z , the K , and the D variability begins similarly at $z = 0$, the difference in damping of the flux variation of the two soils differs with increasing depth. The profiles include symmetrical and asymmetrical patterns around the steady values below approximately 6 m for clay and 30 m for loamy sand.

The profile of the flux variability with depth is smaller in the homogeneous clay than in the homogeneous loamy sand (Figure 8). The hydraulic conductivity, initial pressure head condition, water content variations and diffusivity profiles are also smaller in the clay than the loamy sand (Figure 8b-d). While the mean water content value was greater in clay than loamy sand for all depths, θ in both soils was skewed towards lower water contents near the land surface (Figure 8d). For all systems, the water content decreased more during low flux than it increased during high flux at any given depth, in agreement with Dickinson et al. (2014). This skew toward lower water contents affects the time-averaged diffusivity. Although both soils tended towards lower water contents and began with similar flux and K values near land surface, the difference in their respective soil parameters becomes stark with increasing depth. The variability in K occurs a function of ψ (Gardner, 1958), and is significantly diminished by a depth of ~ 6 m in the clay profile, whereas the loamy sand profile allows for a great variation in K that extends deeper into the profile until $z = 30$ m (Figure 8b).

In addition to the influence of K on the damping of the flux, the water capacity (eqn.10), which is equal to the $d\theta/d\psi$ from the Gardner-Kozeny model (Mathias and Butler, 2006) can dampen or preserve the flux. From the equation for water capacity (eqn.6) and its relevance in the equation for diffusivity (eqn.5), it is evident that the porosity (n_0) and water content (θ) can also influence flux variability. The clay profile has a greater n_0 , a greater mean θ (Figure 8b) and tends towards being under more negative ψ , indicating a higher soil tension (Figure 8c). The loamy sand has a relatively lower n_0 , a smaller mean θ (Figure 8b) and tends towards being under less negative ψ , indicating a lower soil tension (Figure 8c).

The combined effect of the hydraulic properties shown in Figure 8a-e allows the flux variability to persist with depth in the loamy sand compared to the clay. Despite an equal period and similar flux applied at land surface, the greater and more highly variable hydraulic conductivity of the coarser-grained loamy sand, coupled with its weaker soil tension, and less negative pressure head, allow water pulses to continue to flow downward despite the retention of water in the soil-water-air interface, resulting in deeper damping depths. In comparison, clay has greater soil tension (figure 8c) and lower permeability. This, coupled with a lower hydraulic conductivity, allows the clay to store more water, reducing the variability of the flux, causing the flux variation to damp at a shallower depth than the same flux variation in the loamy sand (Figure 8a). All of this can be explained by the diffusivity of the clay compared to the loamy sand.

The diffusivity envelope of the loamy sand is much greater than the clay and preserves the flux amplitude deeper into the profile, for greater damping depths (Figure 8e). The damping depth in the loamy sand is ~30 m, which is five times greater than the damping depth in clay (5.5 m) (Table 6). Of the 12 soils, the coarser-grained soils, sandy loam, loamy sand, and sand have greater hydraulic conductivities, weaker soil tension, a lower range of θ values, and a larger diffusivity envelope, resulting in much deeper damping depths relative to the finer-grained soils (Figure 7, Figure 9). Additionally, while damping occurs at deeper depths over greater fluxes or periods, the damping depths in coarser-grained soils differ more and more by orders of magnitude as the flux or period

increases. Figures 9, 10, and 11 illustrates this pattern for all 12 soils over a range of periods, from 30 days to 10 years (3,652 days), for three infiltration fluxes (0.1, 1.0, and 2.0 mm/day).

Figure 9 illustrates the damping depths in 12 soil textures, for a mean flux of 0.1 mm/day and seven periods: a 30-d, 90-d, 180-d, 365-d, 731-d, 2,557-d and a 3,652-d period. The damping depths in the coarser-grained soils (sandy loam, loamy sand, sand) vary at greater depths by three to four orders of magnitude, while damping depths in the finer-grained soils (silty clay loam, silty clay, silt loam) are closer to land surface and vary by less than one order of magnitude (Figure 9). There is also relatively greater variability in damping depths values among the soil textures for the longer periods (731 to 3,652 days), and relatively less variability in damping depths among the soil textures for the shorter periods (30 to 365 days). The deepest damping depths relative to the period, are greater for the sand, loamy sand, and sandy loam, than for the finer-grained soil textures (Figures 10, 11). For longer periods (731 to 3,652 days), damping depths in sand, loamy sand, and sandy loam are an order of magnitude greater than damping depths in the other soil textures.

For example, a simulation with a 3,652-d period and an applied mean infiltration flux of 0.1 mm/day, resulted in a damping depth of 2,502 m for sand, but at a relatively shallower depth of 169 m in clay (Figure 9, Table 11). The damping depth difference between the coarser-grained soils (sandy loam, loamy sand, sand) and the finer-grained soils becomes even more pronounced at longer periods for greater mean fluxes (Figure 10, 11). For example, the 1.0 mm/day mean flux with a 3,652-day period results in a damping depth of 40,000 m for sand, but 1,570 m in clay (Figure 11). This is strong evidence to suggest important differences in damping depth as a function of increasing mean flux, particularly for the shorter periods.

For a simulation with a mean flux of 0.01 mm/day run in separate homogeneous clay, silt, loam and loamy sand profiles, the damping depths over the 30-day, 90-day, 180-day, 365-day and 731-day periods were within an order of magnitude from each other (Figure 12a, 12b). For a simulation with a mean flux of 0.1 mm/day run in separate

homogeneous clay, silt, loam and loamy sand profiles, the damping depths over the 30-day, 90-day, 180-day, 365-day and 731-day periods were also within an order of magnitude from each other (Figure 12b). However, the damping depth in the loamy sand is noticeably different by the 365-day and 731-day period.

For a simulation with a mean flux of 1.0 mm/day, the damping depths at the 30-day, 90-day, and 180-day period mark were within an order of magnitude of each other (Figure 13a). For a simulation with a mean flux of 2.0 mm/day, the damping depths at the 30-day, 90-day, and 180-day period mark were within an order of magnitude of each other (Figure 13b). Overall, there was a greater difference in damping depths for the 365-day and 731-day periods at the larger mean fluxes (1.0 and 2.0 mm/day) (Figure 13a, 13b). In particular, the damping depth in loamy sand was about an order of magnitude greater than in other soil textures at the 365-day and 731-day period mark for greater mean fluxes (Figure 13a, 13b).

Damping depths as a function of soil texture for a q_z of 2.0 mm/day, show a highly nonlinear and possibly exponential relationship between the soil texture and period (Figure 13b). At a q_z of 2.0 mm/day, there is considerably more difference in damping depths among the soil textures for the shortest periods. For example, the damping depth in a sand with a mean infiltration flux of 2.0 mm/day and a 30-day period is 23 m, while the damping depths in finer-grained soils are an order of magnitude lower, ~2 to 5 m, in the other eleven textures (Figure 11, Table 5). The difference in damping depths between the coarser- and finer-grained soil textures is more pronounced at longer periods. At a period of 731 days, the three coarsest soils are at least an order of magnitude deeper than the finer-grained soils, with d_{num} at 713 m (sandy loam), 2091 m (loamy sand), and 2,965 m (sand) (Figure 11, Table 9).

While the comparison of damping depths at mean fluxes greater than 2.00 mm/day is possible, large fluxes over annual and decadal time periods result in damping depths of thousands if not tens of thousands of meters in homogeneous profiles. Damping depths in sand layers with a $q_s = 1.0$ mm/day and a 3,652-day (10-year P) period have damping depths at 40,000 m (Figure 10), while a $q_s = 2.0$ mm/day and a $P = 3,652$ day have

100,000 m damping depth (Figure 11), which is not at all a realistic model of natural systems or adequate simulation of infiltration events employed here, which already take into account the loss of water to evapotranspiration (Sanford and Selnick, 2013; Velasco et al., 2015).

To put it in perspective, back-calculating the amount of precipitation from an infiltration flux of 2.0 mm/day, for a climate described by Sanford and Selnick (2013) as high rainfall with moderate temperatures, and an evapotranspiration rate of at least 50% (double the infiltration), calculates to ~1,830 mm/yr of precipitation, a high rate of precipitation. For comparison, the average annual rainfall of one of the wettest states in the United States, Georgia, for the third wettest year on record showed an annual rainfall of ~1,650 mm for 2013 (Southeast Regional Climate Center, 2014). Thus, a mean flux of 2.00 mm/day represents the upper limit of infiltration, one that varies sinusoidally between 0.001 mm/day and 4 mm/day for a mean flux of 2 mm/day.

3.2. Effects of Varying Layer Thickness on Damping Depth

Using the four soil textures, a mean flux of 1.0 mm/day, 3 periods (30, 90, and 365 days), I created 30, two-layered profiles with an upper layer that had a thickness equivalent to $\frac{1}{4}$ (thin), $\frac{1}{2}$ (intermediate), $\frac{3}{4}$ (thick) of its homogeneous damping depth.

Clay as the upper layer

For all profiles involving clay as the upper layer, the two-layered simulations result in greater damping depths than the homogeneous clay profile (Figure 14). Two-layer profiles with clay overlying silt or loam, for any period of 30 days, 90 days, and 365 days, were within 50% of clay's original damping depth (Figure 14, Table 12). Outputs from two-layer profiles where loamy sand was the lower layer, had damping depth differences of 100-200% over a period of 30 days, and 200-500% over a period of 90 days and 365 days (Table 13, 14).

The lower layer affects the damping depth, particularly where the lower layer is made up of a coarser soil. Here, a thinning clay layer over a thickening silt, loam, or

loamy sand layer consistently resulted in a greater difference between the two-layered d_{num} and the homogeneous d_{num} .

Silt as the upper layer

For profiles where silt was the upper layer overlying clay or loam, a pattern of increasing or decreasing percent differences from the homogeneous case was minimal (Figure 15). Comparison of damping depths between the homogeneous silt layer and the two-layered cases showed a negative percent difference for systems where silt overlay loam, indicating a shallower damping depth than the homogeneous system. The difference between values began at +5% where a relatively “thick” silt layer was present, and decreased negatively with a decreasing silt layer thickness to ~ - 20 to 40%, implying that the damping depth in the two-layer system was shallower than the homogeneous silt layer (Tables 15-17). There is a negative increase in percent change, from a thick layer of silt to a thinner layer. Over a 365-day period, the percent difference ranged from 20 to 30%, and stayed within that range with varying layer thickness (Table 17).

Loam as the upper layer

For all profiles involving loam as the upper layer, the two-layered simulations result in greater damping depths than the homogeneous loam profile (Figure 16). Two-layer profiles with loam overlying clay or silt, for any period of 30 days, 90 days, and 365 days, were within + or - 33% of loam’s original damping depth (Tables 18-20). The two-layer profiles where loamy sand was the lower layer had damping depth differences of 100-175% for a period of 30 days, 150-360% for a period of 90 days and 236-487% change for a period of 365 days. Observing the influence of the lower layer on the damping depth, a relatively thinner loam layer overlying a thicker clay, silt, or loamy sand layer consistently resulted in an increase in percent difference between the two-layered d_{num} and the homogeneous d_{num} .

Loamy Sand as the upper layer

For all profiles involving loamy sand as the upper layer, the two-layered simulations resulted in shallower damping depths than the homogeneous loamy sand profile (Figure

17). Two-layer profiles with loamy sand overlying clay or loam for a 30-day period, decreased in percent difference from a -15% at the thickest possible loamy sand, towards a -50% difference, indicating a shallower damping depth than the ~30 m depth of a loamy sand profile (Tables 21-23). Profiles showed similar pattern at 90 days, where the decrease occurred from -20% to -65%. Profiles of loamy sand overlaying clay or overlaying loam, at 365 days began with a positive percent difference of ~15% at a “thick” loamy sand upper layer, but decreased significantly towards -50% as the period increased. Overall, a relatively thinner loamy sand results in a shallower damping depth, regardless of soil type or period (Figure 18).

Figure 18 compares the damping depths from the two-layered simulations of varying layer thickness with the damping depths from the homogeneous simulations. The percent difference is not substantially affected by changes in the upper layer thickness for eight of the ten cases over a 30-day, 90-day and 365-day period. The two cases that show a significant percent difference damping depth as a result of a varying layer thickness both have loamy sand as the lower layer. To reiterate, where loamy sand was the lower layer, the damping depth in the two-layered system was deeper by a positive percent change of ~100% to ~500%. No other lower layer had such a pronounced effect on increasing the damping depth (deeper damping depth) between the two-layered and homogeneous simulations. Additionally, profiles with loamy sand as the upper layer also resulted in large percent differences, but all between -25% and -50%, indicating decreases in damping depth (shallower damping). For all two-layered simulations, if the lower layer is composed of sand, the flux variability will be maintained for greater depths, especially as the upper layer decreases in thickness.

3.3. Does the interaction of soil layers influence the damping of variable water flux?

I am also interested in understanding whether the damping depth in a two-layered system can be obtained by approximating the layered system as two superimposed one-layered systems. To quantify how layer interactions influence the damping depth, I consider a change of more than +10% in compared damping to be a significant influence

(eqn.14). Any negative percent changes are considered underestimates and indicative of shallower damping, which may also create the possibility of linear superposition. The detailed objective was to explore which layer interactions caused minimal and pronounced changes in damping depths. The aim was to examine how the interaction and changes in soil parameters like pressure head (ψ), water content (θ) and diffusivity (D) from the upper layer to the bottom layer is linked to damping of flux variability.

For a 30-day period with an applied flux variation of 1.0 mm/day

The results of the damping depths from the two-layered simulations compared to the homogeneous simulations using a 30-day period are shown in Tables 24-27. A positive percent change indicated an increase in damping depth (deeper damping depth), while a negative percent change indicated a decrease in damping depth (shallower damping depth). Of the 30 two-layered profiles, 15 profiles had 20% or less change in damping depth between the two- and one-layered simulations. Of the 15 profiles with changes in damping depth $>20\%$, nine had a change in damping depth ranging from 25 to 49%, and six had a change in damping depth $>100\%$, all indicating deeper damping depths (Tables 24-27). Regardless of upper layer soil texture or thickness, a bottom layer made of loamy sand resulted in damping depths that were 100% deeper than their homogeneous counterparts.

For a 90-day period with an applied flux variation of 1.0 mm/day,

The results of the damping depths from the two-layered simulations compared to the homogeneous simulations using a 90-day period are shown in Tables 28-31. Of the 30 profiles, 9 profiles had 20% or less change in damping depth between the two- and one-layered simulations. Of the 21 profiles with changes in damping depth $>20\%$, 15 had a change in damping depth ranging from 21 to 64% (Tables 28-31). Similar to the 30-day period dataset, six of the 30 profiles exhibited changes $>100\%$. All changes were significantly greater (158–474%) where loamy sand was the bottom layer, resulting in damping depths that were 100% deeper than their homogeneous counterparts.

For a 365-day period with an applied flux variation of 1.0 mm/day,

The results of the damping depths from the two-layered simulations compared to the homogeneous, one-layered simulations using a 365--day period are shown in Tables 32-35. Of the thirty profiles, three profiles exhibited differences of -52%, indicating a curious underestimate, while ten profiles exhibited differences of 23 to 27% from the upper layer's homogeneous system. Consistent with the 30-day, and 90-day period datasets, six of the thirty profiles exhibited changes of more than 100%. These changes showed differences of 215-487% from the respective upper layer's homogeneous damping depth, and were present when loamy sand was the lower layer, regardless of upper layer texture or layer thickness.

3.4. Is linear superposition accurate in two-layered systems?

The next step was to quantify the percent difference of damping depths from two-layered systems with damping depths of homogeneous systems with revised amplitudes. The objective here was to look for cases of linear superposition. To restate the case of linear superposition—the goal is to identify cases where the net sum of damping in the upper layer and bottom layer add up to a damping depth that is within 10% of the damping depth in the two-layered system. If so, then the small percent difference between the two-layered system and the homogeneous system with the revised amplitude is considered a case of accurate linear superposition. If not, then the goal is to understand why by looking at the soil hydraulic parameter plots of the respective simulations.

Clay as the upper layer

For profiles involving clay as the upper layer, the two-layered simulations resulted in slightly deeper damping depths than the simulations with the revised bottom layer for all systems except clay over silt and clay over loam over a period of 365-d (Table 32), which showed a +4% and +1% difference. The percent difference between both systems was less than +/- 10% when clay overlay silt or loam (Figure 19a, 19b, 19c). The percent difference was more pronounced when loamy sand was a lower layer. The percent change for a clay underlain by loamy sand changed from -28% (thick layer) to -6% (thin layer)

for a 30-day period, -31 to -9% for a 90-day period, and -49% to -30% for a 365-day period (Table 32). For all three periods (Table 24, 28 32), there was no apparent pattern of influence of layer thickness. However, there was a general pattern with lower layer type, where the coarser lower layer resulted in a greater percent change between the two systems.

Silt as the upper layer

Figure 19 shows that for all but three profiles involving loam as the upper layer, the two-layered simulations resulted in shallower damping depths than the simulations with the added bottom layer (positive percent change). The percent difference between both the two-layered system and homogeneous system with the revised amplitude, ranged from -10% to +22%, with the majority of the values tending towards 0% difference (Tables 25, 29, 33). Layer thickness does not seem to be an influential factor of the damping depth. Interestingly, the smallest percent differences (and therefore the most accurate) between the two-layered system and the homogeneous system with the revised amplitude occur at greater time periods.

Loam as the upper layer

Figure 19 shows that for all profiles involving loam as the upper layer, the two-layered simulations resulted in greater damping depths than the simulations with the added bottom layer (all negative percent differences, Tables 26, 30, 34). The percent difference between both systems was less than +/- 10% for all profiles where clay or silt were the lower layer, regardless of varying layer thickness. The percent difference was more pronounced when loamy sand was a lower layer. The percent change for a loam underlain by loamy sand moved from -28% to -6% for a 30-day period (Table 26), -33 to -10% for a 90-day period (Table 30) and -50% to -30% for a 365-day period (Table 34). For all three periods, there seemed to be no pattern of influence of layer thickness, but rather a pattern of lower layer type, where the coarser lower layer led to a greater percent change between the two systems.

Loamy Sand as the upper layer

Figure 19 shows that for all profiles involving loamy sand as the upper layer, the difference in damping depth between the two-layered simulations and the simulations with the revised homogeneous bottom layer ranged from -5% to +11% (Table 27). There was no discernible influence of layer thickness and a small influence by period, where the 30-d period profiles (Table 27) show the relatively greatest percent changes, and the 90-d period profiles (Table 31) shows the least, at 0%. The percent change for a loamy sand underlain by loam showed greater changes in damping depth than profiles underlain by clay.

For example, the percent difference when loam was the lower layer, for all periods, ranges from 0% to 11%, and identified in the 30-d period (Table 24), while the percent differences when clay was the lower layer, ranged from -5% to 6%, and was also identified in the 30-d period (Table 24). For all three periods, there seemed to be no pattern of influence of layer thickness, but rather a pattern of lower layer type, where the coarser lower layer of loam resulted in all positive percent differences across time, indicating that the system with the added bottom layer. Overall, as the period increases from 30 days to 90 days to 365 days, the percent difference between the two-layer d_{num} and one-layer amplitude addition, d_{sum} decreases for two-layer systems that had a percent difference of 20% and increases for systems that had a percent difference of more than 30%.

3.5. Diffusivity and Damping Depth

For all fluxes and periods tested, coarser-grained soils cause deeper damping depths for all fluxes and all periods. For two-layered systems, coarser-grained soils are most influential on the damping depth when they are set as the lower layer (Figure 20a-e). A coarser-grained soil, like loamy sand, has a greater hydraulic conductivity, is under lower soil tension, has a relatively small water content and a large and highly variable diffusivity. A finer-grained soil, like clay, has a lower hydraulic conductivity, is under higher soil tension, has a larger water content and a smaller diffusivity envelope. When a

clay layer overlies a loamy sand in a two-layered system, the influence of the coarser-grained soil is noticeable.

Clay Overlying Loamy Sand

A two-layer model of clay over loamy sand, in a 50-meter profile, for a mean flux applied at land surface of 1.0 mm/d and a 90-day period shows a sharp enlargement of the flux envelope at the ~ 3 m layer transition (Figure 20a). At this depth, the hydraulic conductivity also increases in a step-wise manner, indicating the transition from the finer-grained clay to the coarser-grained loamy sand (Figure 20b). Figure 20c shows the pressure head changing from a more negative ψ (higher soil tension) in the finer-grained upper soil to a less negative ψ in the coarser-grained loamy sand. Water flows downward from high soil tension, where water is held more tightly (more negative pressure head) to lower soil tension, where water is held less tightly (less negative pressure head, closer to zero). There is an overall decrease in water content from the upper layer to the lower layer (Figure 20d).

The diffusivity envelope of the homogeneous loamy sand is larger and wider than the homogeneous clay, indicating that the flux variation is preserved with increasing depth, encouraging damping at deeper depths (Figure 20e). If the diffusivity envelope of one soil is larger than the soil with which it is paired, then the soil with the larger diffusivity will be the primary influencer of the damping depth (Dickinson et al., 2014). In figure 20, the mean diffusivity of both soils is very similar, with the sinusoidal component of the flux transitioning from a mean diffusivity of ~ 0.005 m²/day to a lower layer diffusivity of ~ 0.005 m²/day (Figure 20e). Though the mean diffusivity values are similar, the diffusivity envelope of the loamy sand is much larger, wider and persists deeper into the profile than that of clay. Thus, once the flux has permeated the coarser-grained loamy sand, the larger diffusivity envelope of the loamy sand will preserve more of the flux variability with depth, allowing it to dampen a depth of ~ 21 m, a +268% change from the homogeneous upper soil case of ~ 6 m. This case serves as evidence for the positive influence of loamy sand on the damping depth. The next section examines whether this is the case when loamy sand is the upper layer.

Loamy Sand Overlying Clay

A two-layer model of loamy sand over clay, in a 50-meter profile, for a mean flux applied at land surface of 1.0 mm/d and a 90-day period shows a sharp reduction in the flux variability at a depth of ~15 m (Figure 21a). At this depth of 15 m, the hydraulic conductivity decreases in a step-wise manner, indicating the transition from the coarser-grained loamy sand to the finer-grained clay (Figure 21b). Figure 21c shows a change in pressure head (ψ), migrating from a place of lower (less negative ψ) soil tension, a characteristic of clay, towards higher soil tension (more negative ψ) in the coarser-grained loamy sand. As a result, the water content of the profile increases from ~0.05, where water is held less tightly (due to less negative ψ) to ~0.10, where water is held more tightly (more negative pressure head) to lower soil tension, where water is held less tightly (less negative pressure head, closer to 0) as it travels downward (Figure 21d).

In this profile, the mean diffusivity of both soils is very similar. Thus, the sinusoidal component of the flux transitions from a mean diffusivity of ~0.005 m²/day to a lower layer diffusivity of ~0.005 m²/day (Figure 21e). Though the mean diffusivity values are similar, the diffusivity envelope of the clay layer is much smaller, narrower and does not persist as deeply with depth as the homogeneous profile of the loamy sand. Thus, once the flux has permeated the finer-grained clay layer, the smaller diffusivity envelope of the clay will filter out the flux variability at a shallower depth, allowing it to dampen a depth of ~17 m, a -30% change from the simulation in a homogeneous loamy sand layer of ~21 m. This case serves as evidence of the influence that a finer-grained soil can have on the damping depth when its smaller diffusivity envelope causes a sharp reduction in the flux variation in the lower layer of a two-layered system.

3.6. Using Statistical Tools to Understand Parameter Influence

The FDR LogWorth nonparametric test showed that all parameters are statistically significant influencers of the damping depth at an alpha-level of 0.05 (Table 36). These P-values compared to an $\alpha = 0.05$ serve as statistical evidence that all parameters are significant, but the mean infiltration flux is the most significant. The FDR LogWorth

transformation, uses the P-values and solves a mathematical equation that qualitatively describes the amount of influence any one parameter has. values almost double the threshold at ~ 3 (Table 37). Overall, the results of the nonparametric factor test support the hypothesis that the mean flux has the largest influence on damping depth, which has huge implications for the at-large question: “How does climate variability influence groundwater levels and recharge rates?”. Natural climate variability controls the amount of precipitation and evapotranspiration rates that occurs at any one location over a period of time, which results in the infiltration rates that subsurface flow models simulate. If the flux variability is a highly influential factor of the damping depth, that may indicate that areas with low infiltration rates, like desert or arid regions, will have significantly shallower damping depths, regardless of soil texture, in relation to areas with high infiltration rates, representative of wetter, more humid climates, where the flux variability will be preserved to deeper depths. Understanding the statistical significant of the flux and period inputs, are serves as evidence for the strong connection between climate, which causes the infiltration events, and steady or transient groundwater recharge, which is affected by the damping depth.

4.0 IMPLICATIONS

These are crucial findings for engineering projects dealing with the subsurface and accurate groundwater management and recharge planning. Several areas across the U.S., and the world, have a subsurface composed of natural soils that may be approximated as two-layer systems. For example, agriculturally-modified soils tend to exhibit two-layered profiles (Mohseni-Astani et al., 2010). The most prominent example of this are plough layers, where the act of ploughing and constant farming practices cause the pore structure of the upper layer to compact creating a layer that influences water infiltration differently than the underlying parent material. Agriculturally-intensive areas and their respective aquifers like those of the Central Valley and the High Plains regions, may be especially affected as a result of intensive farming with practices of frequent soil mixing (Scanlon et al., 2012).

If in these farming areas, coarser-grained soils have been emplaced as the lower layer, then water moving through these modified systems could persist deeper in the vadose zone and become transient recharge. Theoretically, it is possible that a water flux (say of 1 mm/day), could reach a water table in a season (90 days), provided the water table is at a depth of 25 m (Table 6). This is ideal for states in a water-emergency, like California, that are hoping for aquifer recharge from the 2015-2016 El Niño precipitation pattern. However, if the water table has dropped significantly from 25 m to 100 m or 200 m or 300 m, then a season of infiltration (1 mm/day over a period of 90 days) may not be enough to allow water to reach deeper water tables.

For example, water tables have declined upwards of 90 m in parts of California's Tulare Basin, due to low rainfall rates from 2010-2015, coupled with subsequent minimal infiltration, natural evapotranspiration and excessive groundwater pumping (Bartolino and Cunningham, 2003; Faunt and Geological Survey (U.S.), 2009). With all these factors in mind, the results from this study show that a greater amount of infiltration for a longer period of time are more capable of creating recharge events. In this scenario, if water tables have dropped due to anthropogenic influence, then the natural order of subsurface flow must prevail for four times as long than before our influence, in order to produce the same amount of groundwater recharge. Findings from this study help enhance understanding of the vadose zones influence on transient water flux and improve the simulation of recharge processes and climate variability effects in groundwater models.

5.0 CONCLUSIONS

I investigated the effects of climate variability on groundwater resources by exploring the physical processes in the vadose zone that partially control transient infiltration and recharge fluxes. Infiltration events become time-varying water flux in the vadose zone and are controlled by highly nonlinear, complex interactions between mean infiltration flux, infiltration period, soil textures, and depth to water table. Modeling of a homogeneous vadose zone shows that the flux and period are the greatest influencers of

damping depth. Results for homogeneous profiles show that shorter-period oscillations, smaller mean fluxes, and finer-grained soil textures, cause water flux to dampen at shallower depths. Two-layered systems, however, allow for an influx of water through one layer of a certain soil followed by another layer of a different soil.

Movement of water from one layer to another requires a change in pressure head, water content, and ultimately diffusivity, in order for the water flux to permeate the second material. In two-layered systems, coarse-grained soils cause the greatest differences in damping depth relative to homogeneous systems. Flow simulations show that coupled finer-grained soil profiles result in damping depths closer to land surface, and are more similar to their homogeneous counterparts, than are coupled fine-grained/coarse-grained profiles. Simulations in fine-grained soils over short periods allow for linear superposition while longer periods and coarser-grained soils fail to provide accurate cases. From these highly nonlinear, yet influential relations, it is evident that we must consider how the vadose zone shapes climate variability-groundwater teleconnections for the improvement of our water resource management, especially with increasing demands from population growth, agricultural activities, and changes in climate.

6.0 REFERENCES

- Bakker, M., and Nieber, N.L. 2009. Damping of Sinusoidal Surface Flux Fluctuations with Soil Depth. *Vadose Zone J.* 8(1): 119.
- Bartolino, J.R. and W.L. Cunningham. 2003. Ground-Water Depletion Across the Nation. Available at http://wrrc.arizona.edu/sites/wrrc.arizona.edu/files/USGS_Groundwater%20Depletion%20Across%20the%20Nation.pdf (verified 2 May 2016).
- Benjamini, Y., and Hochberg, Y. 1995. Controlling the false discovery rate: a practical and powerful approach to multiple testing. *J. R. Stat. Soc. Ser. B Methodol.*: 289–300.
- Dickinson, J.E., T.P.A. Ferré, M. Bakker, and B. Crompton. 2014a. A Screening Tool for Delineating Subregions of Steady Recharge within Groundwater Models. *Vadose Zone J.* 13(6): 15.
- Earman, S., and M. Dettinger. 2011. Potential impacts of climate change on groundwater resources – a global review. *J. Water Clim. Change* 2(4): 213.
- Fan, Y., G. Miguez-Macho, C.P. Weaver, R. Walko, and A. Robock. 2007. Incorporating water table dynamics in climate modeling: 1. Water table observations and equilibrium water table simulations. *J. Geophys. Res.* 112(D10) Available at <http://www.agu.org/pubs/crossref/2007/2006JD008111.shtml> (verified 21 February 2013).
- Faunt, C.C., and Geological Survey (U.S.) (Edited). 2009. Groundwater availability of the Central Valley Aquifer, California. U.S. Geological Survey, Reston, Va.
- Ghil, M. (Ed). 2002. Encyclopedia of global environmental change. Wiley; Worcester, New York.
- Gleick, Peter H., A., D.B. 2000. Water: the potential consequences of climate variability and change. A Report of the National Assessment, US Global Change Research Program. US Geological Survey, US Department of the Interior, and the Pacific Institute for Studies in Development, Environment, and Security, Oakland, California.
- Gardner, W.R. 1958. Some Steady-state Solutions of the Unsaturated Moisture Flow: Soil Science. LWW. Available at http://journals.lww.com/soilsci/Fulltext/1958/04000/Some_Steady_State_Solutions_of_the_Unsaturated.6.aspx (verified 27 April 2016).

- Gurdak, J.J., R.T. Hanson, P.B. McMahon, B.W. Bruce, J.E. McCray, G.D. Thyne, and R.C. Reedy. 2007. Climate variability controls on unsaturated water and chemical movement, High Plains aquifer, USA. *Vadose Zone J.* 6(3): 533.
- Hanson, R.T., M.W. Newhouse, and M.D. Dettinger. 2004. A methodology to assess relations between climatic variability and variations in hydrologic time series in the southwestern United States. *J. Hydrology.* 287(1–4): 252–269.
- Helsel, D.R., and Hirsch. R.M 1992. *Statistical methods in water resources.* Elsevier.
- Kuss, A.J.M., and Gurdak, J.J. 2014a. Groundwater level response in U.S. principal aquifers to ENSO, NAO, PDO, and AMO. *J. Hydrology.* 519: 1939–1952.
- Leconte, R., and F.P. Brissette. 2001. Soil moisture profile model for two-layered soil based on sharp wetting front approach. *J. Hydrol. Eng.* 6(2): 141–149.
- Mathias, S.A., and A.P. Butler. 2006. Linearized Richards' equation approach to pumping test analysis in compressible aquifers: Richards' Equation Approach to Pumping Test Analysis. *Water Resources Research.* 42(6).
- Mohseni-Astani, R., P. Haghparast, S. Bidgoli-Kashani, and others. 2010. Assessing and Predicting the Soil Layers Thickness and Type Using Artificial Neural Networks-Case Study in Sari City of Iran. *Middle-East J. Sci. Res.* 6(1): 62–68.
- Nimmo, J.R. 2005. Unsaturated Zone Flow Processes. *In* Anderson, M.G., McDonnell, J.J. (eds.), *Encyclopedia of Hydrological Sciences.* John Wiley & Sons, Ltd, Worchester, UK.
- Radeliffe, D.E., Simunek, J., 2010. *Soil Physics with HYDRUS: modeling and applications.* CRC press.
- Reilly, T.E., L. Franke, and G.D. Bennett. 1984. *Techniques of Water-Resources Investigations of the United States Geological Survey.* Available at http://windowoutdoors.com/Teaching/CE%205302%20Groundwater%20Hydrology/Literature/twri_3-B6_a%20Superposition%20in%20Ground%20Water.pdf (verified 7 May 2016).
- Richards, L.A. 1931a. Capillary Conduction of Liquids through Porous Mediums. *J. Applied. Physics.* 1(5): 318–333.
- Rimon, Y., O. Dahan, R. Nativ, and S. Geyer. 2007. Water percolation through the deep vadose zone and groundwater recharge: Preliminary results based on a new vadose zone monitoring system. *Water Resources. Res.* 43(5): W05402.

- Sanford, W.E., and D.L. Selnick. 2013. Estimation of Evapotranspiration Across the Conterminous United States Using a Regression with Climate and Land-Cover Data. *JAWRA J. Am. Water Resources. Assoc.* 49(1): 217–230.
- Scanlon, B.R., C.C. Faunt, L. Longuevergne, R.C. Reedy, W.M. Alley, V.L. McGuire, and P.B. McMahon. 2012. Groundwater depletion and sustainability of irrigation in the US High Plains and Central Valley. *Proc. Natl. Acad. Sci.* 109(24): 9320–9325.
- Scanlon, B.R., R.W. Healy, and P.G. Cook. 2002. Choosing appropriate techniques for quantifying groundwater recharge. *Hydrogeology. J.* 10(1): 18–39.
- Šimunek, J., M.T. van Genuchten, and M. Šejna. 2008. Development and Applications of the HYDRUS and STANMOD Software Packages and Related Codes. *Vadose Zone J.* 7(2): 587–600.
- Simunek, J., K. Huang, and M.T. van Genuchten. 1995. The SWMS 3D Code for Simulating Water Flow-and Solute Transport in Three-Dimensional Variably-Saturated Media. Available at http://www.pc-progress.com/documents/programs/swms_3d.pdf (verified 3 December 2015).
- Southeast Regional Climate Center. 2014. 2013 Annual Climate Summary for the Southeast United States. Available at <http://www.sercc.com/2013AnnualClimateSummaryfortheSoutheast.pdf>.
- Tompkins, W.J. (Ed). 1993. Biomedical digital signal processing: C-language examples and laboratory experiments for the IBM PC. Prentice Hall, Englewood Cliffs, N.J.
- Taylor, R.G., B. Scanlon, P. Döll, M. Rodell, R. van Beek, Y. Wada, L. Longuevergne, M. Leblanc, J.S. Famiglietti, M. Edmunds, L. Konikow, T.R. Green, J. Chen, M. Taniguchi, M.F.P. Bierkens, A. MacDonald, Y. Fan, R.M. Maxwell, Y. Yechieli, J.J. Gurdak, D.M. Allen, M. Shamsudduha, K. Hiscock, P.J.-F. Yeh, I. Holman, and H. Treidel. 2012. Ground water and climate change. *Nat. Climate Change* 3(4): 322–329.
- USDA. Soil Texture Calculator | NRCS Soils. Nat. Resource Conservation Service Soils. Available at http://www.nrcs.usda.gov/wps/portal/nrcs/detail/soils/survey/?cid=nrcs142p2_054167 (verified 19 May 2016).
- Velasco, E.M., J.J. Gurdak, J.E. Dickinson, T.P.A. Ferré, and C.R. Corona. 2015. Interannual to multidecadal climate forcings on groundwater resources of the U.S. West Coast. *J. Hydrology. Reg. Study.* Available at <http://www.sciencedirect.com/science/article/pii/S2214581815001330> (verified 30 April 2016).

7.0 FIGURES

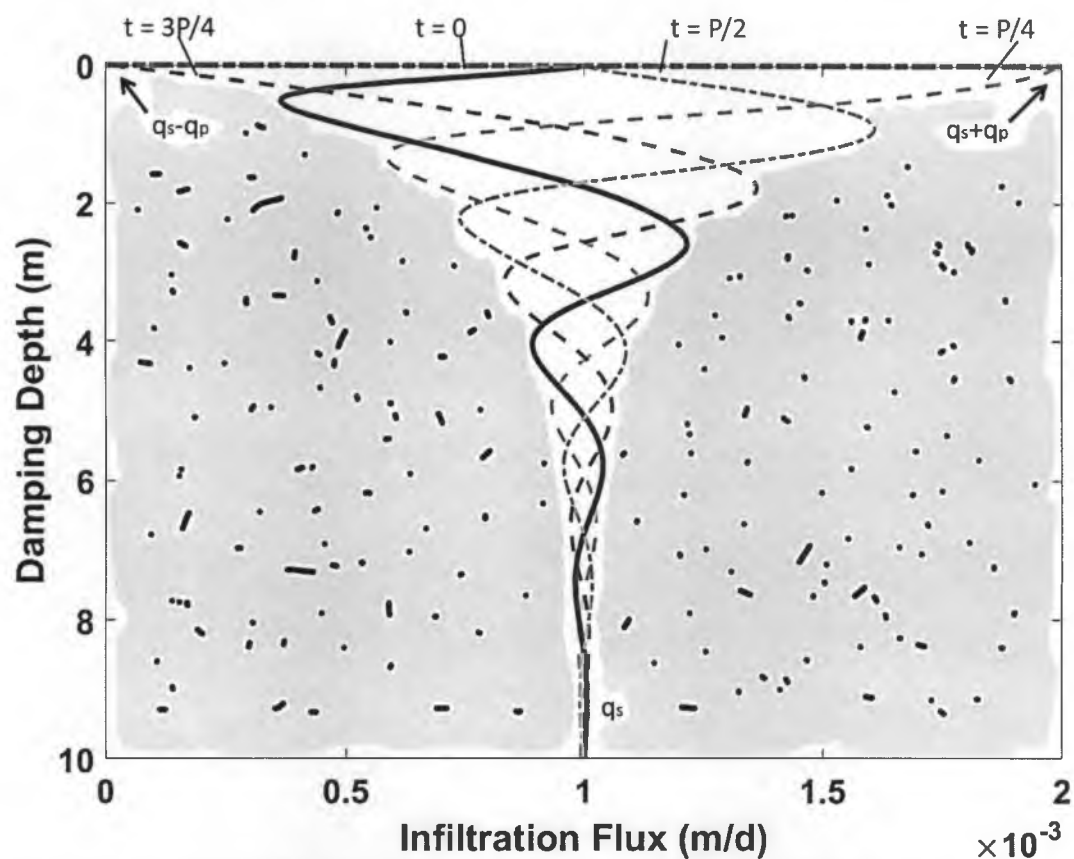


Figure 1. Damping of a sinusoidal vertical flux, q_z , applied at land surface, where $z = 0$. Profiles of the flux with depth at times $P/4$ and $3P/4$, where P is the sinusoidal wave period, and the envelopes encompass the variations in the profiles of the soil. The flux travels vertically downward and has a steady component, q_s , plus a sinusoidal component with amplitude q_p .

Soil Textural Triangle

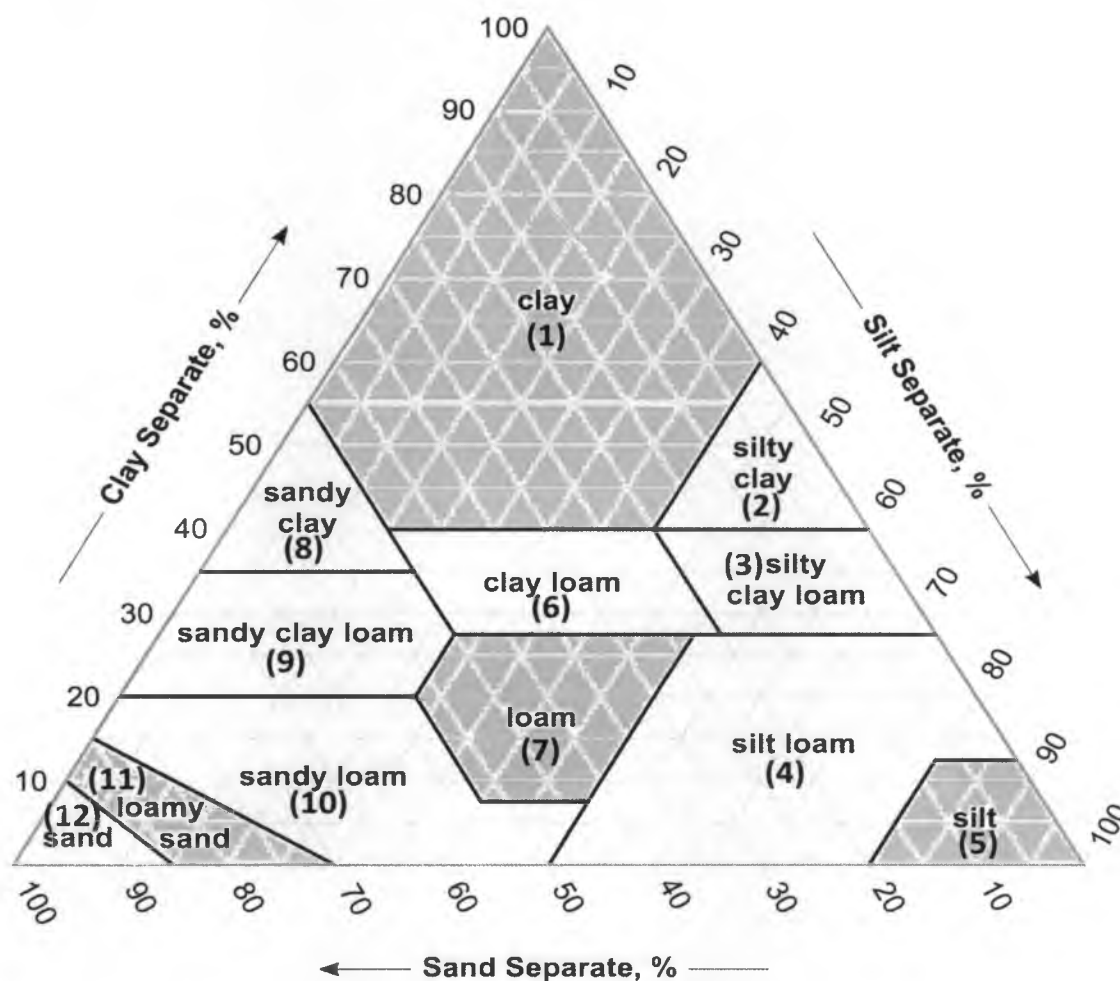


Figure 2. Soil textural triangle showing percentages of sand, silt and clay for the 12 USDA soil texture classifications. The colored polygons are the selected reference soil textures used in the models of the two-layered system.

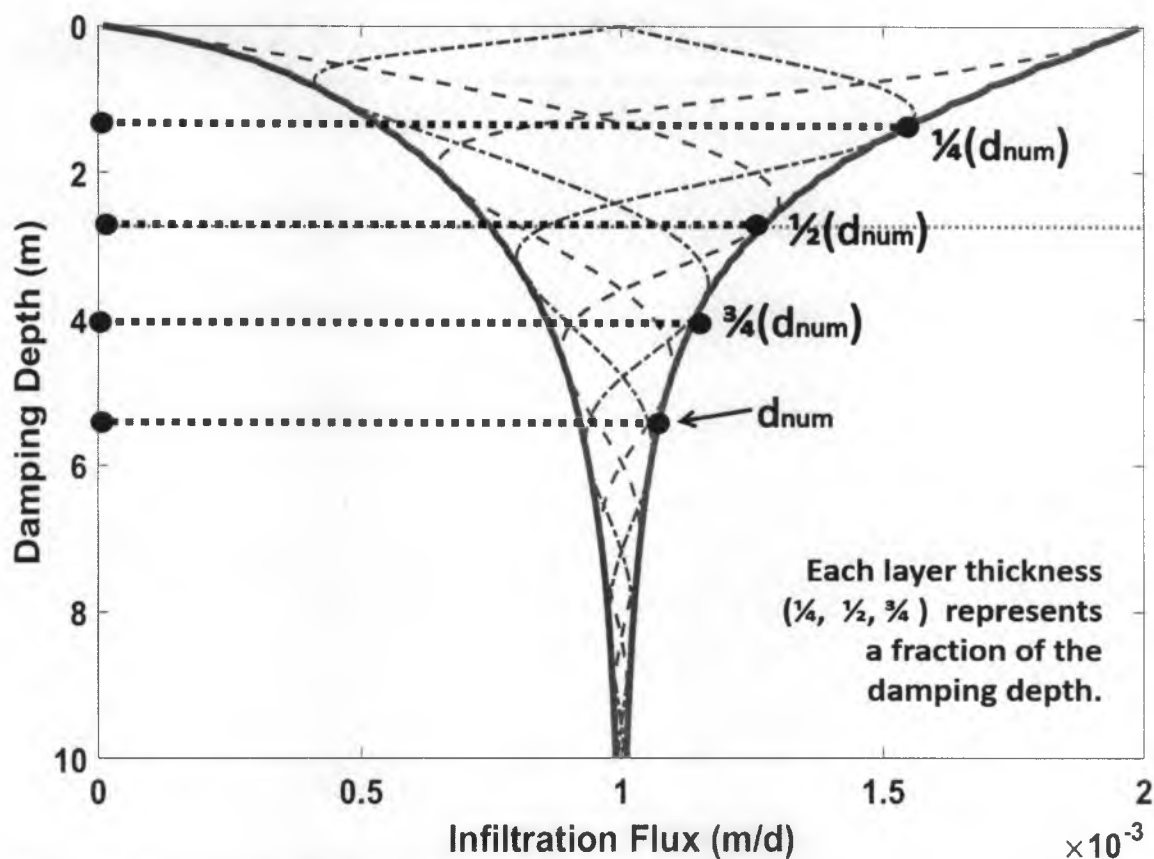


Figure 3. Damping of sinusoidal flux applied at land surface ($z = 0$) to some depth, d_{num} . Layer thickness for subsequent model runs are quarter-fractions of the total d_{num} , as a means of simulating potentially thin, intermediate, and thick upper layers relative to the respective soil.

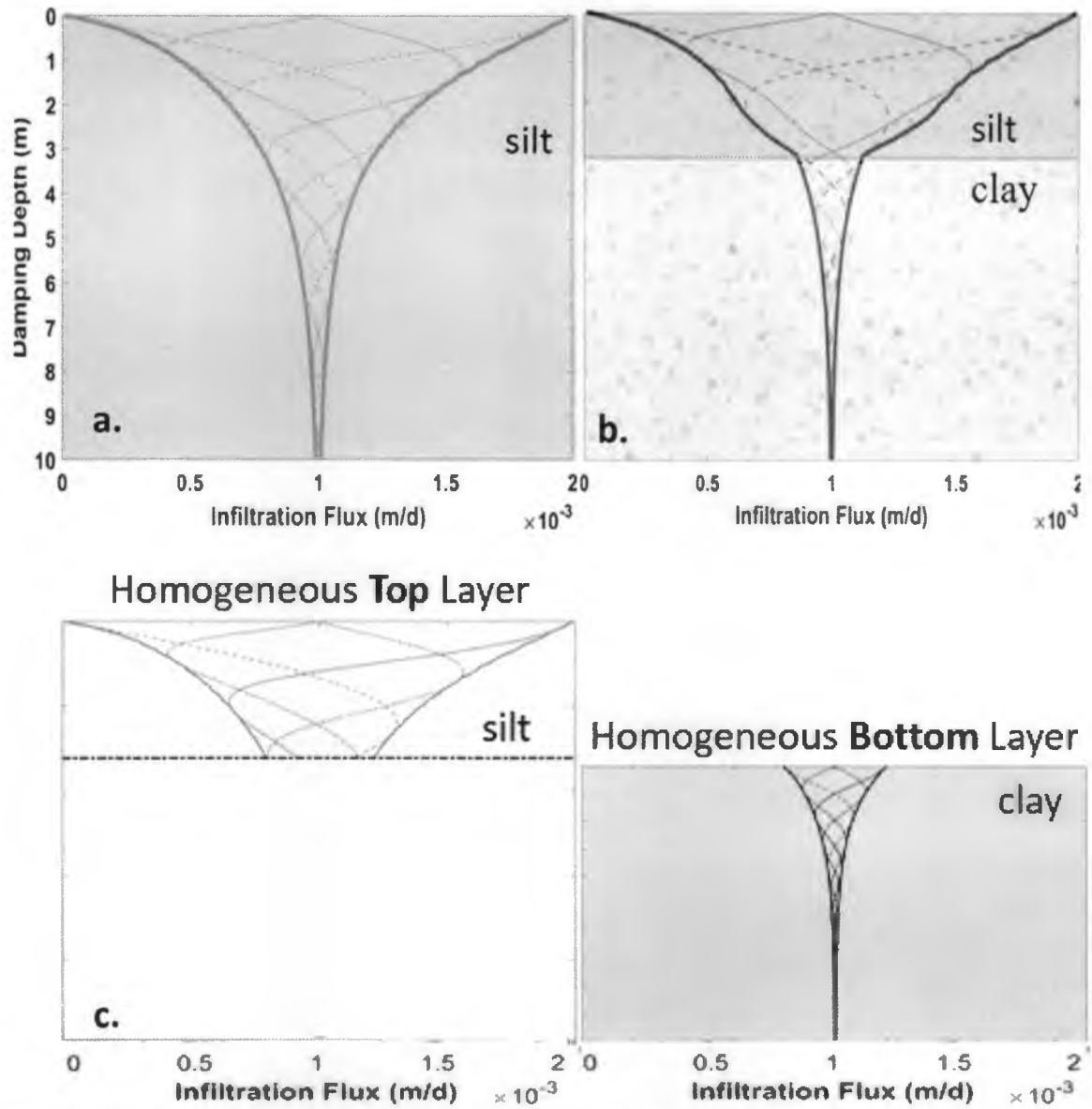


Figure 4(a, b, c). Damping of sinusoidal flux applied at land surface ($z = 0$) in (a) a homogeneous system composed of silt, a (b) a two-layered system composed of silt (soil #1) underlain by clay (soil #2) and (c) a discontinuous homogeneous system with a revised amplitude. The sinusoidal envelopes show how the flux varies with depth at different times, t . The flux has a steady component q_s plus a sinusoidal component with amplitude q_p .

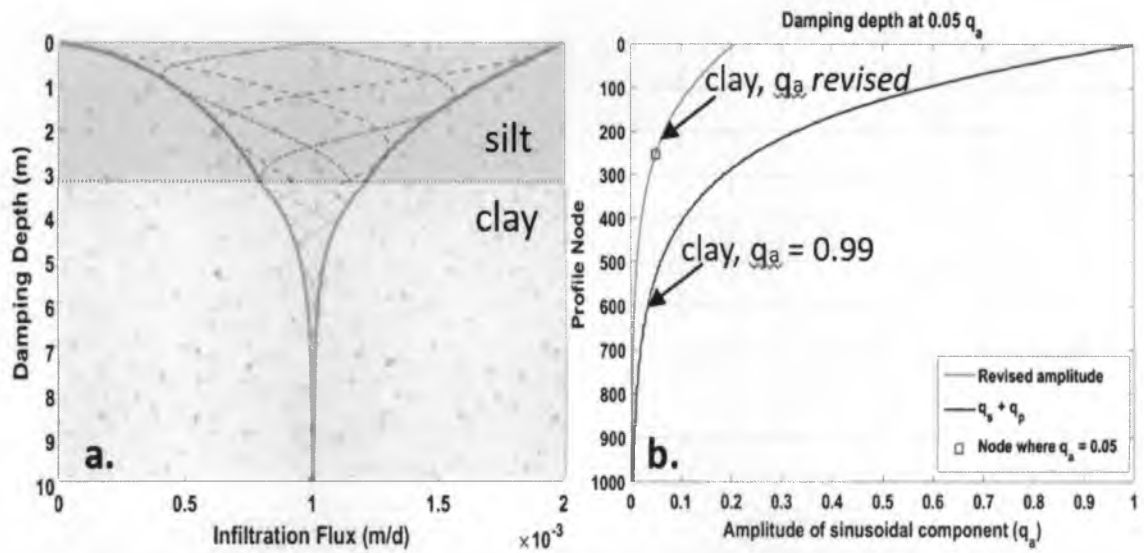


Figure 5(a, b). Damping of sinusoidal flux in (a) made of two distinct homogeneous layers, an upper layer (silt) and a lower layer (clay). (b) Plot of the steady flux component q_s plus a sinusoidal component with amplitude q_p for the lower layer, where the lower line defines an amplitude of 0.99 and the higher line denotes the revised amplitude. The box indicates the node at which the flux variation is 5% of what it was of the revised, starting at q_a .

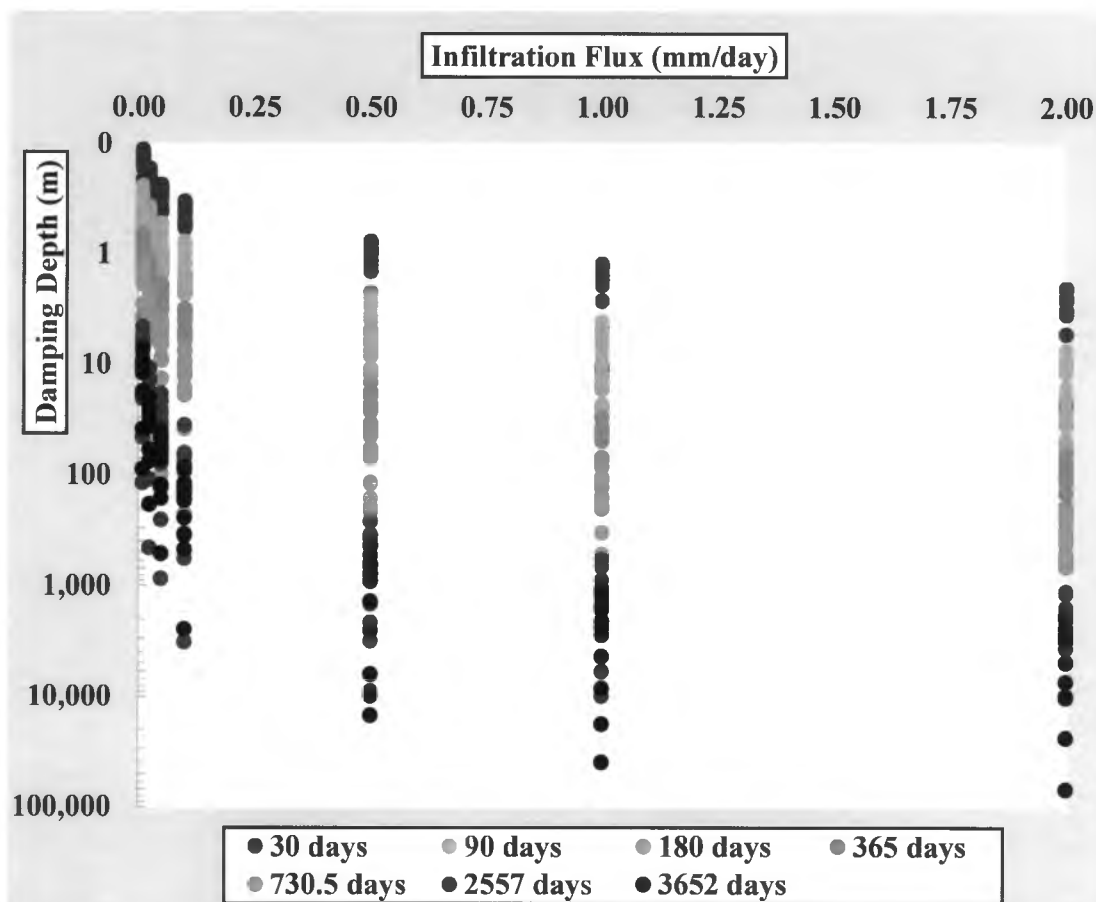


Figure 6. Damping depths (m) from 588 simulations of homogeneous profiles of 12 soil textures, using a range of mean fluxes (0.01 to 2.0 mm/day) and periods (30 to 3,652 days). The range of mean fluxes represents long-term net infiltration flux of climate and land-cover regions of the U.S., and the range of periods represents variability on monthly, seasonal, annual, and interannual timescales.

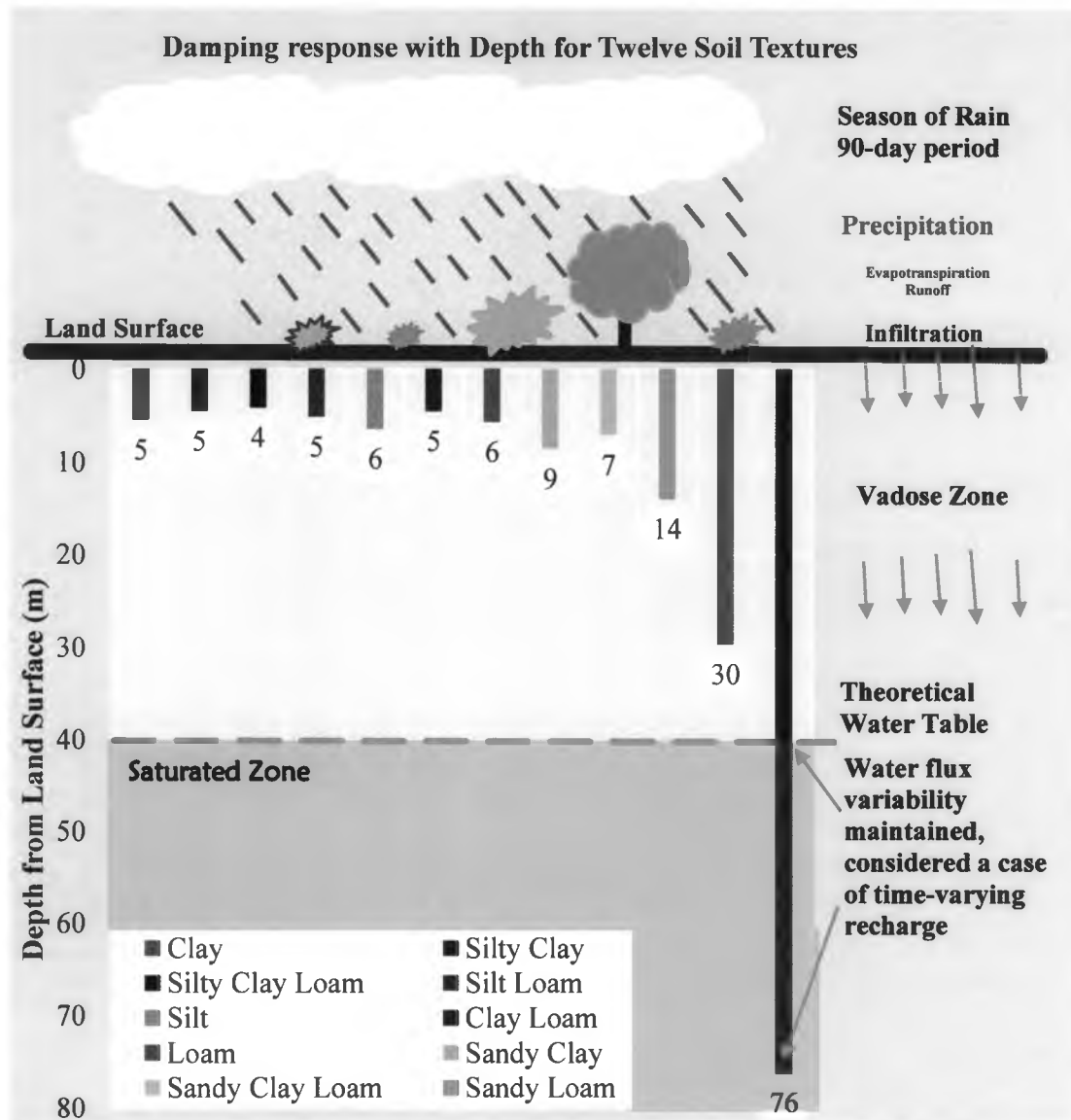


Figure 7. Comparison of the damping depths for all twelve soil texture classes. The flux amplitude damps to 5% of the applied flux variation over a period, $P = 90$ days, where the steady flux component $q_s = 1.00 \times 10^3$ m/d, plus a sinusoidal component with amplitude $q_p = 0.99 \times 10^3$ m/d.

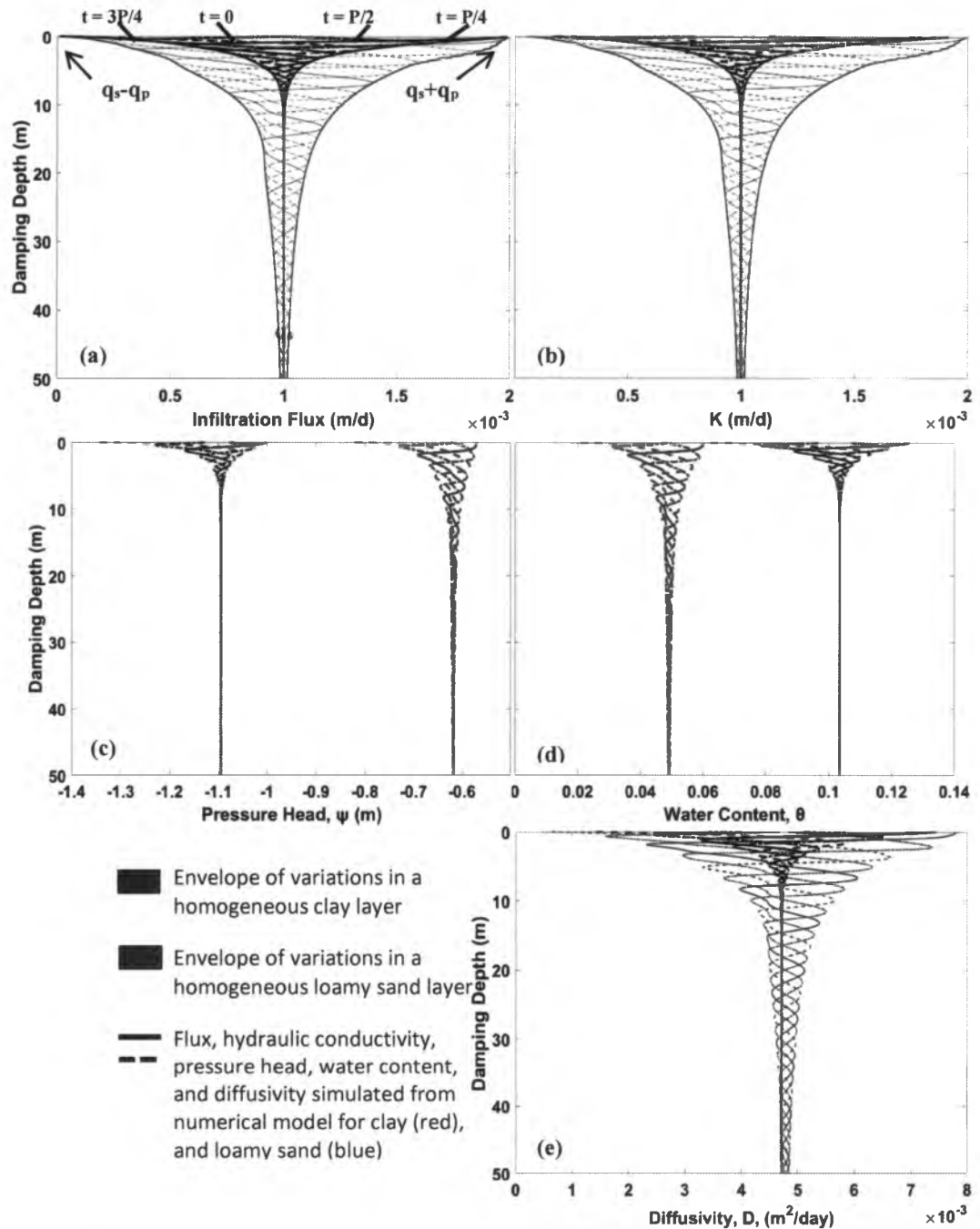


Figure 8. Comparison of (a) flux, q_z , (b) hydraulic conductivity, K , (c) initial pressure head condition, ψ , (d) water content θ , and (e) diffusivity, D , profiles at times $P/4$ and $3P/4$, where P is the sinusoidal wave period, and the envelopes encompass the variations in the profiles of clay and loamy sand layers for a period of 90 days, and a mean flux $q_s = 1.00 \times 10^3$ m/d.

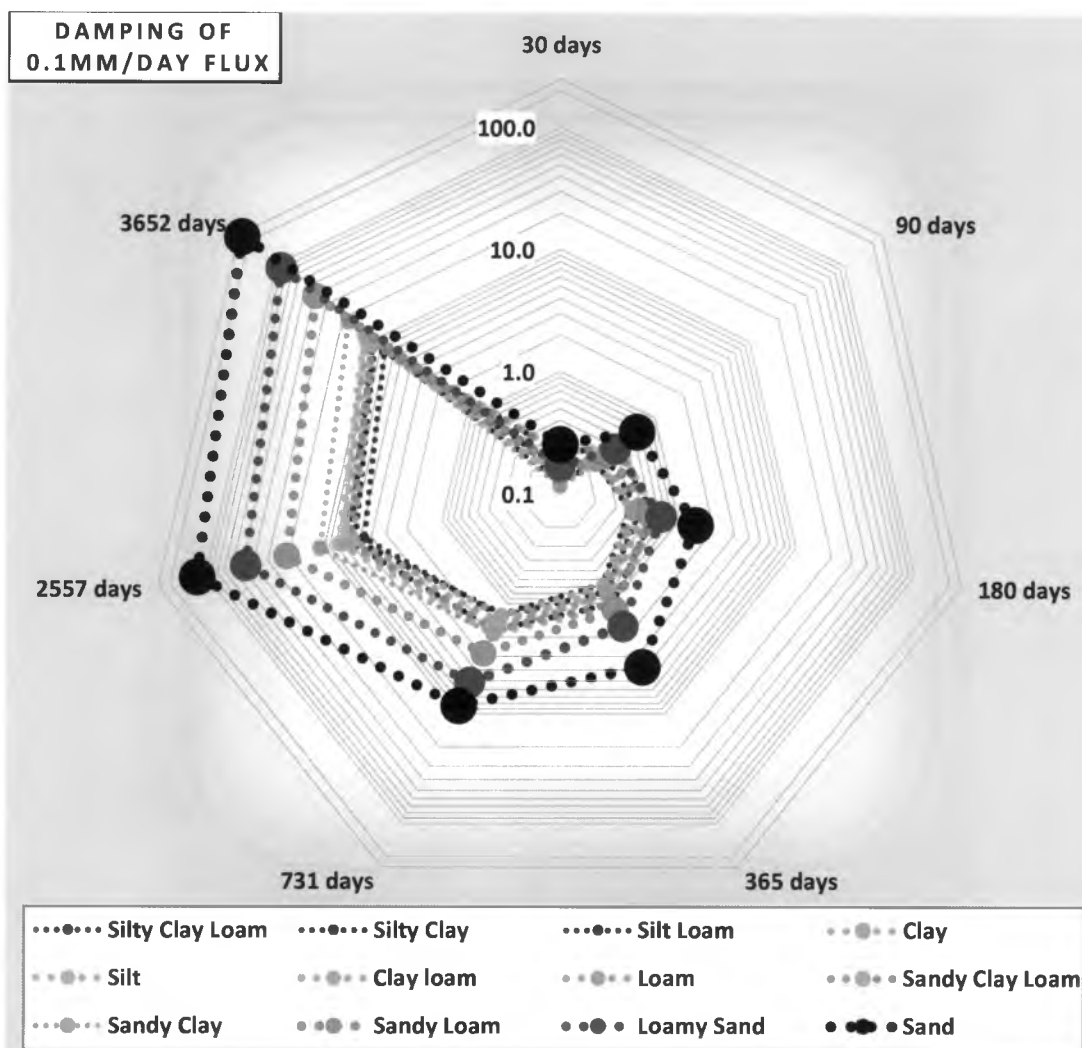


Figure 9. Damping of 0.1 mm/day flux over time ranging from a monthly period (30 days) to a possible 10 years (3,652 days). Color differentiates soil tendency for shallow damping (reds) compared to deep damping (blues), with in-between damping depths in yellow. Small symbols represent fine-grained soils, and large circles represent sandy loam, loamy sand and sand—all coarse-grained textures.

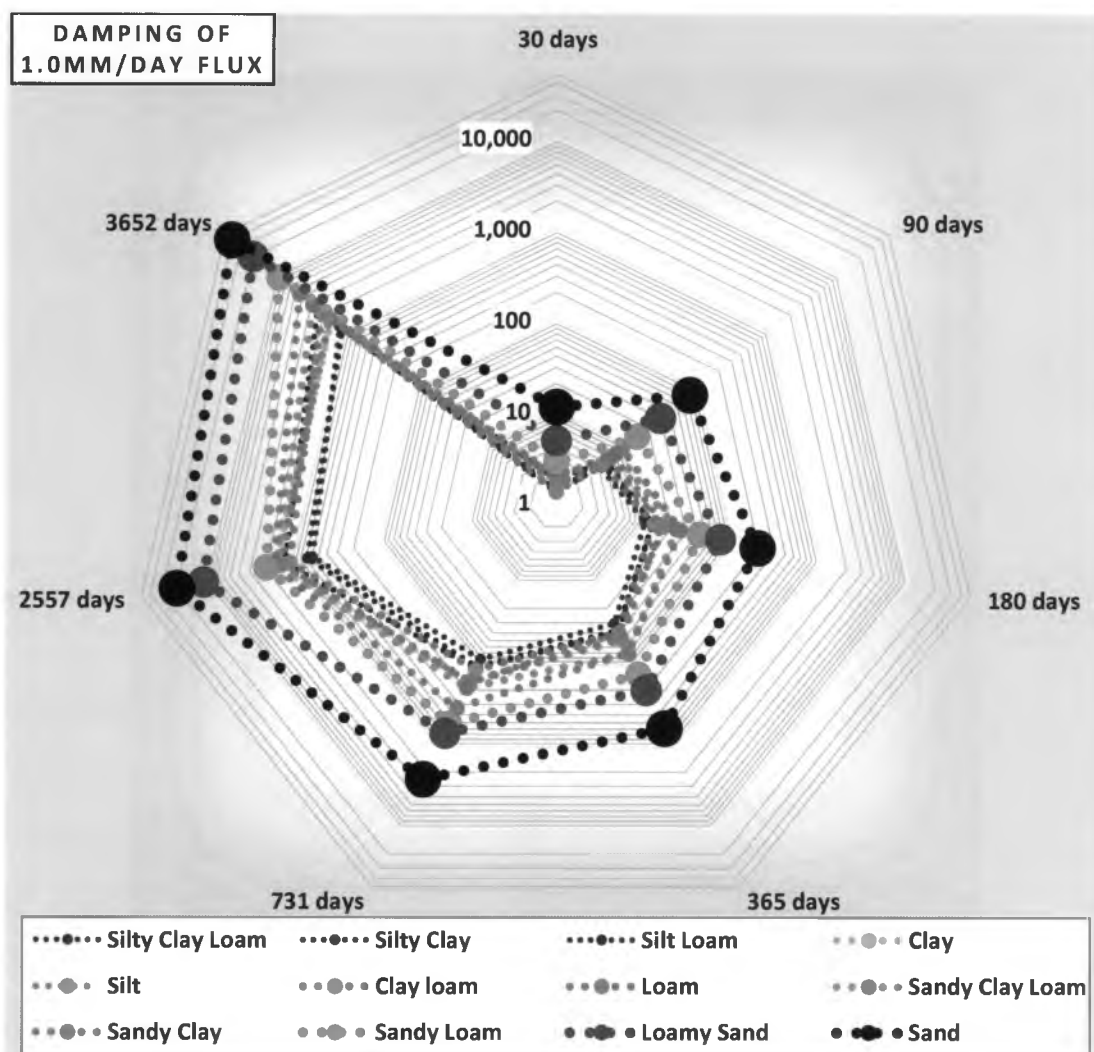


Figure 10. Damping depths of 1.0 mm/day flux over time ranging from a monthly period (30 days) to a possible 10 years (3,652 days). Color differentiates soil tendency for shallow damping (reds) compared to deep damping (blues), with in-between damping depths in yellow. Small symbols represent fine-grained soils, and large circles represent sandy loam, loamy sand and sand—all coarse-grained textures.

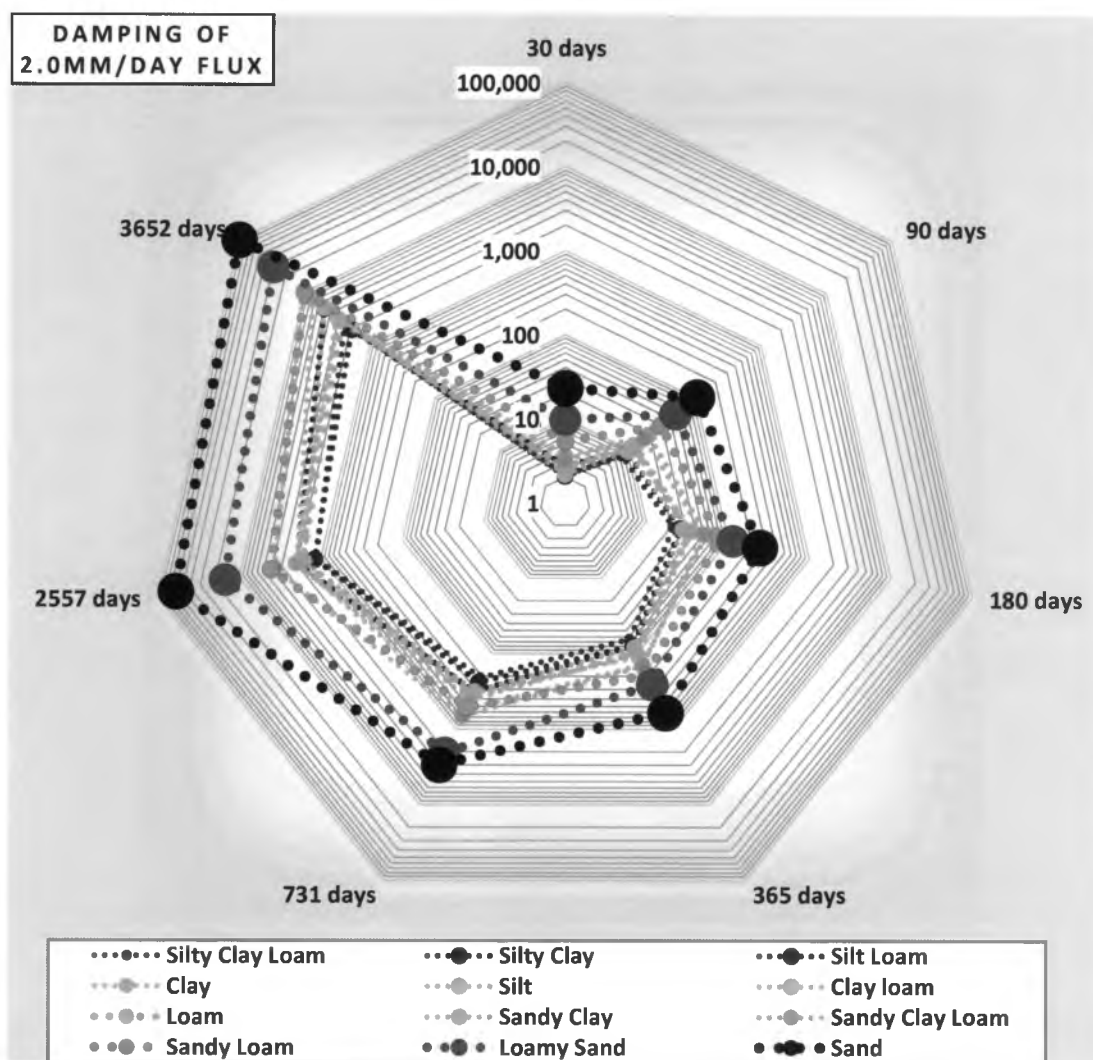


Figure 11. Damping of 2.0 mm/day flux over time ranging from a monthly period (30 days) to a possible 10 years (3,652 days). Color differentiates soil tendency for shallow damping (reds) compared to deep damping (blues), with in-between damping depths in yellow. Small symbols represent fine-grained soils, and large circles represent sandy loam, loamy sand and sand—all coarse-grained textures.

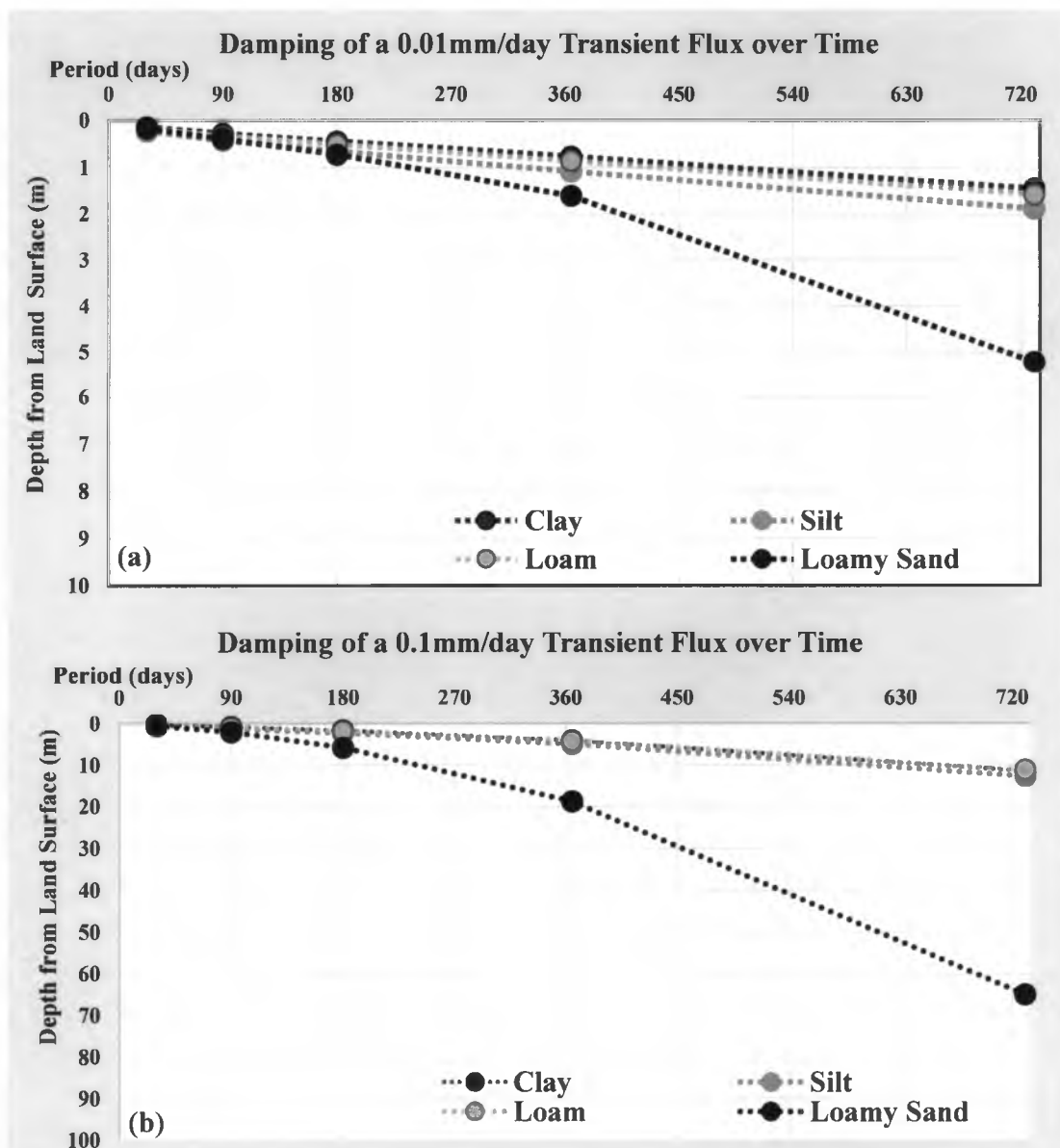


Figure 12(a, b). Damping in the vadose zone for clay, silt, loam, and loamy sand with four increasing infiltration fluxes: (a) 0.01mm/day, (b) 0.1mm/day, over time that may represent irrigation patterns (30 days), seasonal patterns (90 days), annual cycles (365 days) and the lower end of climate variability modes like El Niño (730.5 days).

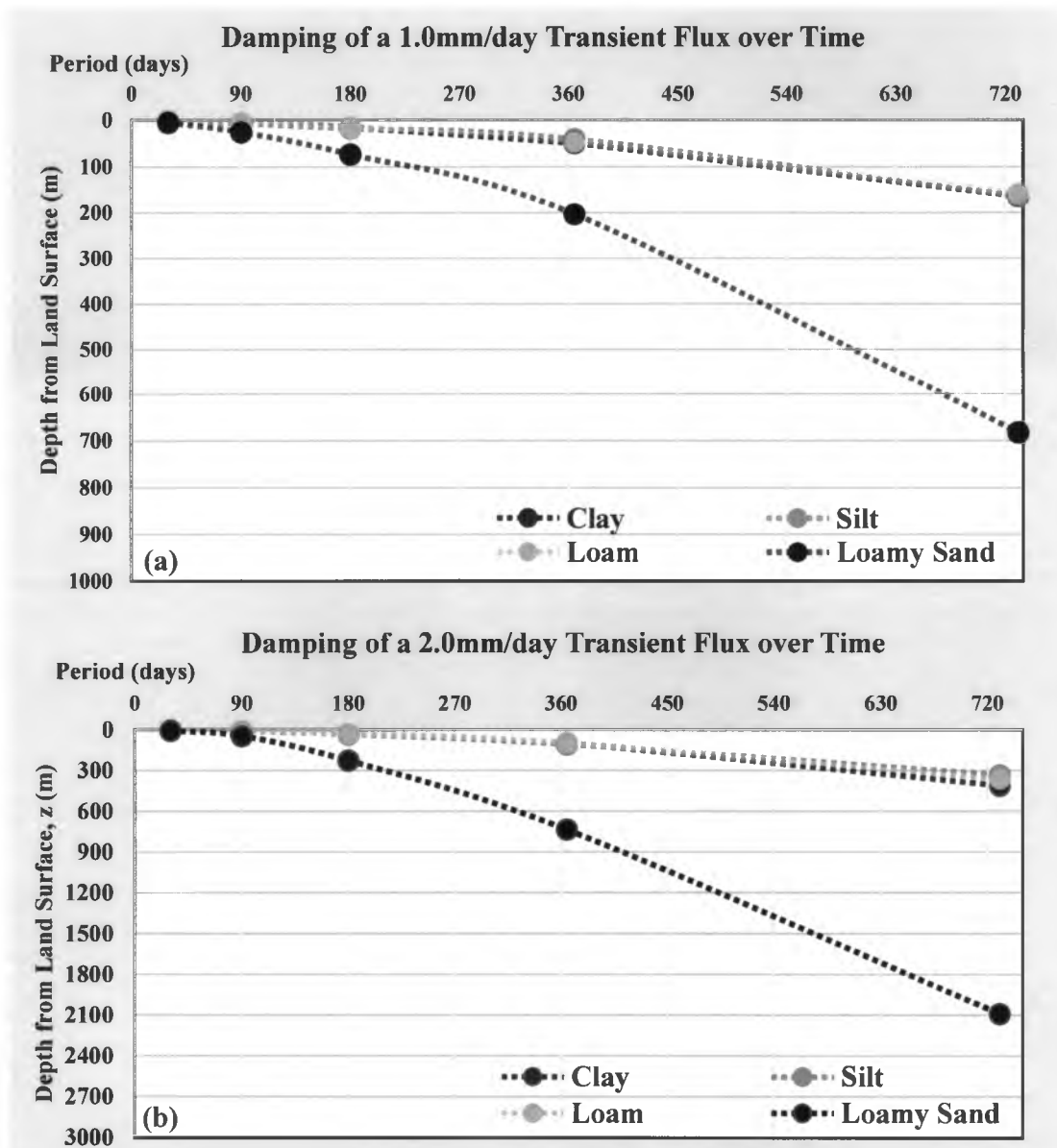


Figure 13(a, b). Damping in the vadose zone for clay, silt, loam, and loamy sand with four increasing infiltration fluxes: (a) 1.0mm/day and (b) 2.0mm/day over time that may represent irrigation patterns (30 days), seasonal patterns (90 days), annual cycles (365 days) and the lower end of climate variability modes like El Niño (730.5 days).

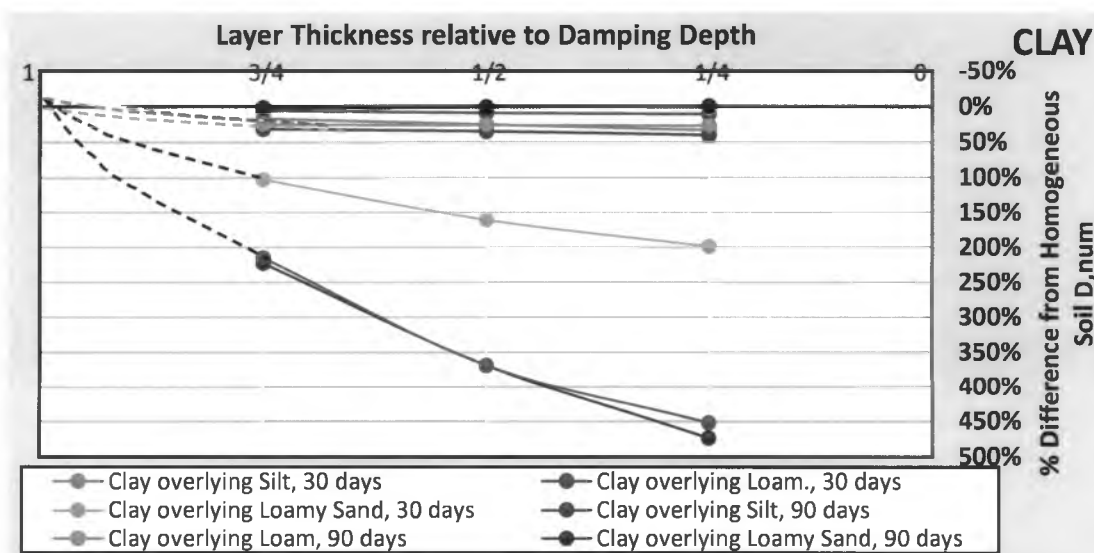


Figure 14. Comparison of damping depths between the homogeneous clay layer and the two-layered cases where clay is the upper layer. Comparisons are made with varying layer thickness that were calculated by dividing the total damping depth of the clay by quarters over 30, 90, and 365 days.

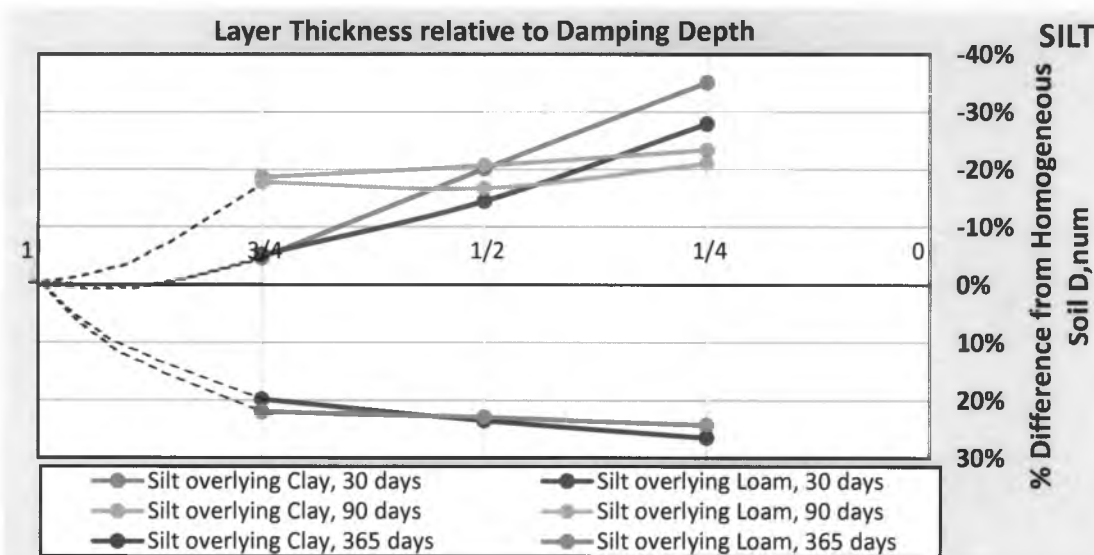


Figure 15. Comparison of damping depths between the homogeneous silt layer and the two-layered cases where silt is the upper layer. Comparisons are made with varying layer thickness that were calculated by dividing the total damping depth of the clay by quarters over 30, 90, and 365 days.

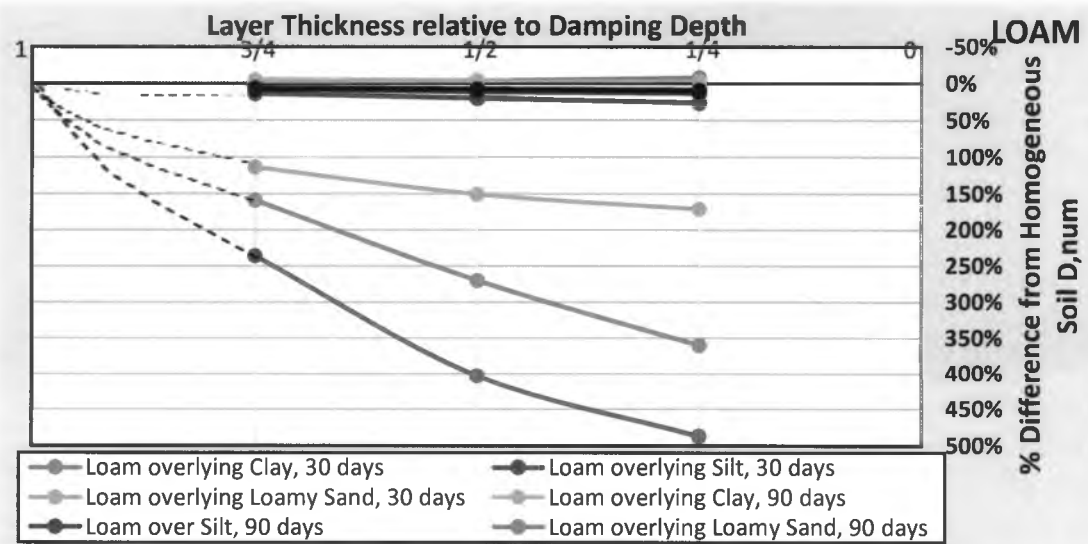


Figure 16. Comparison of damping depths between the homogeneous loam layer and the two-layered cases where loam is the upper layer. Comparisons are made with varying layer thickness that were calculated by dividing the total damping depth of the clay by quarters over 30, 90, and 365 days.

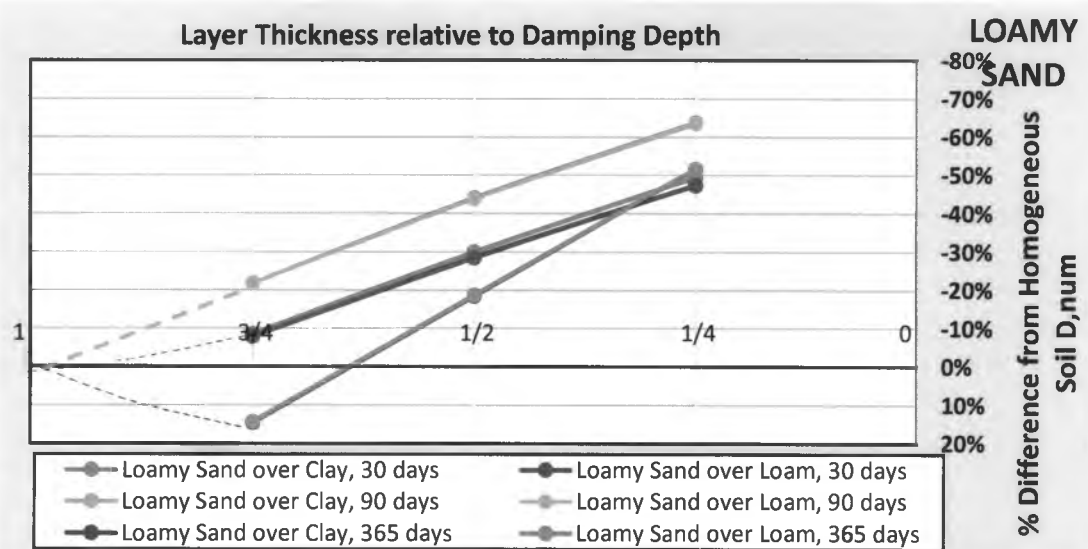


Figure 17. Comparison of damping depths between the homogeneous loam layer and the two-layered cases where loam is the upper layer. Comparisons are made with varying layer thickness that were calculated by dividing the total damping depth of the clay by quarters over 30, 90, and 365 days.

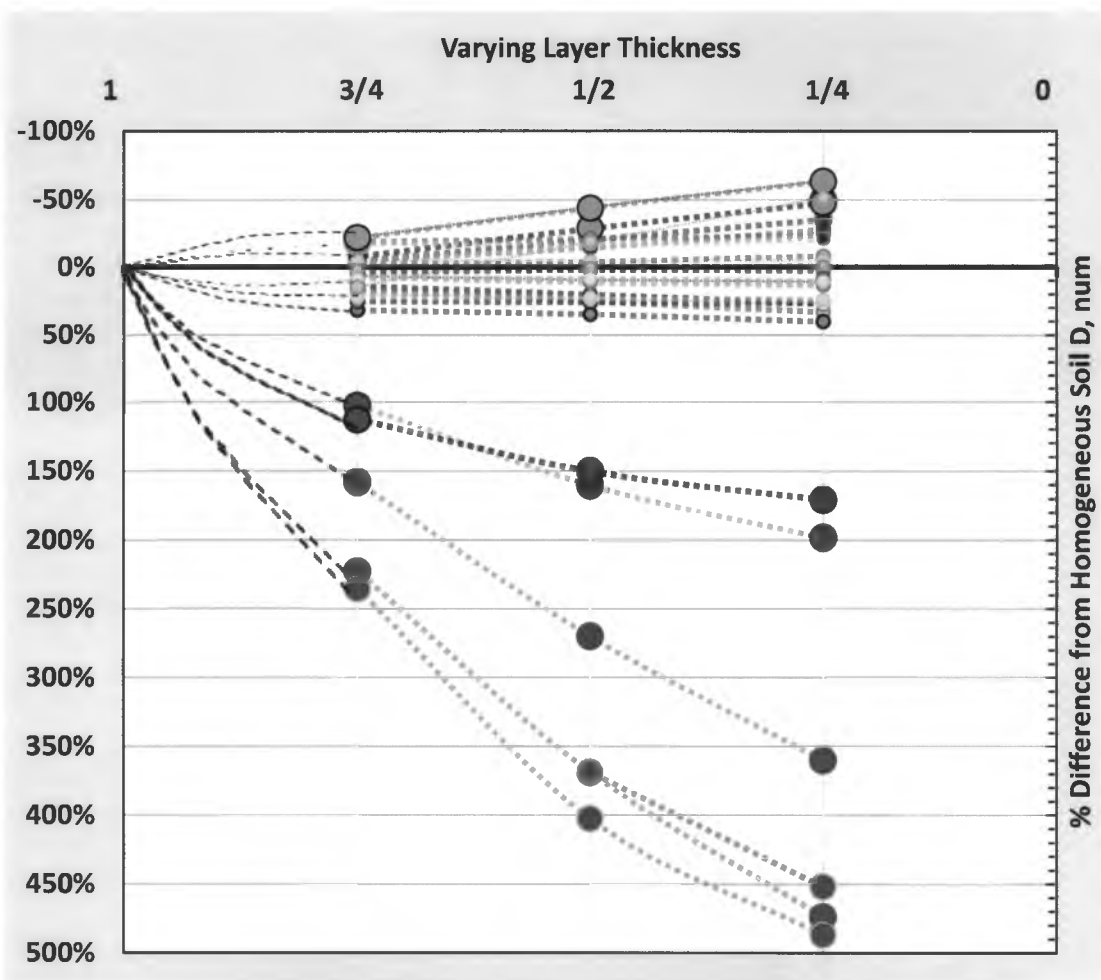


Figure 18. Comparison of all two-layered damping depths with all homogeneous damping depths. Comparisons are made with varying layer thickness that were calculated by dividing the total damping depth of the clay by quarters over 30, 90, and 365 days. In light blue are two-layered systems where loamy sand is the upper layer, ranging from -5% to -65%. Negative percent differences highlight two-layered systems that had shallower damping depths than that of their homogeneous upper layer. Two-layered systems where loamy sand was the lower layer, show damping depth differences of over 100%, with the percent difference becoming more pronounced as the upper layer thins and the bottom layer of loamy sand thickens.

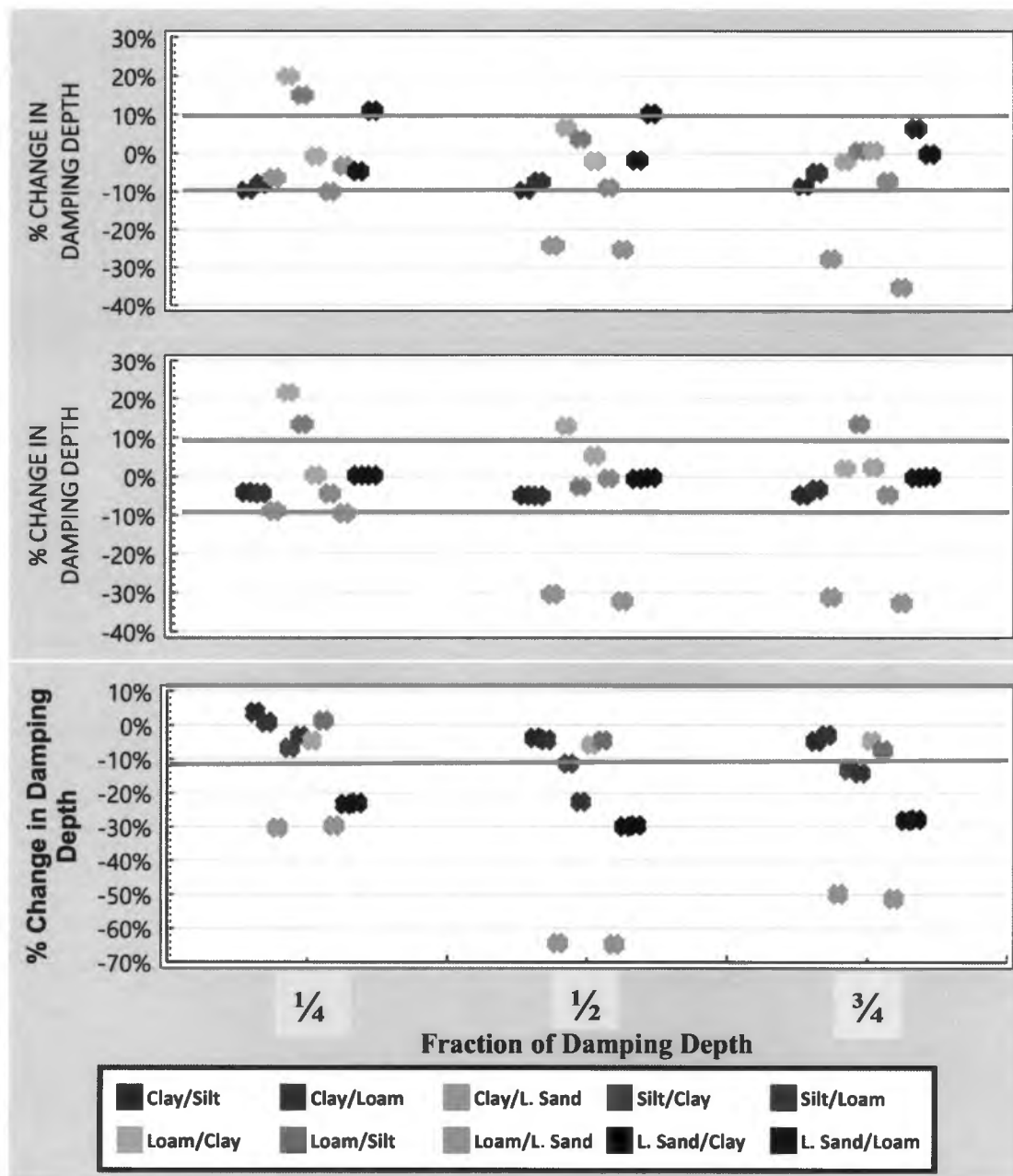


Figure 19(a, b, c). Comparison of the damping depth of the two-layered system and the homogeneous system with the revised amplitude for thin, intermediate, and thick upper layers ($\frac{1}{4}d_{num}$, $\frac{1}{2}d_{num}$, $\frac{3}{4}d_{num}$) for a q_z of 1 mm/day and (a) a 30-day period, a (b) 90-day period and a (c) 365-day period.

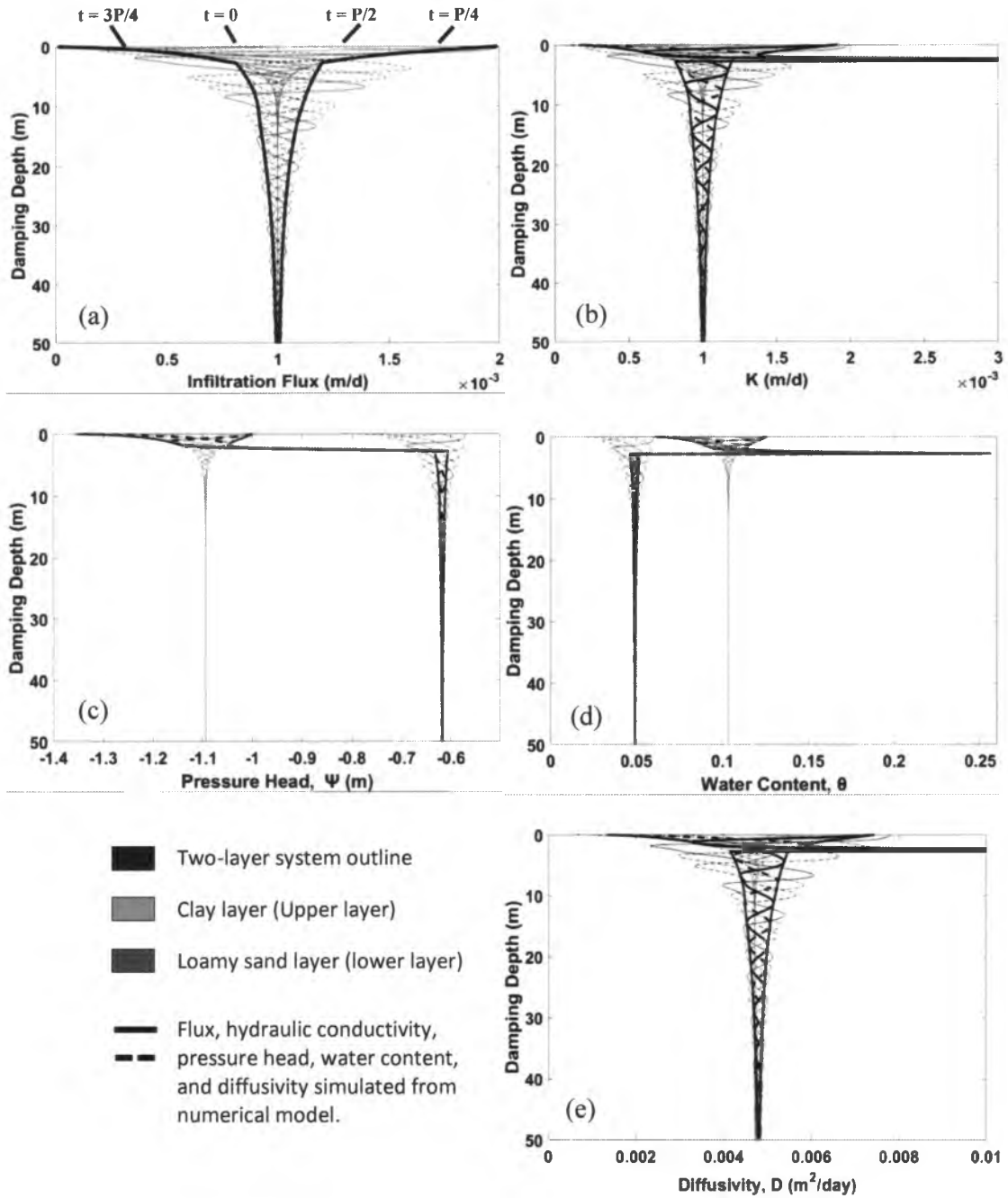


Figure 20(a-e). Two-layered system of a clay layer (upper layer) overlying a loamy sand layer (lower layer) for a period of 90 days, and a mean flux $q_s = 1.00 \times 10^3 \text{ m/d}$. Comparison of (a) flux, q_z , (b) hydraulic conductivity, K , (c) initial pressure head condition, ψ , (d) water content θ , and (e) diffusivity, D , profiles at times $P/4$ and $3P/4$, where P is the sinusoidal wave period. The black envelope represents the water flux response in the two-layered system.

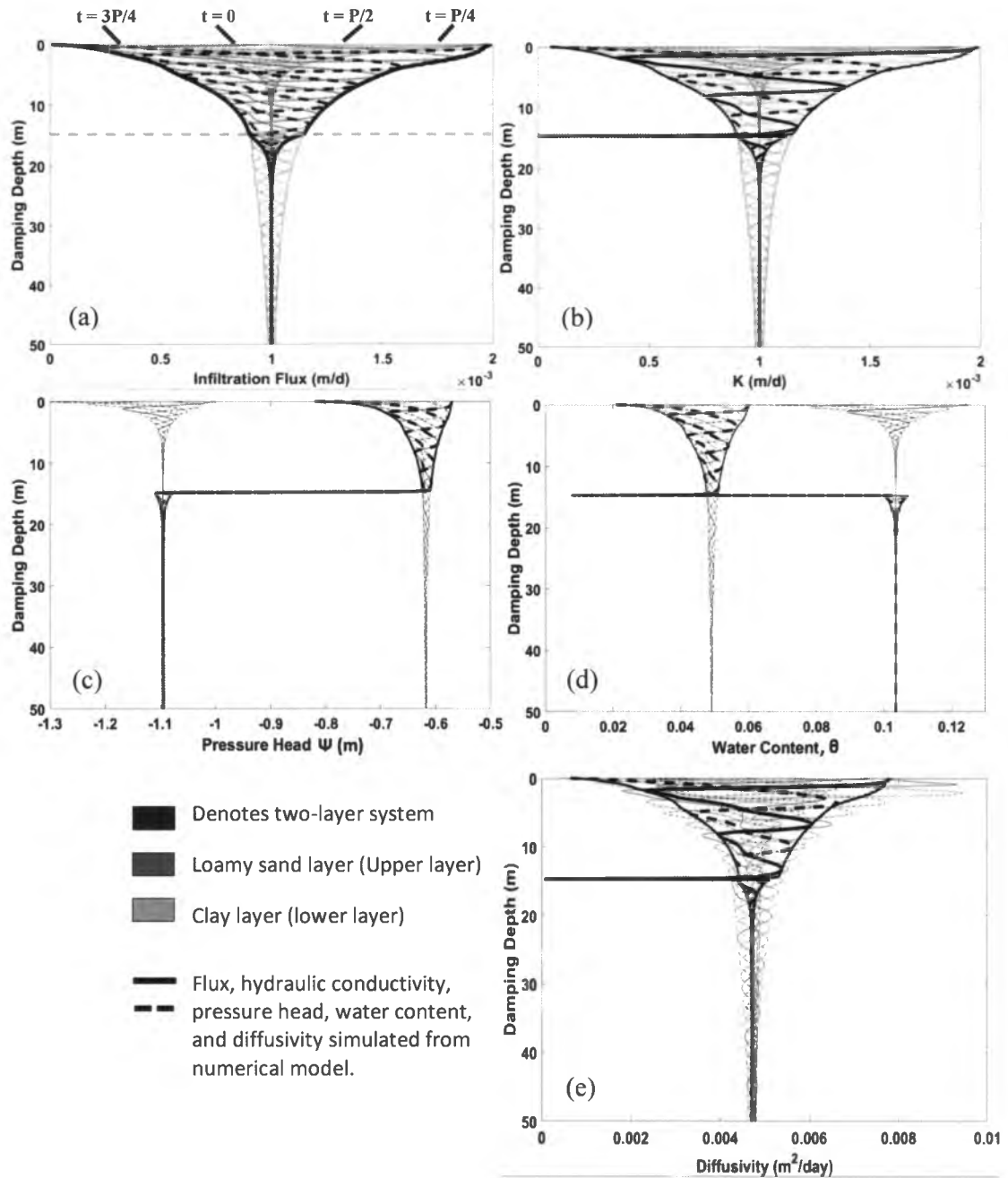


Figure 21(a-e). Two-layered system of a loamy sand (upper layer) overlying a clay layer (lower layer) for a period of 90 days and a mean flux $q_s = 1.00 \times 10^3$ m/d. Comparison of (a) flux, q_z , (b) hydraulic conductivity, K , (c) initial pressure head condition, ψ , (d) water content θ , and (e) diffusivity, D , profiles at times $P/4$ and $3P/4$, where P is the sinusoidal wave period. The black envelope represents the water flux response in the two-layered system.

8.0 TABLES

Table 1. Model conditions and parameters.

Condition or parameter	One-layered system	Two-layered system
Geometric parameters Water-table depth, m	10, 20, 100	100
Soil texture Gardner parameters (Table 1) with specified value given to each soil texture	All (see Table 4)	Upper over lower (1) Over (5), (7), (11) (5) Over (1), (7), (11) (7) Over (1), (5), (11) (11) Over (1), (5), (7)
Initial Conditions Downward water flux, q_s , Amplitude of the sinusoidal flux, q_p , Period (days)	All (see Table 2)	1.0 mm/day 0.99 mm/day 90 days
Boundary Conditions Upper Boundary Condition Lower Boundary Condition	Constant Flux Free Drainage	Constant Flux Free Drainage

Table 2. Infiltration rates represented. Regions from Sanford and Selnick, 2013.

Regions Represented	ET/P ratio	Infiltration Rate	Climate
Arid Southwest	>80%	0.010 mm/d 0.025 mm/d 0.050 mm/d 0.100 mm/d	Little to no rainfall, High temperatures
Temperate	50-70%	0.500 mm/d	Moderate rainfall, Moderate temperatures
WEST: Cascade Mts, Sierra Mts, Northern Rocky Mts, EAST: New England, Appalachian Mountains, Central Gulf Coast	30-50%	1.000 mm/d	Moderate Temperatures, High rainfall
Pacific Northwest	<20%	2.000 mm/d	High rainfall, Low-to-moderate temperatures

Table 3. Water flux values used with conversions to potential annual flux in mm. From Sanford and Selnick, 2013.

Region Represented	Mean Flux, q_z (mm/day)	Mean Amplitude, q_p (mm/day)	Potential Annual Flux (mm/year)
Desert, Arid	0.010	0.00990	3.650
	0.025	0.02475	9.125
Semi-Arid	0.050	0.04950	18.25
	0.100	0.09900	36.50
Shrub-land	0.500	0.49500	182.5
Grassland	1.000	0.99000	365.0
Forest, Marsh	2.000	1.98000	730.0

Table 4. USDA soil textural classes and Gardner hydraulic properties employed in flow simulations (modified from Dickinson et al., 2014).

	Soil Texture	K_{sat} (mm/d)	α (m^{-1})	ψ_e (m)	n_0	μ	$\theta_{residual}$ (m^3/m^3)	$\theta_{saturated}$ (m^3/m^3)
1	Clay	147.6	6.87	-0.366	0.459	2.046	0.098	0.459
2	Silty Clay	96.16	7.34	-0.334	0.481	2.184	0.111	0.481
3	Silty Clay Loam	111.2	4.43	-0.695	0.482	1.323	0.090	0.482
4	Silt Loam	182.4	3.20	-1.189	0.439	0.956	0.065	0.439
5	Silt	437.5	3.76	-0.902	0.489	1.123	0.050	0.489
6	Clay Loam	81.85	7.19	-0.344	0.442	2.139	0.079	0.442
7	Loam	120.5	5.44	-0.511	0.399	1.623	0.063	0.489
8	Sandy Clay	113.5	13.7	-0.134	0.385	4.076	0.061	0.385
9	Sandy Clay Loam	131.8	9.14	-0.244	0.384	2.719	0.063	0.384
10	Sandy Loam	382.8	11.2	-0.182	0.387	3.334	0.039	0.387
11	Loamy Sand	1052	14.2	-0.127	0.390	4.223	0.049	0.390
12	Sand	6427	14.4	-0.124	0.375	4.276	0.375	0.375

Table 5. Numerical solution, d_{num} , of a climate signal in a 30-day periods.

#	Material	Flux (mm/d)	Numerical (m)
1	Clay	0.01	0.14
1	Clay	0.025	0.21
1	Clay	0.05	0.28
1	Clay	0.10	0.39
1	Clay	0.50	0.92
1	Clay	1.00	1.47
1	Clay	2.00	2.47
2	Silty Clay	0.01	0.13
2	Silty Clay	0.025	0.18
2	Silty Clay	0.05	0.25
2	Silty Clay	0.10	0.34
2	Silty Clay	0.50	0.78
2	Silty Clay	1.00	1.25
2	Silty Clay	2.00	2.04
3	Silty Clay Loam	0.01	0.16
3	Silty Clay Loam	0.025	0.23
3	Silty Clay Loam	0.05	0.31
3	Silty Clay Loam	0.10	0.416
3	Silty Clay Loam	0.50	0.90
3	Silty Clay Loam	1.00	1.35
3	Silty Clay Loam	2.00	2.09
4	Silt loam	0.01	0.21
4	Silt loam	0.025	0.31
4	Silt Loam	0.05	0.41
4	Silt Loam	0.10	0.55
4	Silt Loam	0.50	1.18
4	Silt Loam	1.00	1.74
4	Silt Loam	2.00	2.68
5	Silt	0.01	0.22
5	Silt	0.025	0.31
5	Silt	0.05	0.42
5	Silt	0.10	0.57
5	Silt	0.50	1.28
5	Silt	1.00	1.94
5	Silt	2.00	2.68

6	Clay loam	0.01	0.13
6	Clay loam	0.025	0.19
6	Clay loam	0.05	0.26
6	Clay Loam	0.10	0.35
6	Clay loam	0.50	0.82
6	Clay loam	1.00	1.28
6	Clay loam	2.00	2.12
7	Loam	0.01	0.17
7	Loam	0.025	0.24
7	Loam	0.05	0.32
7	Loam	0.10	0.44
7	Loam	0.50	1.02
7	Loam	1.00	1.58
7	Loam	2.00	2.63
8	Sandy Clay	0.01	0.12
8	Sandy Clay	0.025	0.17
8	Sandy Clay	0.05	0.24
8	Sandy Clay	0.10	0.34
8	Sandy Clay	0.50	0.99
8	Sandy Clay	1.00	1.77
8	Sandy Clay	2.00	3.55
9	Sandy Clay Loam	0.01	0.14
9	Sandy Clay Loam	0.025	0.20
9	Sandy Clay Loam	0.05	0.28
9	Sandy Clay Loam	0.10	0.39
9	Sandy Clay Loam	0.50	1.02
9	Sandy Clay Loam	1.00	1.76
9	Sandy Clay Loam	2.00	3.21
10	Sandy Loam	0.01	0.16
10	Sandy Loam	0.025	0.24
10	Sandy loam	0.05	0.33
10	Sandy Loam	0.10	0.506
10	Sandy loam	0.50	1.46
10	Sandy loam	1.00	2.70
10	Sandy loam	2.00	5.31
11	Loamy Sand	0.01	0.17
11	Loamy Sand	0.025	0.26

11	Loamy Sand	0.05	0.40
11	Loamy Sand	0.10	0.594
11	Loamy Sand	0.50	2.28
11	Loamy Sand	1.00	4.67
11	Loamy Sand	2.00	9.56
12	Sand	0.01	0.25
12	Sand	0.025	0.43
12	Sand	0.05	0.65
12	Sand	0.10	1.26
12	Sand	0.50	5.0
12	Sand	1.00	11.0
12	Sand	2.00	23.0

Table 6. Numerical solution, d_{num} , of a climate signal in a 90-day period.

#	Material	Flux (mm/d)	Numerical (m)
1	Clay	0.01	0.28
1	Clay	0.025	0.43
1	Clay	0.05	0.62
1	Clay	0.10	0.91
1	Clay	0.50	2.85
1	Clay	1.00	5.48
1	Clay	2.00	11.15
2	Silty Clay	0.01	0.25
2	Silty Clay	0.025	0.38
2	Silty Clay	0.05	0.53
2	Silty Clay	0.10	0.78
2	Silty Clay	0.50	2.35
2	Silty Clay	1.00	4.53
2	Silty Clay	2.00	8.85
3	Silty Clay Loam	0.01	0.31
3	Silty Clay Loam	0.025	0.46
3	Silty Clay Loam	0.05	0.63
3	Silty Clay Loam	0.10	0.88
3	Silty Clay Loam	0.50	2.38
3	Silty Clay Loam	1.00	4.11
3	Silty Clay Loam	2.00	7.50
4	Silt loam	0.01	0.41
4	Silt loam	0.025	0.60
4	Silt Loam	0.05	0.82
4	Silt Loam	0.10	1.17
4	Silt Loam	0.50	3.05
4	Silt Loam	1.00	5.12
4	Silt Loam	2.00	9.30
5	Silt	0.01	0.42
5	Silt	0.025	0.63
5	Silt	0.05	0.85
5	Silt	0.10	1.27
5	Silt	0.50	3.60
5	Silt	1.00	6.43
5	Silt	2.00	12.20

6	Clay loam	0.01	0.26
6	Clay loam	0.025	0.39
6	Clay loam	0.05	0.55
6	Clay Loam	0.10	0.8
6	Clay loam	0.50	2.48
6	Clay loam	1.00	4.52
6	Clay loam	2.00	9.20
7	Loam	0.01	0.32
7	Loam	0.025	0.49
7	Loam	0.05	0.69
7	Loam	0.10	1.00
7	Loam	0.50	3.05
7	Loam	1.00	5.67
7	Loam	2.00	11.10
8	Sandy Clay	0.01	0.24
8	Sandy Clay	0.025	0.39
8	Sandy Clay	0.05	0.60
8	Sandy Clay	0.10	0.93
8	Sandy Clay	0.50	4.13
8	Sandy Clay	1.00	8.61
8	Sandy Clay	2.00	19.30
9	Sandy Clay Loam	0.01	0.28
9	Sandy Clay Loam	0.025	0.44
9	Sandy Clay Loam	0.05	0.66
9	Sandy Clay Loam	0.10	0.99
9	Sandy Clay Loam	0.50	3.83
9	Sandy Clay Loam	1.00	7.11
9	Sandy Clay Loam	2.00	16.55
10	Sandy Loam	0.01	0.33
10	Sandy Loam	0.025	0.56
10	Sandy loam	0.05	0.86
10	Sandy Loam	0.10	1.53
10	Sandy loam	0.50	6.53
10	Sandy loam	1.00	14.01
10	Sandy loam	2.00	29.10
11	Loamy Sand	0.01	0.39
11	Loamy Sand	0.025	0.68

11	Loamy Sand	0.05	1.19
11	Loamy Sand	0.10	2.07
11	Loamy Sand	0.50	12.03
11	Loamy Sand	1.00	29.70
11	Loamy Sand	2.00	48.70
12	Sand	0.01	0.65
12	Sand	0.025	1.37
12	Sand	0.05	2.00
12	Sand	0.10	5.95
12	Sand	0.50	27.0
12	Sand	1.00	76.2
12	Sand	2.00	103.0

Table 7. Numerical solution, d_{num} , of a climate signal in a 180-day period.

#	Material	Flux (mm/d)	Numerical (m)
1	Clay	0.01	0.45
1	Clay	0.025	0.73
1	Clay	0.05	1.11
1	Clay	0.10	1.77
1	Clay	0.50	7.44
1	Clay	1.00	15.72
1	Clay	2.00	33.32
2	Silty Clay	0.01	0.39
2	Silty Clay	0.025	0.63
2	Silty Clay	0.05	0.94
2	Silty Clay	0.10	1.5
2	Silty Clay	0.50	5.95
2	Silty Clay	1.00	12.48
2	Silty Clay	2.00	26.40
3	Silty Clay Loam	0.01	0.48
3	Silty Clay Loam	0.025	0.73
3	Silty Clay Loam	0.05	1.06
3	Silty Clay Loam	0.10	1.56
3	Silty Clay Loam	0.50	5.30
3	Silty Clay Loam	1.00	10.24
3	Silty Clay Loam	2.00	21.20
4	Silt loam	0.01	0.62
4	Silt loam	0.025	0.97
4	Silt Loam	0.05	1.38
4	Silt Loam	0.10	2.06
4	Silt Loam	0.50	6.62
4	Silt Loam	1.00	12.56
4	Silt Loam	2.00	25.76
5	Silt	0.01	0.65
5	Silt	0.025	1.03
5	Silt	0.05	1.51
5	Silt	0.10	2.33
5	Silt	0.50	8.49
5	Silt	1.00	16.92
5	Silt	2.00	35.68

6	Clay loam	0.01	0.41
6	Clay loam	0.025	0.65
6	Clay loam	0.05	0.98
6	Clay Loam	0.10	1.53
6	Clay loam	0.50	6.27
6	Clay loam	1.00	12.88
6	Clay loam	2.00	27.64
7	Loam	0.01	0.51
7	Loam	0.025	0.82
7	Loam	0.05	1.21
7	Loam	0.10	1.89
7	Loam	0.50	7.58
7	Loam	1.00	15.56
7	Loam	2.00	33.15
8	Sandy Clay	0.01	0.42
8	Sandy Clay	0.025	0.74
8	Sandy Clay	0.05	1.26
8	Sandy Clay	0.10	2.16
8	Sandy Clay	0.50	12.43
8	Sandy Clay	1.00	25.80
8	Sandy Clay	2.00	54.32
9	Sandy Clay Loam	0.01	0.47
9	Sandy Clay Loam	0.025	0.79
9	Sandy Clay Loam	0.05	1.28
9	Sandy Clay Loam	0.10	2.10
9	Sandy Clay Loam	0.50	10.96
9	Sandy Clay Loam	1.00	23.40
9	Sandy Clay Loam	2.00	49.60
10	Sandy Loam	0.01	0.58
10	Sandy Loam	0.025	1.08
10	Sandy loam	0.05	1.88
10	Sandy Loam	0.10	3.87
10	Sandy loam	0.50	19.60
10	Sandy loam	1.00	42.42
10	Sandy loam	2.00	78.43
11	Loamy Sand	0.01	0.72
11	Loamy Sand	0.025	1.49

11	Loamy Sand	0.05	3.01
11	Loamy Sand	0.10	5.80
11	Loamy Sand	0.50	37.16
11	Loamy Sand	1.00	73.20
11	Loamy Sand	2.00	229.8
12	Sand	0.01	1.41
12	Sand	0.025	3.59
12	Sand	0.05	7.00
12	Sand	0.10	18.52
12	Sand	0.50	71.0
12	Sand	1.00	194.0
12	Sand	2.00	248.0

Table 8. Numerical solution, d_{num} , of a climate signal in a 365-day period.

#	Material	Flux (mm/d)	Numerical (m)
1	Clay	0.01	0.77
1	Clay	0.025	1.38
1	Clay	0.05	2.31
1	Clay	0.10	4.14
1	Clay	0.50	22.98
1	Clay	1.00	49.60
1	Clay	2.00	99.48
2	Silty Clay	0.01	0.66
2	Silty Clay	0.025	1.16
2	Silty Clay	0.05	1.90
2	Silty Clay	0.10	3.42
2	Silty Clay	0.50	18.10
2	Silty Clay	1.00	39.10
2	Silty Clay	2.00	78.69
3	Silty Clay Loam	0.01	0.78
3	Silty Clay Loam	0.025	1.26
3	Silty Clay Loam	0.05	1.96
3	Silty Clay Loam	0.10	3.18
3	Silty Clay Loam	0.50	14.65
3	Silty Clay Loam	1.00	31.00
3	Silty Clay Loam	2.00	64.66
4	Silt loam	0.01	1.01
4	Silt loam	0.025	1.66
4	Silt Loam	0.05	2.53
4	Silt Loam	0.10	4.14
4	Silt Loam	0.50	17.90
4	Silt Loam	1.00	37.60
4	Silt Loam	2.00	79.30
5	Silt	0.01	1.08
5	Silt	0.025	1.84
5	Silt	0.05	2.92
5	Silt	0.10	5.01
5	Silt	0.50	24.80
5	Silt	1.00	40.30
5	Silt	2.00	110.00

6	Clay loam	0.01	0.69
6	Clay loam	0.025	1.20
6	Clay loam	0.05	2.00
6	Clay Loam	0.10	3.48
6	Clay loam	0.50	19.05
6	Clay loam	1.00	40.30
6	Clay loam	2.00	83.57
7	Loam	0.01	0.87
7	Loam	0.025	1.50
7	Loam	0.05	2.44
7	Loam	0.10	4.23
7	Loam	0.50	22.95
7	Loam	1.00	47.01
7	Loam	2.00	100.40
8	Sandy Clay	0.01	0.81
8	Sandy Clay	0.025	1.66
8	Sandy Clay	0.05	3.25
8	Sandy Clay	0.10	6.15
8	Sandy Clay	0.50	38.95
8	Sandy Clay	1.00	70.60
8	Sandy Clay	2.00	141.52
9	Sandy Clay Loam	0.01	0.85
9	Sandy Clay Loam	0.025	1.60
9	Sandy Clay Loam	0.05	2.98
9	Sandy Clay Loam	0.10	5.49
9	Sandy Clay Loam	0.50	34.60
9	Sandy Clay Loam	1.00	72.00
9	Sandy Clay Loam	2.00	145.79
10	Sandy Loam	0.01	1.15
10	Sandy Loam	0.025	2.52
10	Sandy loam	0.05	5.06
10	Sandy Loam	0.10	11.9
10	Sandy loam	0.50	58.00
10	Sandy loam	1.00	130.00
10	Sandy loam	2.00	192
11	Loamy Sand	0.01	1.61
11	Loamy Sand	0.025	4.04

11	Loamy Sand	0.05	9.17
11	Loamy Sand	0.10	18.8
11	Loamy Sand	0.50	117.4
11	Loamy Sand	1.00	203
11	Loamy Sand	2.00	738
12	Sand	0.01	3.8
12	Sand	0.025	11.3
12	Sand	0.05	19
12	Sand	0.10	63.4
12	Sand	0.50	194
12	Sand	1.00	591
12	Sand	2.00	609

Table 9. Numerical solution, d_{num} , of a climate signal in a 731-day period.

#	Material	Flux (mm/d)	Numerical (m)
1	Clay	0.01	1.46
1	Clay	0.025	3.00
1	Clay	0.05	5.4
1	Clay	0.10	11.5
1	Clay	0.50	63.5
1	Clay	1.00	164.5
1	Clay	2.00	414
2	Silty clay	0.01	1.25
2	Silty clay	0.025	2.52
2	Silty clay	0.05	4.2
2	Silty clay	0.10	9.2
2	Silty clay	0.50	43.7
2	Silty clay	1.00	110.4
2	Silty clay	2.00	321
3	Silty Clay Loam	0.01	1.31
3	Silty Clay Loam	0.025	2.44
3	Silty Clay Loam	0.05	4.0
3	Silty Clay Loam	0.10	7.5
3	Silty Clay Loam	0.50	26.9
3	Silty Clay Loam	1.00	84.9
3	Silty Clay Loam	2.00	210
4	Silt loam	0.01	1.75
4	Silt loam	0.025	3.08
4	Silt loam	0.05	5.3
4	Silt loam	0.10	9.7
4	Silt loam	0.50	45.1
4	Silt loam	1.00	105.8
4	Silt loam	2.00	243
5	Silt	0.01	1.89
5	Silt	0.025	3.60
5	Silt	0.05	6.4
5	Silt	0.10	12.8
5	Silt	0.50	66.5
5	Silt	1.00	163.3
5	Silt	2.00	336

6	Clay loam	0.01	1.29
6	Clay loam	0.025	2.56
6	Clay loam	0.05	4.5
6	Clay loam	0.10	9.4
6	Clay loam	0.50	45.1
6	Clay loam	1.00	112.7
6	Clay loam	2.00	318
7	Loam	0.01	1.59
7	Loam	0.025	3.20
7	Loam	0.05	5.5
7	Loam	0.10	11.2
7	Loam	0.50	66.3
7	Loam	1.00	158.7
7	Loam	2.00	363
8	Sandy Clay	0.01	1.89
8	Sandy Clay	0.025	4.60
8	Sandy Clay	0.05	8.9
8	Sandy Clay	0.10	19.1
8	Sandy Clay	0.50	164
8	Sandy Clay	1.00	333.5
8	Sandy Clay	2.00	564
9	Sandy Clay Loam	0.01	1.85
9	Sandy Clay Loam	0.025	3.60
9	Sandy Clay Loam	0.05	9.3
9	Sandy Clay Loam	0.10	16.2
9	Sandy Clay Loam	0.50	121
9	Sandy Clay Loam	1.00	190.5
9	Sandy Clay Loam	2.00	678
10	Sandy loam	0.01	2.84
10	Sandy loam	0.025	5.88
10	Sandy loam	0.05	13.6
10	Sandy loam	0.10	38.5
10	Sandy loam	0.50	218
10	Sandy loam	1.00	524.4
10	Sandy loam	2.00	713
11	Loamy Sand	0.01	5.23
11	Loamy Sand	0.025	12.16

11	Loamy Sand	0.05	28.1
11	Loamy Sand	0.10	64.9
11	Loamy Sand	0.50	259
11	Loamy Sand	1.00	683
11	Loamy Sand	2.00	2091
12	Sand	0.01	8.50
12	Sand	0.025	43.03
12	Sand	0.05	100
12	Sand	0.10	228
12	Sand	0.50	1406
12	Sand	1.00	2474
12	Sand	2.00	2965

Table 10. Numerical solution, d_{num} , of a climate signal in a 2556-day period.

#	Material	Flux (mm/d)	Numerical (m)
1	Clay	0.01	6.76
1	Clay	0.025	17.6
1	Clay	0.05	32.7
1	Clay	0.10	87.2
1	Clay	0.50	530
1	Clay	1.00	1532
1	Clay	2.00	2035
2	Silty clay	0.01	5.46
2	Silty clay	0.025	13.4
2	Silty clay	0.05	21.8
2	Silty clay	0.10	35.6
2	Silty clay	0.50	434
2	Silty clay	1.00	1190
2	Silty clay	2.00	1960
3	Silty Clay Loam	0.01	4.58
3	Silty Clay Loam	0.025	10.9
3	Silty Clay Loam	0.05	18.6
3	Silty Clay Loam	0.10	133
3	Silty Clay Loam	0.50	264
3	Silty Clay Loam	1.00	580
3	Silty Clay Loam	2.00	1130
4	Silt loam	0.01	6.11
4	Silt loam	0.025	13.4
4	Silt loam	0.05	28.1
4	Silt loam	0.10	64.8
4	Silt loam	0.50	374
4	Silt loam	1.00	668
4	Silt loam	2.00	1181
5	Silt	0.01	7.41
5	Silt	0.025	18.5
5	Silt	0.05	38.9
5	Silt	0.10	93.6
5	Silt	0.50	428
5	Silt	1.00	1262
5	Silt	2.00	1970

6	Clay loam	0.01	5.72
6	Clay loam	0.025	14.1
6	Clay loam	0.05	26.1
6	Clay loam	0.10	69.6
6	Clay loam	0.50	348
6	Clay loam	1.00	1060
6	Clay loam	2.00	1580
7	Loam	0.01	6.76
7	Loam	0.025	17.6
7	Loam	0.05	34.4
7	Loam	0.10	80.0
7	Loam	0.50	540
7	Loam	1.00	1382
7	Loam	2.00	1671
8	Sandy Clay	0.01	10.8
8	Sandy Clay	0.025	36.1
8	Sandy Clay	0.05	80.0
8	Sandy Clay	0.10	147
8	Sandy Clay	0.50	1474
8	Sandy Clay	1.00	1605
8	Sandy Clay	2.00	1940
9	Sandy Clay Loam	0.01	10.5
9	Sandy Clay Loam	0.025	22.0
9	Sandy Clay Loam	0.05	68.0
9	Sandy Clay Loam	0.10	122
9	Sandy Clay Loam	0.50	920
9	Sandy Clay Loam	1.00	891
9	Sandy Clay Loam	2.00	3680
10	Sandy loam	0.01	20.7
10	Sandy loam	0.025	34.9
10	Sandy loam	0.05	64.2
10	Sandy loam	0.10	359
10	Sandy loam	0.50	2156
10	Sandy loam	1.00	2145
10	Sandy loam	2.00	1800
11	Loamy Sand	0.01	45.9
11	Loamy Sand	0.025	110

11	Loamy Sand	0.05	255
11	Loamy Sand	0.10	572
11	Loamy Sand	0.50	3175
11	Loamy Sand	1.00	6000
11	Loamy Sand	2.00	5000
12	Sand	0.01	118
12	Sand	0.025	459
12	Sand	0.05	870
12	Sand	0.10	3263
12	Sand	0.50	9000
12	Sand	1.00	10000
12	Sand	2.00	10000

Table 11. Numerical solution, d_{num} , of a climate signal in a 3652-day period.

#	Material	Flux (mm/d)	Numerical (m)
1	Clay	0.01	11.6
1	Clay	0.025	34.8
1	Clay	0.05	57.5
1	Clay	0.10	169
1	Clay	0.50	783
1	Clay	1.00	1570
1	Clay	2.00	3171
2	Silty clay	0.01	9.2
2	Silty clay	0.025	27.6
2	Silty clay	0.05	45.5
2	Silty clay	0.10	137
2	Silty clay	0.50	651
2	Silty clay	1.00	2425
2	Silty clay	2.00	4921
3	Silty Clay Loam	0.01	7.3
3	Silty Clay Loam	0.025	20.0
3	Silty Clay Loam	0.05	41.0
3	Silty Clay Loam	0.10	87.0
3	Silty Clay Loam	0.50	441
3	Silty Clay Loam	1.00	1180
3	Silty Clay Loam	2.00	2422
4	Silt loam	0.01	9.6
4	Silt loam	0.025	24.8
4	Silt loam	0.05	54.0
4	Silt loam	0.10	120
4	Silt loam	0.50	633
4	Silt loam	1.00	1085
4	Silt loam	2.00	1911
5	Silt	0.01	12.0
5	Silt	0.025	33.4
5	Silt	0.05	73.5
5	Silt	0.10	172
5	Silt	0.50	669
5	Silt	1.00	2125
5	Silt	2.00	3010

6	Clay loam	0.01	9.6
6	Clay loam	0.025	28.4
6	Clay loam	0.05	48.5
6	Clay loam	0.10	133
6	Clay loam	0.50	648
6	Clay loam	1.00	2095
6	Clay loam	2.00	4935
7	Loam	0.01	11.2
7	Loam	0.025	33.2
7	Loam	0.05	61.5
7	Loam	0.10	146
7	Loam	0.50	906
7	Loam	1.00	1650
7	Loam	2.00	2730
8	Sandy Clay	0.01	17.6
8	Sandy Clay	0.025	75.6
8	Sandy Clay	0.05	164
8	Sandy Clay	0.10	345
8	Sandy Clay	0.50	2553
8	Sandy Clay	1.00	4380
8	Sandy Clay	2.00	7419
9	Sandy Clay Loam	0.01	18.6
9	Sandy Clay Loam	0.025	36.6
9	Sandy Clay Loam	0.05	132
9	Sandy Clay Loam	0.10	246
9	Sandy Clay Loam	0.50	1392
9	Sandy Clay Loam	1.00	2815
9	Sandy Clay Loam	2.00	10344
10	Sandy loam	0.01	38.8
10	Sandy loam	0.025	60.0
10	Sandy loam	0.05	124
10	Sandy loam	0.10	475
10	Sandy loam	0.50	6335
10	Sandy loam	1.00	8586
10	Sandy loam	2.00	10000
11	Loamy Sand	0.01	89.8
11	Loamy Sand	0.025	186

11	Loamy Sand	0.05	520
11	Loamy Sand	0.10	2502
11	Loamy Sand	0.50	10000
11	Loamy Sand	1.00	18000
11	Loamy Sand	2.00	24000
12	Sand	0.01	89.8
12	Sand	0.025	186
12	Sand	0.05	520
12	Sand	0.10	2502
12	Sand	0.50	15000
12	Sand	1.00	40000
12	Sand	2.00	70000

Table 12. Two-layered profile with clay as the upper layer and different bottom layers. Changes from the one-layer d_{num} are based on varying later thickness and varying lower layer for a q_z of 1 mm/day and period of 30 days.

Upper layer	One-layer d_{num} (m)	Fraction of d_{num}	Layer Thickness (m)	Lower layer	Two-layer d_{num} (m)	Percent Change
Clay	1.5	$\frac{1}{4}$	0.4	Silt	2.0	33%
				Loam	1.6	11%
				Loamy Sand	4.4	199%
	1.5	$\frac{1}{2}$	0.7	Silt	1.8	25%
				Loam	1.6	10%
				Loamy Sand	3.8	161%
	1.5	$\frac{3}{4}$	1.1	Silt	1.7	17%
				Loam	1.6	7%
				Loamy Sand	3.0	103%

Table 13. Two-layered profile with clay as the upper layer and different bottom layers. Changes from the one-layer d_{num} are based on varying later thickness and varying lower layer for a q_z of 1 mm/day and period of 90 days.

Upper layer	One-layer d_{num} (m)	Fraction of d_{num}	Layer Thickness (m)	Lower layer	Two-layer d_{num} (m)	Percent Change
Clay	4.5	$\frac{1}{4}$	1.1	Silt	6.3	40%
				Loam	5.7	27%
				Loamy Sand	26	474%
	4.5	$\frac{1}{2}$	2.3	Silt	6.1	35%
				Loam	5.7	26%
				Loamy Sand	21	369%
	4.5	$\frac{3}{4}$	3.4	Silt	6.0	32%
				Loam	5.7	25%
				Loamy Sand	15	223%

Table 14. Two-layered profile with clay as the upper layer and different bottom layers. Changes from the one-layer d_{num} are based on varying later thickness and varying lower layer for a q_z of 1 mm/day and period of 365 days.

Upper layer	One-layer d_{num} (m)	Fraction of d_{num}	Layer Thickness (m)	Lower layer	Two-layer d_{num} (m)	Percent Change
Clay	50	$\frac{1}{4}$	12.7	Silt	51	3%
				Loam	50	0%
				Loamy Sand	274	452%
	50	$\frac{1}{2}$	25.4	Silt	51	2%
				Loam	50	1%
				Loamy Sand	233	369%
	50	$\frac{3}{4}$	38.0	Silt	52	4%
				Loam	51	2%
				Loamy Sand	156	215%

Table 15. Two-layered profile with silt as the upper layer and different bottom layers. Changes from the one-layer d_{num} are based on varying later thickness and varying lower layer for a q_z of 1 mm/day and period of 30 days.

Upper layer	One-layer d_{num} (m)	Fraction of d_{num}	Layer Thickness (m)	Lower layer	Two-layer d_{num} (m)	Percent Change
Silt	2.0	$\frac{1}{4}$	0.5	Clay	1.3	-35%
				Loam	1.4	-28%
	2.0	$\frac{1}{2}$	1.0	Clay	1.6	-20%
				Loam	1.7	-14%
	2.0	$\frac{3}{4}$	1.5	Clay	1.9	-5%
				Loam	1.8	-5%

Table 16. Two-layered profile with silt as the upper layer and different bottom layers. Changes from the one-layer d_{num} are based on varying later thickness and varying lower layer for a q_z of 1 mm/day and period of 90 days.

Upper layer	One-layer d_{num} (m)	Fraction of d_{num}	Layer Thickness (m)	Lower layer	Two-layer d_{num} (m)	Percent Change
Silt	6.4	$\frac{1}{4}$	1.6	Clay	4.9	-23%
				Loam	5.1	-21%
	6.4	$\frac{1}{2}$	3.2	Clay	5.1	-21%
				Loam	5.4	-17%
	6.4	$\frac{3}{4}$	4.8	Clay	5.2	-19%
				Loam	5.3	-18%

Table 17. Two-layered profile with silt as the upper layer and different bottom layers. Changes from the one-layer d_{num} are based on varying later thickness and varying lower layer for a q_z of 1 mm/day and period of 365 days.

Upper layer	One-layer d_{num} (m)	Fraction of d_{num}	Layer Thickness (m)	Lower layer	Two-layer d_{num} (m)	Percent Change
Silt	40	$\frac{1}{4}$	10.1	Clay	51	27%
				Loam	50	24%
	40	$\frac{1}{2}$	20.2	Clay	50	24%
				Loam	50	24%
	40	$\frac{3}{4}$	30.2	Clay	48	20%
				Loam	50	23%

Table 18. Two-layered profile with loam as the upper layer and different bottom layers. Changes from the one-layer d_{num} are based on varying later thickness and varying lower layer for a q_z of 1 mm/day and period of 30 days.

Upper layer	One-layer d_{num} (m)	Fraction of d_{num}	Layer Thickness (m)	Lower layer	Two-layer d_{num} (m)	Percent Change
Loam	1.6	$\frac{1}{4}$	0.4	Clay	1.5	-8%
				Silt	2.0	27%
				Loamy Sand	4.3	171%
	1.6	$\frac{1}{2}$	0.8	Clay	1.5	-4%
				Silt	1.9	20%
				Loamy Sand	4.0	151%
	1.6	$\frac{3}{4}$	1.2	Clay	1.5	-3%
				Silt	1.8	14%
				Loamy Sand	3.4	113%

Table 19. Two-layered profile with loam as the upper layer and different bottom layers. Changes from the one-layer d_{num} are based on varying later thickness and varying lower layer for a q_z of 1 mm/day and period of 90 days.

Upper layer	One-layer d_{num} (m)	Fraction of d_{num}	Layer Thickness (m)	Lower layer	Two-layer d_{num} (m)	Percent Change
Loam	5.7	$\frac{1}{4}$	1.4	Clay	5.4	-5%
				Silt	6.4	13%
				Loamy Sand	26	360%
	5.7	$\frac{1}{2}$	2.8	Clay	5.4	-4%
				Silt	6.3	11%
				Loamy Sand	21	270%
	5.7	$\frac{3}{4}$	4.3	Clay	5.4	-5%
				Silt	6.1	7%
				Loamy Sand	15	158%

Table 20. Two-layered profile with loam as the upper layer and different bottom layers. Changes from the one-layer d_{num} are based on varying later thickness and varying lower layer for a q_z of 1 mm/day and period of 365 days.

Upper layer	One-layer d_{num} (m)	Fraction of d_{num}	Layer Thickness (m)	Lower layer	Two-layer d_{num} (m)	Percent Change
Loam	47	$\frac{1}{4}$	11.8	Clay	51	8%
				Silt	52	10%
				Loamy Sand	276	487%
	47	$\frac{1}{2}$	23.5	Clay	50	7%
				Silt	51	8%
				Loamy Sand	236	403%
	47	$\frac{3}{4}$	35.3	Clay	50	5%
				Silt	51	8%
				Loamy Sand	158	236%

Table 21. Two-layered profile with loamy sand as the upper layer and different bottom layers. Changes from the one-layer d_{num} are based on varying later thickness and varying lower layer for a q_z of 1 mm/day and period of 30 days.

Upper layer	One-layer d_{num} (m)	Fraction of d_{num}	Layer Thickness (m)	Lower layer	Two-layer d_{num} (m)	Percent Change
Loamy Sand	4.7	$\frac{1}{4}$	1.2	Clay	2.4	-49%
				Loam	2.5	-47%
	4.7	$\frac{1}{2}$	2.3	Clay	3.3	-30%
				Loam	3.3	-28%
	4.7	$\frac{3}{4}$	3.5	Clay	4.3	-9%
				Loam	4.3	-8%

Table 22. Two-layered profile with loamy sand as the upper layer and different bottom layers. Changes from the one-layer d_{num} are based on varying later thickness and varying lower layer for a q_z of 1 mm/day and period of 90 days.

Upper layer	One-layer d_{num} (m)	Fraction of d_{num}	Layer Thickness (m)	Lower layer	Two-layer d_{num} (m)	Percent Change
Loamy Sand	30	$\frac{1}{4}$	7.4	Clay	11	-64%
				Loam	11	-63%
	30	$\frac{1}{2}$	14.9	Clay	17	-44%
				Loam	17	-44%
	30	$\frac{3}{4}$	22.3	Clay	23	-22%
				Loam	23	-22%

Table 23. Two-layered profile with loamy sand as the upper layer and different bottom layers. Changes from the one-layer d_{num} are based on varying later thickness and varying lower layer for a q_z of 1 mm/day and period of 365 days.

Upper layer	One-layer d_{num} (m)	Fraction of d_{num}	Layer Thickness (m)	Lower layer	Two-layer d_{num} (m)	Percent Change
Loamy Sand	203	$\frac{1}{4}$	50.8	Clay	98	-52%
				Loam	98	-52%
	203	$\frac{1}{2}$	101.6	Clay	166	-19%
				Loam	165	-19%
	203	$\frac{3}{4}$	152.4	Clay	233	15%
				Loam	233	14%

Table 24. Percent change in damping depth comparisons for clay for a q_z of 1.0 mm/day and a period of 30 days. A difference of less than 10% between the two-layered and the one-layered systems indicates possible linear superposition.

Upper layer	Layer thickness	Lower layer	Two-layer d_{num}	One-layered, imposed d_{num}	Percent Change
Clay	$1/4$	Silt	2.0	1.8	-10%
		Loam	1.6	1.5	-8%
		Loamy Sand	4.4	4.1	-6%
	$1/2$	Silt	1.8	1.7	-10%
		Loam	1.6	1.5	-7%
		Loamy Sand	3.8	2.9	-24%
	$3/4$	Silt	1.7	1.6	-9%
		Loam	1.6	1.5	-5%
		Loamy Sand	3.0	2.2	-28%

Table 25. Percent change in damping depth comparisons for silt for a q_z of 1.0 mm/day and a period of 30 days. A difference of less than 10% between the two-layered and the one-layered systems indicates possible linear superposition.

Upper layer	Layer thickness	Lower layer	Two-layer d_{num}	One-layered, imposed d_{num}	Percent Change
Silt	$1/4$	Clay	1.3	1.5	20%
		Loam	1.4	1.6	15%
	$1/2$	Clay	1.6	1.7	6%
		Loam	1.7	1.7	4%
	$3/4$	Clay	1.9	1.8	-2%
		Loam	1.8	1.9	1%

Table 26. Percent change in damping depth comparisons for loam for a q_z of 1.0 mm/day and a period of 30 days. A difference of less than 10% between the two-layered and the one-layered systems indicates possible linear superposition.

Upper layer	Layer thickness	Lower layer	Two-layer d_{num}	One-layered, imposed d_{num}	Percent Change
Loam	$\frac{1}{4}$	Clay	1.5	1.4	-1%
		Silt	2.0	1.8	-10%
		Loamy Sand	4.3	4.1	-3%
	$\frac{1}{2}$	Clay	1.5	1.5	-2%
		Silt	1.9	1.7	-9%
		Loamy Sand	4.0	3.0	-25%
	$\frac{3}{4}$	Clay	1.5	1.6	1%
		Silt	1.8	1.7	-7%
		Loamy Sand	3.4	2.2	-35%

Table 27. Percent change in damping depth comparisons for loamy sand for a q_z of 1.0 mm/day and a period of 30 days. A difference of less than 10% between the two-layered and the one-layered systems indicates possible linear superposition.

Upper layer	Layer thickness	Lower layer	Two-layer d_{num}	One-layered, imposed d_{num}	Percent Change
Loamy Sand	$\frac{1}{4}$	Clay	2.4	2.3	-5%
		Loam	2.5	2.7	11%
	$\frac{1}{2}$	Clay	3.3	3.2	-2%
		Loam	3.3	3.7	10%
	$\frac{3}{4}$	Clay	4.3	4.5	6%
		Loam	4.3	4.3	0%

Table 28. Percent change in damping depth comparisons for clay for a q_z of 1.0 mm/day and a period of 90 days. A difference of less than 10% between the two-layered and the one-layered systems indicates possible linear superposition.

Upper layer	Layer thickness	Lower layer	Two-layer d_{num}	One-layered, imposed d_{num}	Percent Change
Clay	$\frac{1}{4}$	Silt	6.3	6.1	-4%
		Loam	5.7	5.5	-4%
		Loamy Sand	26	24	-9%
	$\frac{1}{2}$	Silt	6.1	5.8	-5%
		Loam	5.7	5.4	-5%
		Loamy Sand	21	15	-30%
	$\frac{3}{4}$	Silt	6.0	5.7	-5%
		Loam	5.7	5.5	-3%
		Loamy Sand	15	10	-31%

Table 29. Percent change in damping depth comparisons for silt for a q_z of 1.0 mm/day and a period of 90 days. A difference of less than 10% between the two-layered and the one-layered systems indicates possible linear superposition.

Upper layer	Layer thickness	Lower layer	Two-layer d_{num}	One-layered, imposed d_{num}	Percent Change
Silt	$\frac{1}{4}$	Clay	4.9	6.0	22%
		Loam	5.1	5.8	13%
	$\frac{1}{2}$	Clay	5.1	5.8	13%
		Loam	5.4	5.2	-3%
	$\frac{3}{4}$	Clay	5.2	5.3	2%
		Loam	5.3	6.0	13%

Table 30. Percent change in damping depth comparisons for loam for a q_z of 1.0 mm/day and a period of 90 days. A difference of less than 10% between the two-layered and the one-layered systems indicates possible linear superposition.

Upper layer	Layer thickness	Lower layer	Two-layer d_{num}	One-layered, imposed d_{num}	Percent Change
Loam	$\frac{1}{4}$	Clay	5.4	5.4	0%
		Silt	6.4	6.1	-4%
		Loamy Sand	26	24	-10%
	$\frac{1}{2}$	Clay	5.4	5.7	5%
		Silt	6.3	6.3	0%
		Loamy Sand	21	14	-32%
	$\frac{3}{4}$	Clay	5.4	5.5	2%
		Silt	6.1	5.8	-5%
		Loamy Sand	15	9.9	-33%

Table 31. Percent change in damping depth comparisons for loamy sand for a q_z of 1.0 mm/day and a period of 90 days. A difference of less than 10% between the two-layered and the one-layered systems indicates possible linear superposition.

Upper layer	Layer thickness	Lower layer	Two-layer d_{num}	One-layered, imposed d_{num}	Percent Change
Loamy Sand	$\frac{1}{4}$	Clay	11	11	0%
		Loam	11	11	0%
	$\frac{1}{2}$	Clay	17	17	-1%
		Loam	17	17	0%
	$\frac{3}{4}$	Clay	23	23	0%
		Loam	23	23	0%

Table 32. Percent change in damping depth comparisons for clay for a q_z of 1.0 mm/day and a period of 365 days. A difference of less than 10% between the two-layered and the one-layered systems indicates possible linear superposition.

Upper layer	Layer thickness	Lower layer	Two-layer d_{num} (m)	One-layered, imposed d_{num}	Percent Change
Clay	$1/4$	Silt	51	53	4%
		Loam	50	50	1%
		Loamy Sand	274	191	-30%
	$1/2$	Silt	51	49	-3%
		Loam	50	48	-3%
		Loamy Sand	233	83	-64%
	$3/4$	Silt	52	50	-3%
		Loam	51	50	-1%
		Loamy Sand	156	79	-49%

Table 33. Percent change in damping depth comparisons for silt for a q_z of 1.0 mm/day and a period of 365 days. A difference of less than 10% between the two-layered and the one-layered systems indicates possible linear superposition.

Upper layer	Layer Thickness	Lower layer	Two-layer d_{num} (m)	One-layered, imposed d_{num}	Percent Change
Silt	$1/4$	Clay	51	51	0%
		Loam	50	52	3%
	$1/2$	Clay	50	51	2%
		Loam	50	45	-10%
	$3/4$	Clay	48	52	7%
		Loam	50	52	6%

Table 34. Percent change in damping depth comparisons for loam for a q_z of 1.0 mm/day and a period of 365 days. A difference of less than 10% between the two-layered and the one-layered systems indicates possible linear superposition.

Upper layer	Layer thickness	Lower layer	Two-layer d_{num} (m)	One-layered, imposed d_{num}	Percent Change
Loam	$\frac{1}{4}$	Clay	51	49	-3%
		Silt	52	53	3%
		Loamy Sand	276	195	-30%
	$\frac{1}{2}$	Clay	50	49	-3%
		Silt	51	50	-1%
		Loamy Sand	236	85	-64%
	$\frac{3}{4}$	Clay	50	50	0%
		Silt	51	50	-3%
		Loamy Sand	158	79	-50%

Table 35. Percent change in damping depth comparisons for loamy sand for a q_z of 1.0 mm/day and a period of 365 days. A difference of less than 10% between the two-layered and one-layered systems indicates possible linear superposition.

Upper layer	Layer thickness	Lower layer	Two-layer d_{num} (m)	One-layered, imposed d_{num}	Percent Change
Loamy Sand	$\frac{1}{4}$	Clay	98	100	1%
		Loam	98	100	1%
	$\frac{1}{2}$	Clay	166	164	-1%
		Loam	165	165	0%
	$\frac{3}{4}$	Clay	233	240	3%
		Loam	233	240	3%

Table 36. The False Discovery Rate (FDR) p-values of mean flux, period, and K_{sat} , shown alongside a statistically significant level of $\alpha = 0.05$.

		Mean Flux	Period	K_{sat}	α
1	Clay	0.0009	0.0022	0.017	0.05
2	Silty Clay	0.0009	0.0022	0.017	0.05
3	Silty Clay Loam	0.0008	0.0023	0.020	0.05
4	Silt Loam	0.0008	0.0023	0.020	0.05
5	Silt	0.0010	0.0036	0.024	0.05
6	Clay Loam	0.0009	0.0023	0.018	0.05
7	Loam	0.0009	0.0024	0.018	0.05
8	Sandy Clay	0.0004	0.0015	0.014	0.05
9	Sandy Clay Loam	0.0008	0.0022	0.016	0.05
10	Sandy Loam	0.0004	0.0010	0.013	0.05
11	Loamy Sand	0.0004	0.0005	0.013	0.05
12	Sand	0.0029	0.0029	0.048	0.05

Table 37. The FDR LogWorth values highlight the statistically significant influence that the flux and period have on the damping depth.

FDR LogWorth Values						
		Mean Flux	Period	K_{sat}	R^2 value	R^2 value (adjusted)
1	Clay	3.06	2.66	1.77	0.61	0.57
2	Silty Clay	3.06	2.66	1.77	0.61	0.57
3	Silty Clay Loam	3.09	2.65	1.77	0.61	0.57
4	Silt Loam	3.09	2.64	1.70	0.61	0.57
5	Silt	3.01	2.44	1.65	0.59	0.55
6	Clay Loam	3.04	2.63	1.76	0.60	0.57
7	Loam	3.05	2.62	1.75	0.60	0.57
8	Sandy Clay	3.38	2.82	1.87	0.63	0.60
9	Sandy Clay Loam	3.56	2.84	1.80	0.61	0.57
10	Sandy Loam	3.37	3.02	1.90	0.64	0.61
11	Loamy Sand	3.46	3.32	1.90	0.66	0.63
12	Sand	2.54	2.54	1.32	0.55	0.51

9.0 APPENDIX

Model Input

The numerical script has 7 lines of code that may be changed to reflect a desired hypothetical vadose zone profile and boundary conditions. Line 1 asks for the soil catalog, either VanGenuchten 'VG' or Gardner 'GA', for this research, I used the 'Gardner' soil catalog.

Lines 2-3 define the profile geometry and soils in the layered system. Line 2 defines the node (out of 1001), at the bottom of the first layer and Line 3 defines the node (out of 1001) at the bottom of the second layer. If the node on Line 3 is less than 1001, then the first layer will repeat. Additionally, Line 2 asks for an integer (of 12 possible values) that will define the starting position along a 1-D vector. Line 3 asks for an integer (from same 12 values) to define the ending position along a 1-D vector. The 12 values represent the 12 soils: clay (1), silty clay (2), silty clay loam (3), silt loam (4), silt (5), clay loam (6), loam (7), sandy clay (8), sandy clay loam (9), sandy loam (10), loamy sand (11), and sand (12). When the script is executed, it will "call upon" HYDRUS-1D (Simunek, 1992), which will use the input soils (Table 4).

Line 4 defines the vertical cell thickness (mm) of the profile, depth "z", starting at $z = 0$ and ending at the defined value. Lines 5-7 create the properties of the sinusoidal infiltration cycle at the surface, where Line 5 asks for the number of days that will define a period. Line 6 defines the mean flux of the sinusoidal boundary in mm/d, and Line 7 defines the amplitude of the sinusoidal boundary, also in mm/d. To maintain consistency across the modeling exercise, the amplitude was always set as 99.0% of the respective mean flux.

Model Output

Once the numerical script is executed, it uses the input parameters in HYDRUS to solve Richards' equation (Richards, 1931b). Once the numerical solution has converged, it organizes the solution into 6 data profiles with values describing changes over the set period: water capacity [dimensions], infiltration flux [dimensions], hydraulic conductivity [dimensions], pressure head [dimensions], water content [dimensions], profile amplitude [dimensions], and damping depth [L]. The model output can then be plotted in MATLAB or most other data programs to visually observe changes in the sinusoid over time.